UNIVERSITY OF CALIFORNIA, SAN DIEGO

BIOMECHANICS OF CARTILAGE ARTICULATION: EFFECTS OF DEGENERATION, LUBRICATION, AND FOCAL ARTICULAR DEFECTS

A dissertation submitted in partial satisfaction of the

requirements for the degree Doctor of Philosophy

in

Bioengineering

by

Benjamin L. Wong

Committee in charge:

Professor Robert L. Sah, Chair
Professor William D. Bugbee
Professor Shu Chien
Professor Jeffrey H. Omens
Professor Samuel R. Ward

2009

The dissertation of Benjamin L. Wong is approved, and it is acceptable in quality and form for publication on microfilm and electronically:

_____

_____

_____

_____

_____

_____

Chair

University of California, San Diego

2009

TABLE OF CONTENTS

LIST OF FIGURES AND TABLES

ACKNOWLEDGMENTS

The completion of this work has been made possible only with the invaluable support of many individuals that I acknowledge herein. To them, I am dearly grateful and appreciative because each one of them has contributed immensely to my growth not only as a bioengineer, but also as a person.

First and foremost, I would like to thank Dr. Robert L. Sah for his mentorship, guidance, and tutelage. His generosity to take me on as an undergraduate researcher was pivotal in the career path that I have taken. The 8 years of research experience under his guidance has enabled me to grow as a critical thinker, a better scientific writer and a more sound researcher. I am greatly indebted to Dr. Sah for his endless support; for he is a large reason for all my successes in research and education as both an undergraduate and graduate student at UCSD. The skills and knowledge I have gained are in large part due to Dr. Sah and will empower me for all my future endeavors. As a result, he is among the most instrumental people in my life and career.

Funding sources as well as collaborators has made this dissertation possible. I would like to acknowledge the San Diego Fellowship for the supplemental financial support it has provided me through the first 4 years of my graduate studies. Furthermore, I would like to acknowledge support by the National Institute of Heath, National Science Foundation and the Howard Hughes Medical Institute. I thank my thesis committee members, Drs. William Bugbee, Shu Chien, Jeffery Omens, and Samuel Ward for their time and discussions. Finally, I would like to thank Dr. Martin

Lotz and his visiting orthopedic surgeons for their time and skill at harvesting and providing the human samples for these studies.

Permission has been requested to John Wiley & Sons, Inc. and Tech Press Science for the reprinting of Chapters 2 and 3 in full, respectively. I would like to sincerely thank co-authors: Drs. Won Bae, Kenneth Gratz, Martin Lotz, and Robert Sah, as well as June Chun for their contributions to these chapters. Additionally, Chapter 5 will be submitted to Arthritis and Rheumatism, and I like to thank co-authors: Drs. C Wayne McIlwraith and Robert Sah, as well as, Seung Hyun (Chris) Kim and Jennifer Antonacci for their contributions to this work.

During my experience in the CTE lab, I have had wonderful mentors throughout my time here that have taken me under their wing to train and teach me the in and outs of research. I have to thank Dr Kyle Jadin, who at the time was entering his 2nd year as a graduate student, for his mentorship and guidance during my first experience in the CTE lab as an undergraduate. A special thanks to Dr. Won Bae who took me under his wing when I entered the lab as a gradate student and was in the trenches with me doing experimental pilot work in MRI and shear testing of cartilage. It was because of your aid that this work has become what it has. You are a great teacher and would be a great addition to any academic department as a faculty member. I would also like to thank Barbara Schumacher for her invaluable teachings in histology, fixation, sectioning, and staining of cartilage.

I would also like to acknowledge all the current and past CTE staff including Van Wong, Carrie Wirt, Leo Schumacher, and Michael Voegtline, who have made my daily life in CTE run so much smoother than it would have otherwise. In addition to

them, Project Scientists Drs Albert Chen and Michele Temple-Wong have been an immense source of expertise in compressive and wear testing of cartilage.

Throughout my time here, I have had the tremendous privilege of working with many undergraduate students. I would like to acknowledge June Chun, my first undergraduate researcher, Chris Kim, and Alexander Cigan for all of their help in my experiments. Their help in tissue harvesting, running tests, chamber design, and data analysis took a large burden off my shoulders. Their cooperativeness, motivation, and pleasant personalities made it an enjoyment to work with them.

To the past and present graduate students of the CTE lab, you were a large part in making the rigors of graduate research enjoyable as well as memorable. To the elder grad students of the past, Drs. Tannin Schmidt, Kyle Jadin, Gayle Nugent-Derfus, Ken Gratz, and Megan Blewis, thank you for all the good times and stories shared in and out of lab. To the current grad students who entered graduate school near my time, Greg Williams, Jennifer Hwang, and Jennifer Antonacci, I will cherish the good times spent in and definitely outside of lab. To the current grad students that followed, Eun Hee Han, Hoa Nguyen, Andrea Pallante, Bill McCarty, Elaine Chan, and Brad Hansen, thank you for the fun memories during our ORS outings as well as lab social functions.

I would like to especially thank my close friends Sheila Singson Bruschi, Giancarlo Bruschi, Quyen Nguyen, Darren Gin, Kevin Tsang, Leslie Hsu, and Minna Tran for keeping me sane outside of graduate school by allowing me to have a good balance between work and play. Thank you for always being there for me in my times of need. Also, I would like to thank my friends and classmates from the “BE Group”

of my undergraduate days, Leslie, Sheila, Quyen, John Lin, Tihua Chen, Zeb Lee, and Diana Hsue for making my undergraduate experiences with bioengineering bearable. If it weren't for you guys, I probably would not have pursued a graduate degree in BE.

I would especially like to thank my girlfriend, Alda Chang, for her support and patience. Your company, friendship, and unwavering support have been pivotal in my personal happiness and accomplishments.

Most of all, I would like to finally thank my parents, Shiu Wai Tam Wong, and Wei Sing Wong. Their unwavering belief and trust in me has enabled me to pursue what I desire to do and accomplish. I am very lucky to have parents like them, whom provide unyielding support while giving me absolute freedom and trust. I can only hope that I have made them proud with my accomplishments and rewarded their trust in me by becoming a son they envisioned.

VITA

2003	B.S., Bioengineering University of California, San Diego, La Jolla, California
2003-2009	Graduate Student Researcher Cartilage Tissue Engineering Laboratory University of California, San Diego, La Jolla, California
2005	M.S., Bioengineering University of California, San Diego, La Jolla, California
2009	Ph.D., Bioengineering University of California, San Diego, La Jolla, California

Journal Articles

Wong BL, Sah RL: Cartilage mechanics during tibio-femoral articulation: local and overall compressive and shear deformation and properties. *J Biomech* (submitted), 2009

Gratz KR, Wong BL, Bae WC, Sah RL: The effects of focal articular defects on cartilage contact mechanics. *J Orthop Res* 27:584-92.

Gratz KR, Wong BL, Bae WC, Sah RL: The effects of focal articular defects on intra-tissue strain in the surrounding and opposing cartilage. *Biorheology* 45:193-207, 2008.

Wong BL, Bae WC, Gratz KR, Sah RL: Shear deformation kinematics during cartilage articulation: effect of lubrication, degeneration, and stress relaxation. *Mol Cell Biomech* 5:197-206, 2008.

Wong BL, Bae WC, Chun J, Gratz KR, Lotz M, Sah RL: Biomechanics of cartilage articulation: effects of lubrication and degeneration on shear deformation. *Arthritis Rheum* 58:2065-74, 2008.

Selected Abstracts

Wong BL, Cigan AD, Kim SH, Sah RL: The effect of a focal articular defect on cartilage deformation during articulation. *Trans Orthop Res Soc* 34:149, 2009.

Wong, BL, Bae WC, Gratz KR, Sah RL: Shear kinematics of cartilage articulation: effect of lubrication and degeneration. *BMES*, 2008

Wong BL, Bae WC, Chun J, Gratz KR, Kim SHC, Antonacci JM, McIlwraith CW, Sah RL: Biomechanics of cartilage articulation: effect of lubrication & degeneration on shear strain. *GRC* , 2008.

Wong BL, Kim SHC, Antonacci JM, McIlwraith CW, Sah RL: Cartilage shear strain during femoral-tibial articulation: effect of acute joint injury on synovial fluid lubrication. *Trans Orthop Res Soc* 33:627, 2008

Nguyen QT, Wong BL, Chun J, Sah RL: Controlling cartilage shear and sliding in vitro for mechanobiology: effect of synovial fluid and platen surface roughness. *Trans Orthop Res Soc* 33:626, 2008.

Gratz KR, Wong BL, Bae WC, Sah RL: Focal Articular Defects Alter Cartilage Contact Mechanics. *5th International Symposium on Mechanobiology of Cartilage and Chondrocyte, Athens GR*, 2007

Gratz KR, Wong BL, Bae WC, Sah RL: Effects of a focal articular defect on cartilage contact mechanics. *Trans Orthop Res Soc* 32:617, 2007.

Wong BL, Bae WC, Chun J, Gratz KR, Sah RL: Micro-mechanics of cartilage articulation: effect of degeneration on shear deformation. *Trans Orthop Res Soc* 32:100, 2007.

Gratz KR, Wong BL, Bae WC, Sah RL: Focal articular defects modify cartilage contact mechanics. *Proc 25th SPRBM Conf*, in *MCB* 3:199-200, 2006.

Wong BL, Bae WC, Chun J, Gratz KR, Sah RL: Lubricating effect of synovial fluid on cartilage biomechanics during articulation. *BMES*, 2006.

Lee JJ, Lewis CW, Chen AC, Bae WC, Wong BL, Sah RL: Effect of inhomogeneity and boudary conditions during confined compression testing of articular cartilage. *Trans Orthop Res Soc* 31:1493, 2006.

Wong BL, Bae WC, Sah RL: Accelerated stress-relaxation of cartilage due to chondral defects and subchondral bone plate perforation. *Trans Orthop Res Soc* 31:1497, 2006.

ABSTRACT OF THE DISSERTATION

BIOMECHANICS OF CARTILAGE ARTICULATION:
EFFECT OF LUBRICATION, DEGENERATION, AND
FOCAL ARTICULAR DEFECTS

by

Benjamin L. Wong

Doctor of Philosophy in Bioengineering
University of California, San Diego, 2009
Professor Robert L. Sah, Chair

During knee movement, cartilage surfaces, which are lubricated with synovial fluid (SF), contact, compress, and slide relative to each other to facilitate joint motion. However, the mechanical behavior of cartilage during joint loading remains unclear. Surface degeneration, altered SF function, and focal articular defects are common following joint injury and may markedly alter the mechanical deformation of cartilage during joint motion. Changes in cartilage mechanics due to such factors may make cartilage more susceptible to further degeneration and wear, predisposing the joint to osteoarthritis. Thus, the goal of this dissertation was to further the understanding of cartilage mechanics under normal and pathologic conditions during joint loading, by

elucidating the cartilage deformation during cartilage-on-cartilage articulation as well as the effects of degeneration, lubrication, and focal defects.

An experimental approach was developed that allowed the *in vitro* compression and relative sliding of apposing cartilage surfaces while resultant tissue deformation was imaged at a microscopic level. During cartilage-on-cartilage articulation, cartilage shear deformation varied with tissue depth, elevated with tissue degeneration, and was relatively lower with normal SF lubrication than saline. Shear kinematic studies indicated SF reduced peak shear by allowing surfaces to slide sooner. During tibio-femoral cartilage articulation, axial and shear strains were markedly higher in tibial cartilage than femoral cartilage, being reflective of their respective moduli. Also during tibio-femoral cartilage articulation, acute injury impairs SF function as indicated by elevated shear deformation, while hyaluronan (HA) supplementation partially restores SF function as indicated by reducing resultant shear strains towards normal magnitudes. Finally, tests of patello-femoral cartilage articulation with and without a focal defect showed cartilage strains were drastically elevated in cartilage adjacent to, and lowered in cartilage in direct apposition of, a focal defect following lateral motion.

Collectively, this work has further elucidated the contact mechanics of cartilage during joint movement in normal health and following acute injury or trauma. Such characterization may be beneficial to tissue engineering applications, such as engineering implantable cartilage constructs, as well as the development of treatments that address mechanically induced cartilage degeneration and wear.

CHAPTER 1

INTRODUCTION

1.1 General Introduction to the Dissertation

Articular cartilage covers the ends of all long bones and functions normally to provide a load-bearing, low-friction, wear-resistant surface so that diarthroidal joints articulate smoothly. Synovial fluid (SF) is present within articular joints and supplements articulation by reducing surface friction and wear [85]. During joint movement, cartilage surfaces contact, compress, and slide relative to each other, being subjected to both compressive and shear loads [60]. While cartilage deformation under compression alone has been investigated previously [62, 75], the deformation of cartilage during compression *and* shear remains to be elucidated.

Unfortunately, cartilage degeneration [15], altered synovial fluid function [26, 39], and focal defects [23, 32] are common, especially in the knee. If left untreated, such articular maladies are thought to lead to cartilage degeneration and wear, eventually progressing to osteoarthritis [15]. Since articular cartilage provides a mechanical function, biomechanical factors have been thought to contribute to the progressive nature of cartilage degeneration. Thus, quantification of the effects of such pathologically relevant factors on cartilage deformation during compression and shear

could provide insights into how associated changes in tissue mechanics during joint loading contribute to cartilage degeneration and the pathogenesis of osteoarthritis.

Therefore, the overall goal of this dissertation work was to further the understanding of cartilage contact mechanics during joint movement by characterizing the tissue deformation during cartilage-on-cartilage articulation (i.e. compression and relative sliding), and how pathologically relevant factors alter it by assessing the effects of degeneration, lubrication, and focal articular defects. To achieve this goal, (1) the peak shear deformation of cartilage and the effects of mild surface degeneration and SF lubrication were characterized in a simplified *in vitro* model of cartilage-on-cartilage articulation, (2) extending upon the previous aim, the shear kinematics of cartilage and the effects of mild degeneration, SF lubrication, and stress relaxation were then determined, (3) the deformation, and associated cartilage properties, of tibial and femoral cartilage were determined during tibio-femoral cartilage articulation, (4) the effects of acute injury on SF function, as indicated by shear deformation, and the ability of hyaluronan (HA) to restore SF function were assessed, and (5) the deformation of cartilage near and in direct apposition of a focal defect were experimentally determined.

This work has furthered the understanding of cartilage mechanics during joint movement in health and injury as well as provides insight into how changes in mechanical deformation may contribute to cartilage degeneration. Specifically, it provides motivation for, and contributes to the development of, treatments that directly address the abnormal tissue deformation that results from degeneration, altered SF lubrication, and a focal defect during joint articulation.

This chapter begins with a review of cartilage of the biomechanical demands and deformation of articular cartilage. This is followed by a discussion of cartilage degeneration, lubrication, and focal defects and how such factors may affect cartilage deformation during joint movement. Furthermore, the variables of cartilage shear strain, mechanobiology of cartilage, and *in vitro* testing systems for cartilage mechanics are reviewed. Finally, the significance of studying cartilage mechanics during articulation and characterizing the effects of pathologically relevant factors are discussed and summarized.

Chapter 2, which is published in *Arthritis and Rheumatism* [94], describes the shear deformation of cartilage during cartilage-on-cartilage articulation and assesses the effects of mild degeneration and SF lubrication. The study quantified the peak local and overall shear strains in normal and mildly degenerated cartilage, with saline and SF as lubricant, following compression and relative sliding.

While cartilage shear was elucidated at a time when strains were at a peak and surfaces were sliding, cartilage shear kinematics (i.e. during applied lateral motion) would further elucidate the mechanics of cartilage during articulation.

Thus in Chapter 3, which is published in *Molecular and Cellular Biomechanics* [95], the shear deformation kinetics of cartilage-on-cartilage articulation and the effects of degeneration, SF lubrication, and stress relaxation were characterized, building upon the findings of Chapter 2. Cartilage shear strains were determined *during* applied lateral motion for normal and mildly degenerated cartilage, with saline and SF as lubricant, after 5 and 60 minutes of stress relaxation.

Previous studies in Chapters 2 and 3 examined articulation mechanics with a simplified geometry, with apposing cartilage samples being from the femoral condyle. Thus, Chapter 4, which has been submitted to the *Journal of Biomechanics*, investigated the cartilage mechanics (deformation and tissue properties) in a configuration that was more physiologically relevant, with tibial cartilage in articulation with femoral cartilage. Cartilage compressive and shear strains, as well as their moduli, were determined for both tibial and femoral cartilage during articulation.

Chapter 5 builds upon the findings of the previous chapters by specifically investigating the effect of acute injury on SF function and the ability of HA to restore SF function, as indicated by resultant shear deformation during tibio-femoral cartilage articulation. Tibial cartilage was apposed and slid against femoral cartilage in SF from normal joints, the contra-lateral acutely-injured joints (AI-SF), and AI-SF supplemented with HA. Resultant shear strains in both tibial and femoral cartilage were determined.

Chapter 6 assesses the deformation of cartilage near and in direct apposition of a focal defect during patello-femoral cartilage articulation. Trochlear cartilage was apposed and slide against patellar cartilage with an intact surface and then with a focal defect. Shear, axial, and lateral strains were determined in both apposing cartilage tissues.

Finally, Chapter 7 summarizes the major findings of each study and discusses reviews the future directions of this work.

1.2 Composition and Structure of Articular Cartilage

Normal articular cartilage is a connective tissue that is composed of a sparse population of chondrocytes encased in a fluid filled extracellular matrix (ECM). Articular cartilage is mainly comprised of fluid, with 65-80% of its wet weight being attributed to interstitial fluid and electrolytes. The remaining solid components of cartilage consist of mostly collagen (10-20% of wet weight) and proteoglycans (5-10% of the wet weight) [14, 46-48, 60, 61]. The composition of articular cartilage being of both solid and fluid gives rise to its mechanical properties. Proteoglycans can maintain hydration even under considerably high loads due to the high osmotic pressure generated by its high density of negatively charged groups [46, 47, 50, 87]. The osmotic pressure also provides resistance to compression. In turn, the collagen network withstands the swelling pressure generated by the proteoglycans and the high tensile loads that occur during joint articulation [46]. The intricate balance between the fluid and solid components of cartilage is critical to maintain for normal cartilage function.

The cellular organization and matrix structure of mature articular cartilage varies with increasing tissue depth from the articular surface. Cartilage is typically categorized as having three distinct zones that are aligned parallel to the surface: superficial, middle, and deep [34]. In the superficial zone, cartilage is populated with a relatively high density of chondrocytes that have a flattened morphology [34, 84] (Figure 1.1). In the middle zone, chondrocytes exhibit a spherical morphology and are

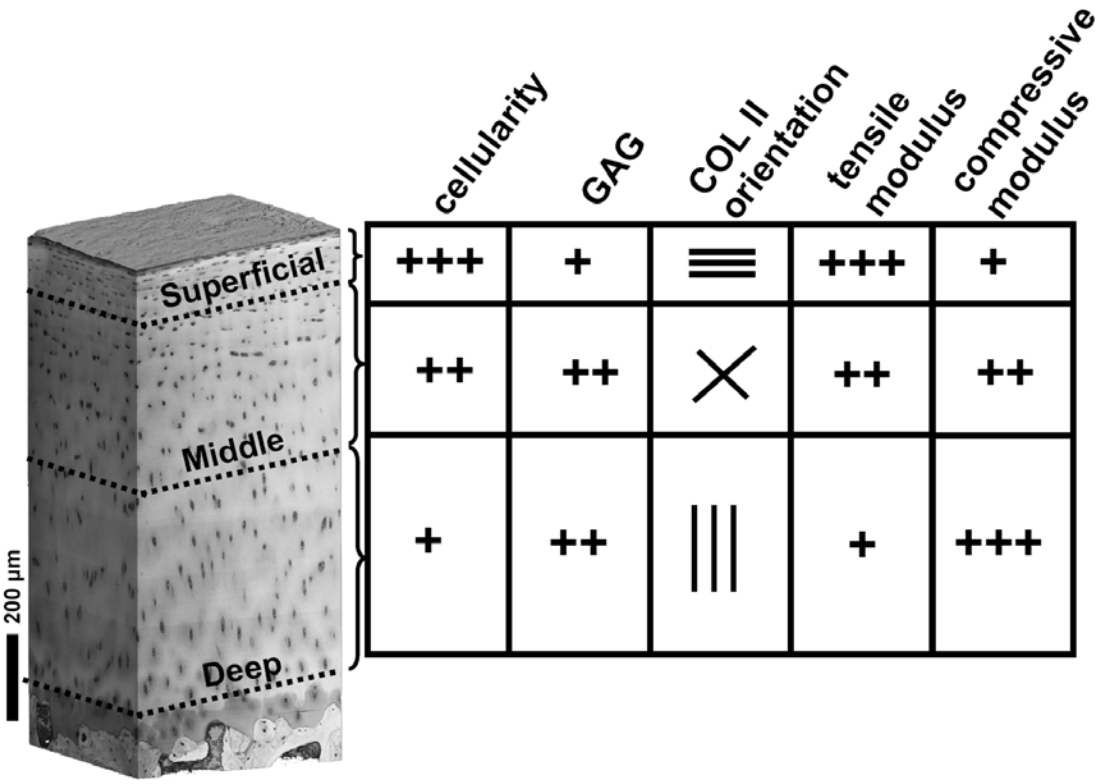

Figure 1.1: The structure, composition, and function of articular cartilage is inhomogeneous and vary between the superficial, middle, and deep regions.

less densely populated. In the deep zone, chondrocytes display an oblong morphology and are arranged in vertical columns. Collagen in the superficial zone is arranged tangential to the articular surface and transitions to an oblique and radial orientation in the middle and deep zones, respectively [21, 54, 73, 92]. Proteoglycan content is relatively low near the surface and increases with increasing depth from the articular surface [49]. Such zonal variations in composition and structure give rise to depth-dependent mechanical properties of cartilage.

1.3 Biomechanical Demands and Deformation of Articular Cartilage

Articular cartilage is subjected to repeated bouts of compressive and shear load during normal activities. Individuals typically take ~1-4 million steps each year,[80] with their joints being subjected to periods of rest and motion (Figure 1.2A). In the knee, the distal femur contacts, rolls, and slides across the tibial plateau during ~60% of the walking cycle [59], with a contact area ranging between 3-4 cm^2 during knee flexion [66] (Figure 1.2D). At heel-strike, joint loads can reach 3 times the body weight [2, 58] and create contact stresses between 1-18 MPa [1, 10, 13, 56] (Figure 1.2C). Joint surfaces also slide across one another, at relative velocities of 0-0.2 m/s and ±0.3 m/s for stance and swing phases, respectively (Figure 1.2B). Thus, throughout a person's lifetime, articular cartilage endures a high biomechanical demand, in both compression and shear.

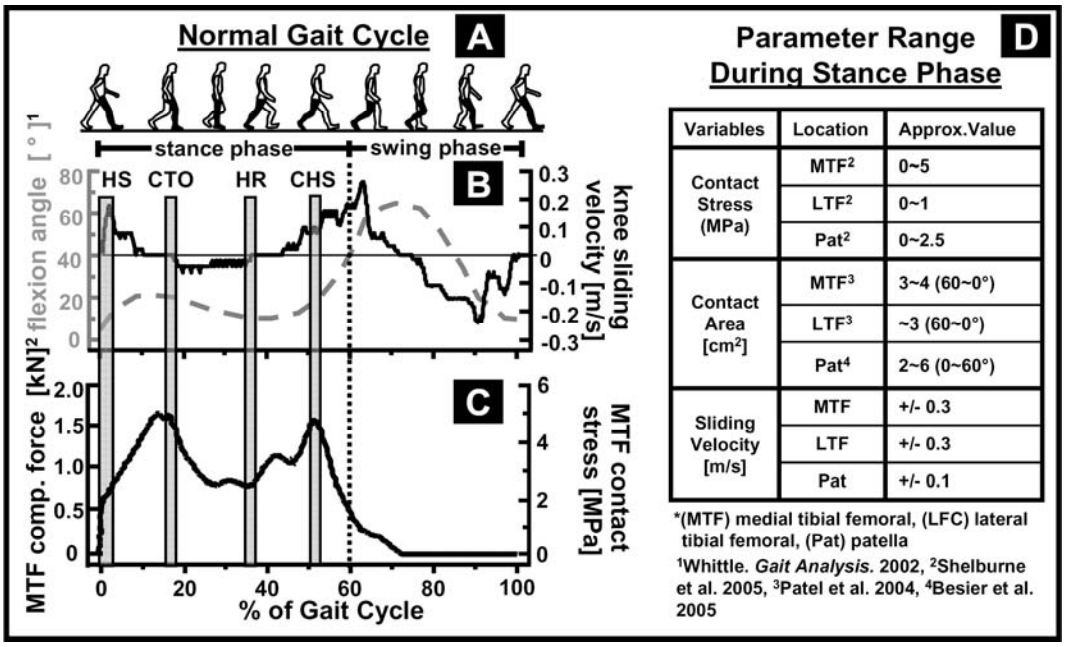

Figure 1.2: Features of normal gait cycle. **(A)** Schematic of stance and swing phases for right leg. **(B)** Knee flexion angle (– –) and sliding velocity (—) values. **(C)** Medial femoral-tibial compressive forces and estimated contact stresses during gait. Indicated are heel strike (HS), contralateral toe-off (CTO), heel rise (HR), and contralateral heel strike (CHS). **(D)** Knee parameters during stance phase.

Under such physiologic loads, cartilage deforms and exhibits a depth-varying magnitude of deformation. Following repeated knee bending [25], impact loading [88], and running [41], articular cartilage is compressed by ~3-20% of its overall thickness. Within statically [75] and dynamically compressed [62] cartilage, the magnitude of compressive strain is highest near the articular surface and minimal in deeper regions, a pattern consistent with the depth-varying compressive stiffness of cartilage [74]. Despite extensive knowledge of cartilage compressive behavior, the overall and depth-varying deformation of cartilage that may result during articulation remains to be elucidated.

Characterization of the mechanical deformation of cartilage during compression and shear would provide novel and critical information on cartilage contact mechanics. Theoretical models of articulating joints predict local cartilage deformation [5, 85], but are highly dependent on assumptions about boundary conditions at articulating surfaces (e.g., friction-less or adherent) and depth-varying mechanical properties [5]. Detailed experimental characterization of apposing cartilage samples sliding relative to each other would further the understanding of cartilage mechanics during joint movement by elucidating both the actual boundary condition at the articulating cartilage surface and the deformation and properties of cartilage in shear.

1.4 Surface Fibrillation & Roughening of Articular Cartilage

Articular cartilage often deteriorates with aging [22] and progresses to complete tissue degeneration and osteoarthritis (OA) [15]. As cartilage undergoes

degeneration, articular surfaces become fibrillated and roughened, as revealed by an increase in India-ink staining [53]. As tissue degeneration progresses, chondral fibrillation and lesions deepen into the tissue and causes cartilage loss. With continued joint loading and time, cartilage eventually erodes down further, exposing the underlying subchondral bone [15] (Figure 1.3). Such a progression of tissue degeneration characteristic in OA can be quite debilitating and painful.

Degeneration of articular cartilage confined to the articular surface may affect the way in which cartilage deforms and functions during joint movement. Roughened surfaces have local asperities that can cause surfaces to adhere slightly longer, increasing friction during sliding, and result in increased deformation. Concomitantly, cartilage degeneration is accompanied by a reduction in overall mechanical integrity during compressive, tensile, and shear loading, [81] i.e., an increase in cartilage deformation and strain magnitude in response to a particular amplitude of applied load. The altered surface topography along with changes in mechanical stiffness associated with tissue degeneration may markedly alter the mechanical behavior of cartilage during joint loading.

Depending on magnitude, cartilage deformation may either stimulate or inhibit chondrocyte metabolism and matrix synthesis. When subjected to excessive levels of compression [42] and shear [68], matrix synthesis of cartilage is inhibited. On the

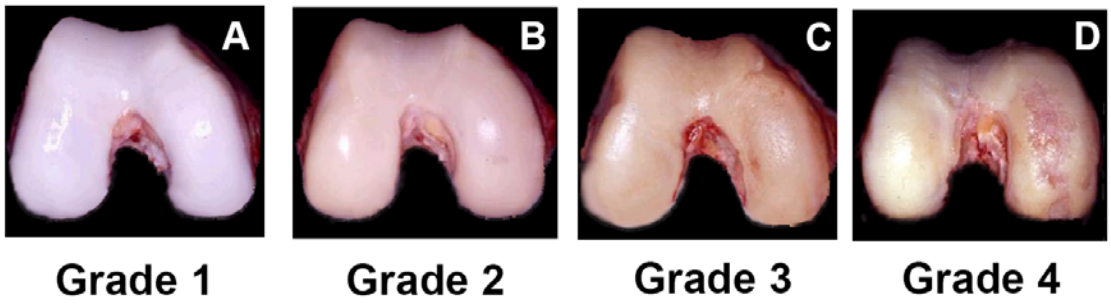

Figure 1.3: Macroscopic images of the distal femur with cartilage that is normal (**A**), mildly fibrillated (**B**), overtly fibrillated (**C**), and eroded down to the cartilage erosion (**D**). Corresponding grades are based on the Noyes grading scheme [63].

other hand, moderate levels of compression [70] and shear [27] stimulate matrix synthsis. Thus, determination of the deformation and strain of articulating cartilage, both with normal and degenerate surfaces, would provide insight into the local mechanical cues that regulate chondrocyte behavior and the consequences of degenerative changes on such cues.

1.5 Lubrication of Articular Cartilage

In healthy joints, synovial fluid (SF) is present between articulating cartilage surfaces and facilitates joint movement by functioning as an effective boundary lubricant. In boundary mode lubrication, load across articular surfaces is supported by direct surface to surface contact, and friction is dependent upon bound lubricant molecules at the surface. In a configuration to reveal boundary lubrication effects, the surface interaction, as indicated by friction [77, 78], is reduced by SF relative to interactions with phosphate buffered saline (PBS). Physiologically, boundary lubrication is relevant because articulating cartilage layers are in direct contact ~10% of the total area [57]. Friction is likely highest in these regions and becomes increasingly dominated by surface boundary lubricant molecules with loading time and dissipation of hydrostatic pressure [52, 55], which increases contact area. Since lubrication of cartilage by SF modulates friction between surfaces, cartilage deformation during articulation is also likely dependent upon the presence of surface lubricants.

The main constituents of SF interact and absorb to the articular surface to reduce cartilage friction during articulation. The main lubricant molecules identified to

contribute to boundary lubrication of cartilage include hyaluronan (HA) [64], proteoglycan 4 (PRG4) [38, 79], and surface-active phospholipids (SAPLs) [72]. The SF lubricant molecules, PRG4 and HA, contribute, both independently and in combination, to reducing articulating cartilage friction under boundary lubrication conditions [77]. Furthermore, effects are dose-dependent. Thus, the boundary lubrication function of SF depends upon the concentrations of lubricant molecules, and if altered, may have marked effects on cartilage deformation during articulation.

With injury and disease, the concentrations of lubricant molecules HA, PRG4, and SAPL can become altered. In acutely injured equine joints, HA concentration decreases markedly (~0.3 mg/ml to 0.2 mg/ml), while PRG4 concentration increases (~4 times) compared to SF from the contra-lateral normal joints [3]. In human joints, HA concentration decreases from 1-4 mg/ml in healthy joints [8, 19, 51, 91] to ~0.1-1.3 mg/ml in arthritic disease[24, 51]. For patients undergoing arthrocentesis procedures, PRG4 concentrations are elevated ~2-5-fold compared to post-mortem joints [76]. Concentrations of phospholipids in human SF increase ~1.5-2-fold with osteoarthritis [51] and decrease ~2-fold following acute injury [67]. Collectively, such results suggest changes in lubricant molecule concentrations may be dependent upon the type of injury and severity of disease.

1.6 Focal Defects in Articular Cartilage

Once thought to be rare [33], focal cartilage defects are prevalent in the knee and associated with accelerating cartilage degeneration. In patients evaluated

arthroscopically, focal defects were found in 20-60% of all symptomatic knees and ranged in size from 0.5 to 4 cm^2 in area [4, 23, 32, 93]. The average area of the defects was 2.1 cm^2, and the lesions extended beyond half the cartilage thickness in depth in 50% of all diagnosed articular defects [32]. With time and joint loading, a focal defect generally enlarges [90], deepens [35, 36], and accelerates cartilage loss [20]. Fibrillation [37, 43], hypocellularity [43], and loss of safranin-O staining [43] occur in tissue adjacent to focal defects (Figure 1.4). Despite the prevalence of focal defects and their tendency to worsen with time, few studies have investigated the effects of a focal defect on cartilage mechanics and deformation.

With the presence of a focal articular defect, cartilage mechanics markedly change during compressive loading. Under compression alone, cartilage geometry and contact between apposing surfaces are altered with the presence of a focal defect [9, 11]. Consequently, contact stress and stress gradients are significantly elevated in the tissue near the edges of the defect [12, 31]. Such elevations in stress translate to increases in macroscopic tissue deformation [11] and local strains [29] [30] in these regions. While marked changes in cartilage mechanics occur under compression alone, joint articulation involves both compression and lateral motion, and further changes in cartilage mechanics could occur during lateral motion. Characterization of the effects of a focal defect on cartilage deformation during articulation would further the understanding of focal defect cartilage mechanics and elucidate the role of mechanical strain in cartilage degeneration associated with focal defects.

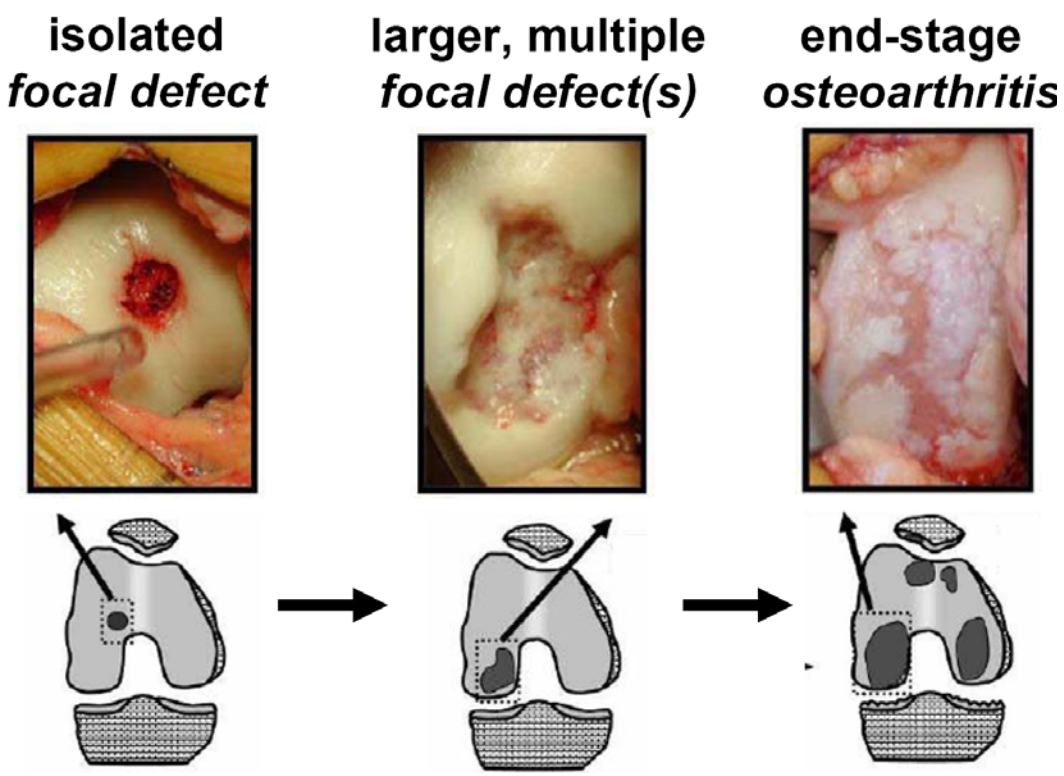

Figure 1.4: Macroscopic images displaying the enlargement of a focal articular defect and progressing to end-stage osteoarthritis.

1.7 Modulators of Shear Strain

Since shear forces are likely high during lateral articulation, shear deformation of cartilage is likely initiated, and the magnitudes of shear strain are dependent upon mechanical parameters. Modeling cartilage as a homogeneous, isotropic, and elastic tissue, the magnitude of shear deformation can be related to contact and tissue properties. The following inter-related equations are considered: equation 1 relating shear modulus (G) to 2nd Piola-Kirchhoff shear stress (S_{xz}) and overall Lagrangian shear strain (E_{xz}), which are measures of finite stress and deformation., and equation 2 relating S_{xz} needed to induce surfaces to slide to coefficient of friction (μ) and 2nd Piola-Kirchhoff normal contact stress (S_n) .[28]

$$G = \frac{S_{xz}}{2E_{xz}} \qquad \text{(Eqn. 1)}$$

$$S_{xz} = \mu S_n \qquad \text{(Eqn. 2)}$$

By combing equations 1 and 2, equation 3 is obtained that relates the overall shear strain when surfaces are sliding to μ, S_n, and G.

$$E_{xz} = \frac{\mu S_n}{G} \qquad \text{(Eqn. 3)}$$

Based on equation 3, shear strain at a time when surfaces are sliding is dependent and modulated by friction, contact stress, and shear modulus. Since boundary lubricants modulate friction,[78] lubrication of cartilage would likely modulate cartilage shear strain through such a mechanism. Similarly, surface degeneration and focal defects likely affect shear strain by modulating shear modulus

and contact stress, respectively. Thus by investigating how surface degeneration, deficient lubrication, and focal defects affect cartilage shear strain, the effect of mechanical parameters friction, shear modulus, and contact stress on cartilage shear deformation can be elucidated.

1.8 *In Vitro* Testing Systems for Cartilage Mechanics

Certain mechanical features of joint articulation can be mimicked and translated to an *in vitro* testing system to elucidate intra-tissue deformation and strain. The load-bearing, sliding, and rolling motion of articulating cartilage surfaces presents a challenging tribological system to test experimentally and model theoretically [6, 82, 85]. Local and bulk compressive properties of cartilage have been investigated with confined [18, 74] and unconfined [89] compression of cartilage explants to give insight into the compressive properties and behavior of cartilage during articulation. Additionally, cartilage-on-cartilage testing configurations that are analogous to contacting cartilage surfaces in the joint have been utilized to determine frictional properties of cartilage lubricants [78]. During joint articulation, cartilage contacts, compresses, and slides relative to an apposing cartilage surface, being subjected to compressive and shear loads. As a result, cartilage articulation is mainly comprised of compression and shear of apposing cartilage surfaces. Thus, combining previously used experimental setups, important mechanical components of cartilage articulation can be tested and modeled *in vitro*. By subjecting contacting cartilage explants to both

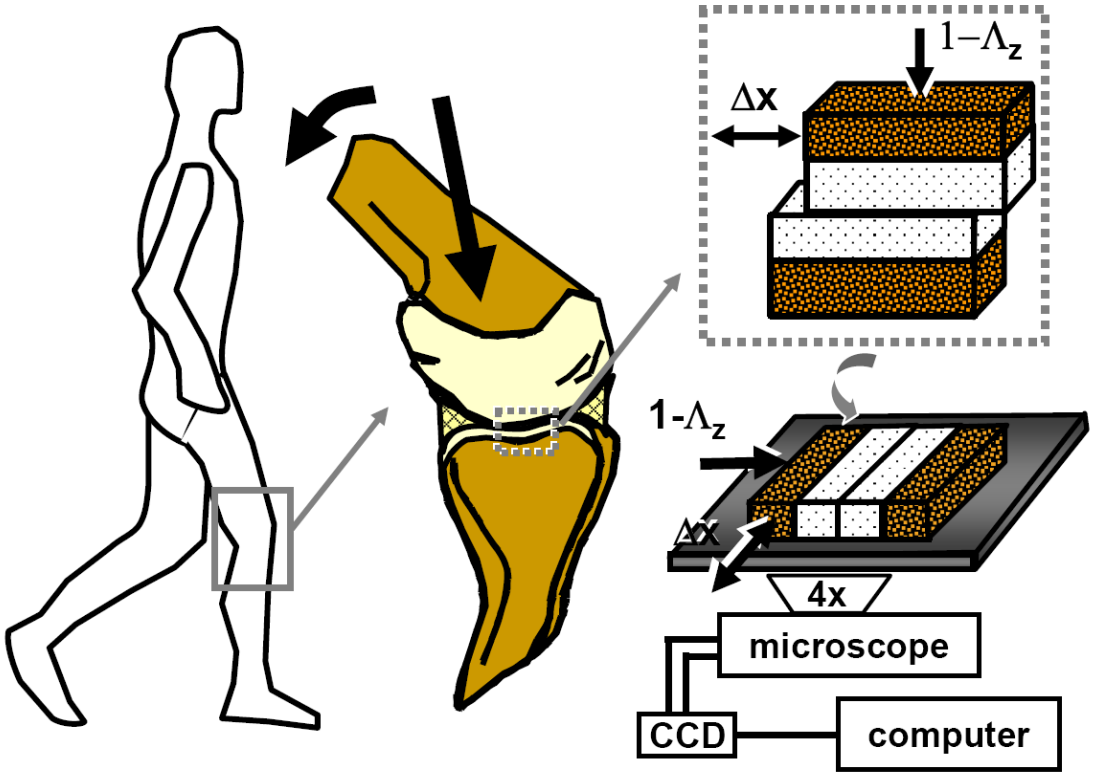

Figure 1.5: Schematic of joint articulation and an *in vitro* mechanical testing system that mimics the compression and lateral sliding of articular cartilage surfaces that occurs during joint articulation.

compression and shear, and visualizing tissue deformation, important aspects of joint articulation can be mimicked (Figure 1.5), and insight into the cartilage deformation during joint articulation may be obtained.

1.9 Mechanobiology of Cartilage

Investigation of cartilage mechanics and the factors that alter it are important because magnitudes of cartilage deformation affect tissue health. Moderate levels of dynamic compression and shear, individually, promote matrix synthesis [40, 70], while dynamic shear also stimulates proteoglycan 4 (PRG4) secretion [65], a surface lubricant molecule. Yet, excessive levels of compressive [42, 44] and shear strain have injurious effects, causing reduced matrix synthesis[83], matrix damage, and cell death [17]. Overall compressive strains of 50% or greater induce cell death near the surface, where local compressive strains are even greater [86]. However, such magnitudes of overall compression are not physiologic and unlikely to occur even in the pathologic state. After relatively low indentation amplitudes, on the other hand, cell death was associated with areas of high local shear strain [7], suggesting elevated localized strains may induce cell death even under physiologic levels of compression and contribute to cartilage degeneration and wear.

1.10 Summary and Significance

Despite the tendency of cartilage to progressively degenerate with time after injury, few studies have investigated cartilage mechanics and deformation under

pathologic conditions. Cartilage deformation likely elevates with deficient lubrication, surface degeneration, and focal defects. To what extent deformation elevates to, and what consequences pathologic deformation has on tissue metabolism and structure remain unknown. Excessive deformation that results in pathologic conditions may contribute to the progressive degeneration of cartilage following injury. Thus, it is important clinically to elucidate the changes in joint contact mechanics that result from such conditions and determine whether such biomechanical changes initiate degeneration. Using this information, clinically-applicable repair strategies may be designed to specifically inhibit the mechanical factors causing degeneration.

Articular cartilage has a limited capacity for intrinsic repair and thus is likely susceptible to osteoarthritis (OA) if injured [45]. This debilitating joint disease is characterized by the progressive degeneration of cartilage and the eventual exposure of the underlying bone as the disease advances. In end-stage OA, large regions of bone to bone contact occur, which can be quite crippling and painful [14]. Osteoarthritis affects ~20 million Americans and causes a substantial economic impact of $60 billion annually [16]. The limited healing capacity of cartilage and the prevalence of OA have motivated a great deal of research into methods of cartilage repair and regeneration [69, 71]. Thus, studies to understand the mechanisms and pathogenesis of cartilage degeneration are clinically important and necessary for the development of such treatments.

1.11 References

1. Ahmed AM, Burke DL: In-vitro measurement of static pressure distribution in synovial joints--part I: tibial surface of the knee. *J Biomech Eng* 105:216-25, 1983.

2. Andriacchi TP, Natarajan RN, Hurwitz DE: Musculoskeletal dynamics, locomotion, and clinical applications. In: *Basic Orthopaedic Biomechanics,* ed. by VC Mow, Hayes WC, Raven Press, New York, 1997, 37-68.

3. Antonacci JM, Ballard BL, Schumacher BL, Sah RL: Role of hyaluronan in bovine synovial fluid in the boundary lubricating of articular cartilage. *Trans Orthop Res Soc* 33:625, 2008.

4. Aroen A, Loken S, Heir S, Alvik E, Ekeland A, Granlund OG, Engebretsen L: Articular cartilage lesions in 993 consecutive knee arthroscopies. *Am J Sports Med* 32:211-5, 2004.

5. Ateshian GA, Lai WM, Zhu WB, Mow VC: An asymptotic solution for the contact of two biphasic cartilage layers. *J Biomech* 27:1347-60, 1994.

6. Ateshian GA, Mow VC: Friction, lubrication, and wear of articular cartilage and diarthrodial joints. In: *Basic Orthopaedic Biomechanics and Mechano-Biology,* ed. by VC Mow, Huiskes R, Lippincott Williams & Wilkins, Philadelphia, 2005, 447-94.

7. Bae WC, Schumacher BL, Sah RL: Indentation probing of human articular cartilage: effect on chondrocyte viability. *Osteoarthritis Cartilage* 15:9-18, 2007.

8. Balazs EA: The physical properties of synovial fluid and the special role of hyaluronic acid. In: *Disorders of the Knee,* ed. by AJ Helfet, Lippincott Co., Philadelphia, 1974, 63-75.

9. Balint L, Park SH, Bellyei A, Luck JV, Jr., Sarmiento A, Lovasz G: Repair of steps and gaps in articular fracture models. *Clin Orthop Relat Res* 430:208-18, 2005.

10. Barker MK, Seedhom BB: The relationship of the compressive modulus of articular cartilage with its deformation response to cyclic loading: does cartilage optimize its modulus so as to minimize the strains arising in it due to prevalent loading regime? *Rheumatology* 40:274-84, 2001.

11. Braman JP, Bruckner JD, Clark JM, Norman AG, Chansky HA: Articular cartilage adjacent to experimental defects is subject to atypical strains. *Clin Orthop Relat Res* 430:202-7, 2005.

12. Brown TD, Pope DF, Hale JE, Buckwalter JA, Brand RA: Effects of osteochondral defect size on cartilage contact stress. *J Orthop Res* 9:559-67, 1991.

13. Brown TD, Shaw DT: In vitro contact stress distributions in the natural human hip. *J Biomech* 16:373-84, 1983.

14. Buckwalter JA, Mankin HJ: Articular cartilage. Part I: tissue design and chondrocyte-matrix interactions. *J Bone Joint Surg Am* 79-A:600-11, 1997.

15. Buckwalter JA, Mankin HJ: Articular cartilage. Part II: degeneration and osteoarthrosis, repair, regeneration, and transplantation. *J Bone Joint Surg Am* 79-A:612-32, 1997.

16. Buckwalter JA, Saltzman C, Brown T: The impact of osteoarthritis: implications for research. *Clin Orthop Rel Res Relat Res*:S6-15, 2004.

17. Chen CT, Burton-Wurster N, Lust G, Bank RA, Tekoppele JM: Compositional and metabolic changes in damaged cartilage are peak-stress, stress-rate, and loading-duration dependent. *J Orthop Res* 17:870-9, 1999.

18. Chen SS, Falcovitz YH, Schneiderman R, Maroudas A, Sah RL: Depth-dependent compressive properties of normal aged human femoral head articular cartilage: relationship to fixed charge density. *Osteoarthritis Cartilage* 9:561-9, 2001.

19. Chmiel IH, Walitza E. On the Rehology of Blood and Synovial Fluids. New York: Research Studies Press; 1980.

20. Cicuttini F, Ding C, Wluka A, Davis S, Ebeling PR, Jones G: Association of cartilage defects with loss of knee cartilage in healthy, middle-age adults: a prospective study. *Arthritis Rheum* 52:2033-9, 2005.

21. Clark JM: Variation of collagen fiber alignment in a joint surface: a scanning electron microscope study of the tibial plateau in dog, rabbit, and man. *J Orthop Res* 9:246-57, 1991.

22. Clark JM, Simonian PT: Scanning electron microscopy of "fibrillated" and "malacic" human articular cartilage: technical considerations. *Microsc Res Tech* 37:299-313, 1997.

23. Curl WW, Krome J, Gordon ES, Rushing J, Smith BP, Poehling GG: Cartilage injuries: a review of 31,516 knee arthroscopies. *Arthroscopy* 13:456-60, 1997.

24. Dahl LB, Dahl IM, Engstrom-Laurent A, Granath K: Concentration and molecular weight of sodium hyaluronate in synovial fluid from patients with rheumatoid arthritis and other arthropathies. *Ann Rheum Dis* 44:817-22, 1985.

25. Eckstein F, Lemberger B, Stammberger T, Englmeier KH, Reiser M: Patellar cartilage deformation in vivo after static versus dynamic loading. *J Biomech* 33:819-25, 2000.

26. Elsaid KA, Jay GD, Warman ML, Rhee DK, Chichester CO: Association of articular cartilage degradation and loss of boundary-lubricating ability of synovial fluid following injury and inflammatory arthritis. *Arthritis Rheum* 52:1746-55, 2005.

27. Fitzgerald JB, Jin M, Grodzinsky AJ: Shear and compression differentially regulate clusters of functionally related temporal transcription patterns in cartilage tissue. *J Biol Chem* 281:24095-103, 2006.

28. Fung YC. A First Course in Continuum Mechanics. 2nd ed. Englewood Cliffs: Prentice-Hall; 1977.

29. Gratz KR, Wong BL, Bae WC, Sah RL: The effects of focal articular defects on intra-tissue strains in the surrounding and opposing cartilage. *Biorheology* 45:193-207, 2008.

30. Gratz KR, Wong BL, Bae WC, Sah RL: The effects of focal articular defects on cartilage contact mechanics. *J Orthop Res* 27:584-92, 2009.

31. Guettler JH, Demetropoulos CK, Yang KH, Jurist KA: Osteochondral defects in the human knee: influence of defect size on cartilage rim stress and load redistribution to surrounding cartilage. *Am J Sports Med* 32:1451-8, 2004.

32. Hjelle K, Solheim E, Strand T, Muri R, Brittberg M: Articular cartilage defects in 1,000 knee arthroscopies. *Arthroscopy* 18:730-4, 2002.

33. Hopkinson WJ, Mitchell WA, Curl WW: Chondral fractures of the knee. Cause for confusion. *Am J Sports Med* 13:309-12, 1985.

34. Hunziker EB: Articular cartilage structure in humans and experimental animals. In: *Articular Cartilage and Osteoarthritis,* ed. by KE Kuettner, Schleyerbach R, Peyron JG, Hascall VC, Raven Press, New York, 1992, 183-99.

35. Hunziker EB: Growth-factor induced healing of partial-thickness defects in adult articular cartilage. *Osteoarthritis Cartilage* 9:22-32, 2001.

36. Hunziker EB, Rosenberg LC: Repair of partial-thickness defects in articular cartilage: Cell recruitment from the synovial membrane. *J Bone Joint Surg Am* 78-A:721-33, 1996.

37. Jackson DW, Lalor PA, Aberman HM, Simon TM: Spontaneous repair of full-thickness defects of articular cartilage in a goat model. A preliminary study. *J Bone Joint Surg Am* 83-A:53-64, 2001.

38. Jay GD: Lubricin and surfacing of articular joints. *Curr Opin Orthop* 15:355-9, 2004.

39. Jay GD, Elsaid KA, Zack J, Robinson K, Trespalacios F, Cha CJ, Chichester CO: Lubricating ability of aspirated synovial fluid from emergency department patients with knee joint synovitis. *J Rheumatol* 31:557-64, 2004.

40. Jin M, Frank EH, Quinn TM, Hunziker EB, Grodzinsky AJ: Tissue shear deformation stimulates proteoglycan and protein biosynthesis in bovine cartilage explants. *Arch Biochem Biophys* 395:41-8, 2001.

41. Kersting UG, Stubendorff JJ, Schmidt MC, Bruggemann GP: Changes in knee cartilage volume and serum COMP concentration after running exercise. *Osteoarthritis Cartilage* 13:925-34, 2005.

42. Kurz B, Jin M, Patwari P, Cheng DM, Lark MW, Grodzinsky AJ: Biosynthetic response and mechanical properties of articular cartilage after injurious compression. *J Orthop Res* 19:1140-6, 2001.

43. Lefkoe TP, Trafton PG, Ehrlich MG, Walsh WR, Dennehy DT, Barrach HJ, Akelman E: An experimental model of femoral condylar defect leading to osteoarthrosis. *J Orthop Trauma* 7:458-67, 1993.

44. Loening A, Levenston M, James I, Nuttal M, Hung H, Gowen M, Grodzinsky A, Lark M: Injurious mechanical compression of bovine articular cartilage induces chondrocyte apoptosis. *Arch Biochem Biophys* 381:205-12, 2000.

45. Mankin HJ: The response of articular cartilage to mechanical injury. *J Bone Joint Surg Am* 64-A:460-6, 1982.

46. Maroudas A: Balance between swelling pressure and collagen tension in normal and degenerate cartilage. *Nature* 260:808-9, 1976.

47. Maroudas A: Physico-chemical properties of articular cartilage. In: *Adult Articular Cartilage,* ed. by MAR Freeman, Pitman Medical, Tunbridge Wells, England, 1979, 215-90.

48. Maroudas A, Bayliss MT, Venn MF: Further studies on the composition of human femoral head cartilage. *Ann Rheum Dis* 39:514-23, 1980.

49. Maroudas A, Venn M: Chemical composition and swelling of normal and osteoarthrotic femoral head cartilage. II. Swelling. *Ann Rheum Dis* 36:399-406, 1977.

50. Maroudas A, Wachtel E, Grushko G, Katz EP, Weinberg P: The effect of osmotic and mechanical pressures on water partitioning in articular cartilage. *Biochim Biophys Acta* 1073:285-94, 1991.

51. Mazzucco D, Scott R, Spector M: Composition of joint fluid in patients undergoing total knee replacement and revision arthroplasty: correlation with flow properties. *Biomaterials* 25:4433-45, 2004.

52. McCutchen CW: Boundary lubrication by synovial fluid: demonstration and possible osmotic explanation. *Fed Proceedings* 25:1061-8, 1966.

53. Meachim G, Emery IH: Quantitative aspects of patello-femoral cartilage fibrillation in Liverpool necropsies. *Ann Rheum Dis* 33:39-47, 1974.

54. Meachim G, Sheffield SR: Surface ultrastructure of mature adult human articular cartilage. *J Bone Joint Surg Br* 51-B:529-39, 1969.

55. Meyer E, Overney RM, Dransfeld K, Gyalog T. Nanoscience: Friction and Rheology on the Nanometer Scale. River Edge, New Jersey: World Scientific Publishing Co. Pte. Ltd; 2002.

56. Morell KC, Hodge WA, Krebs DE, Mann RW: Corroboration of in vivo cartilage pressures with implications for synovial joint tribology and osteoarthritis causation. *Proc Natl Acad Sci U S A* 102:14819-24, 2005.

57. Morrell KC, Hodge WA, Krebs DE, Mann RW: Corroboration of in vivo cartilage pressures with implications for synovial joint tribology and osteoarthritis causation. *Proc Natl Acad Sci U S A* 102:14819-24, 2005.

58. Morrison JB: Bioengineering analysis of force actions transmitted to the knee joint. *Biomed Eng* 3:164, 1968.

59. Mow VC, Ateshian GA: Lubrication and wear of diarthrodial joints. In: *Basic Orthopaedic Biomechanics,* ed. by VC Mow, Hayes WC, Raven Press, New York, 1997, 275-315.

60. Mow VC, Gu WY, Chen FH: Structure and Function of Articular Cartilage and Meniscus. In: *Basic Orthopaedic Biomechanics and Mechano-Biology,* ed. by VC Mow, Huiskes R, Lippincott Williams & Wilkins, Philadelphia, 2005, 720.

61. Muir IHM: Articular cartilage: biochemistry. In: *Adult Articular Cartilage,* ed. by MAR Freeman, Pitman Medical, Tunbridge Wells, England, 1979, 145-214.

62. Neu CP, Hull ML, Walton JH: Heterogeneous three-dimensional strain fields during unconfined cyclic compression in bovine articular cartilage explants. *J Orthop Res* 23:1390-8, 2005.

63. Noyes FR, Stabler CL: A system for grading articular cartilage lesions at arthroscopy. *Am J Sports Med* 17:505-13, 1989.

64. Noyori K, Takagi T, Jasin HE: Characterization of the macromolecular components of the articular cartilage surface. *Rheumatol Int* 18:71-7, 1998.

65. Nugent GE, Aneloski NM, Schmidt TA, Schumacher BL, Voegtline MS, Sah RL: Dynamic shear stimulation of bovine cartilage biosynthesis of proteoglycan 4 (PRG4). *Arthritis Rheum* 54:1888-96, 2006.

66. Patel VV, Hall K, Ries M, Lotz J, Ozhinsky E, Lindsey C, Lu Y, Majumdar S: A three-dimensional MRI analysis of knee kinematics. *J Orthop Res* 22:283-92, 2004.

67. Rabinowitz JL, Gregg JR, Nixon JE: Lipid composition of the tissues of human knee joints. II. Synovial fluid in trauma. *Clin Orthop Rel Res*:292-8, 1984.

68. Raimondi MT, Moretti M, Cioffi M, Giordano C, Boschetti F, Lagana K, Pietrabissa R: The effect of hydrodynamic shear on 3D engineered chondrocyte systems subject to direct perfusion. *Biorheology* 43:215-22, 2006.

69. Sah RL: Interface and bulk regions in the repair, regeneration, and replacement of articular cartilage. *J Musculoskelet Neuronal Interact* 4:393-5, 2004.

70. Sah RL, Kim YJ, Doong JH, Grodzinsky AJ, Plaas AHK, Sandy JD: Biosynthetic response of cartilage explants to dynamic compression. *J Orthop Res* 7:619-36, 1989.

71. Sah RL, Klein TJ, Schmidt TA, Albrecht DR, Bae WC, Nugent GE, McGowan KB, Temple MM, Jadin KD, Schumacher BL, Chen AC, Sandy JD: Articular cartilage repair, regeneration, and replacement. In: *Arthritis and Allied Conditions: A Textbook of Rheumatology,* ed. by WJ Koopman, Lippincott Williams & Wilkins, Philadelphia, 2005, 2277-301.

72. Sarma AV, Powell GL, LaBerge M: Phospholipid composition of articular cartilage boundary lubricant. *J Orthop Res* 19:671-6, 2001.

73. Schenk RK, Eggli PS, Hunziker EB: Articular cartilage morphology. In: *Articular Cartilage Biochemistry,* ed. by K Kuettner, Schleyerbach R, Hascall VC, Raven Press, New York, 1986, 3-22.

74. Schinagl RM, Gurskis D, Chen AC, Sah RL: Depth-dependent confined compression modulus of full-thickness bovine articular cartilage. *J Orthop Res* 15:499-506, 1997.

75. Schinagl RM, Ting MK, Price JH, Sah RL: Video microscopy to quantitate the inhomogeneous equilibrium strain within articular cartilage during confined compression. *Ann Biomed Eng* 24:500-12, 1996.

76. Schmid T, Lindley K, Su J, Soloveychik V, Block J, Kuettner K, Schumacher B: Superficial zone protein (SZP) is an abundant glycoprotein in human synovial fluid and serum. *Trans Orthop Res Soc* 26:82, 2001.

77. Schmidt TA, Gastelum NS, Nguyen QT, Schumacher BL, Sah RL: Boundary lubrication of articular cartilage: role of synovial fluid constituents. *Arthritis Rheum* 56:882-91, 2007.

78. Schmidt TA, Sah RL: Effect of synovial fluid on boundary lubrication of articular cartilage. *Osteoarthritis Cartilage* 15:35-47, 2007.

79. Schumacher BL, Block JA, Schmid TM, Aydelotte MB, Kuettner KE: A novel proteoglycan synthesized and secreted by chondrocytes of the superficial zone of articular cartilage. *Arch Biochem Biophys* 311:144-52, 1994.

80. Seedhom BB, Wallbridge NC: Walking activities and wear of prostheses. *Ann Rheum Dis* 44:838-43, 1985.

81. Setton LA, Elliott DM, Mow VC: Altered mechanics of cartilage with osteoarthritis: human osteoarthritis and an experimental model of joint degeneration. *Osteoarthritis and Cartilage* 7:2-14, 1999.

82. Stachowiak GW, Batchelor AW. Engineering Tribology. 3rd ed. Burlington: Elsevier Butterworth-Heinemann; 2005.

83. Steinmeyer J, Knue S: The proteoglycan metabolism of mature bovine articular cartilage explants superimposed to continuously applied cyclic mechanical loading. *Biochem Biophys Res Commun* 240:216-21, 1997.

84. Stockwell RA, Meachim G: The chondrocytes. In: *Adult Articular Cartilage,* ed. by MAR Freeman, Pitman Medical, Tunbridge Wells, England, 1979, 69-144.

85. Swanson SAV: Friction, wear, and lubrication. In: *Adult Articular Cartilage,* ed. by MAR Freeman, Pitman Medical, Tunbridge Wells, England, 1979, 415-60.

86. Torzilli PA, Deng XH, Ramcharan M: Effect of compressive strain on cell viability in statically loaded articular cartilage. *Biomech Model Mechanobiol* 5:123-32, 2006.

87. Urban JP, Maroudas A, Bayliss MT, Dillon J: Swelling of proteoglycans at the concentrations found in cartilaginous tissues. *Biorheology* 16:447-64, 1979.

88. Van de Velde SK, Bingham JT, Gill TJ, Li G: Analysis of tibiofemoral cartilage deformation in the posterior cruciate ligament-deficient knee. *J Bone Joint Surg Am* 91:167-75, 2009.

89. Wang CC, Deng JM, Ateshian GA, Hung CT: An automated approach for direct measurement of two-dimensional strain distributions within articular cartilage under unconfined compression. *J Biomech Eng* 124:557-67, 2002.

90. Wang Y, Ding C, Wluka AE, Davis S, Ebeling PR, Jones G, Cicuttini FM: Factors affecting progression of knee cartilage defects in normal subjects over 2 years. *Rheumatology (Oxford)* 45:79-84, 2006.

91. Watterson JR, Esdaile JM: Viscosupplementation: therapeutic mechanisms and clinical potential in osteoarthritis of the knee. *J Am Acad Orthop Surg* 8:277-84, 2000.

92. Weiss C, Rosenberg L, Helfet AJ: An ultrastructural study of normal young adult human articular cartilage. *J Bone Joint Surg Am* 50-A:663-74, 1968.

93. Widuchowski W, Widuchowski J, Trzaska T: Articular cartilage defects: study of 25,124 knee arthroscopies. *Knee* 14:177-82, 2007.

94. Wong BL, Bae WC, Chun J, Gratz KR, Sah RL: Biomechanics of cartilage articulation: effects of lubrication and degeneration on shear deformation. *Arthritis Rheum* 58:2065-74, 2008.

95. Wong BL, Bae WC, Gratz KR, Sah RL: Shear deformation kinematics during cartilage articulation: effect of lubrication, degeneration, and stress relaxation. *Mol Cell Biomech* 5:197-206, 2008.

CHAPTER 2

BIOMECHANICS OF CARTILAGE ARTICULATION: EFFECTS OF LUBRICATION AND DEGENERATION ON SHEAR DEFORMATION

2.1 Abstract

Objective: To elucidate cartilage shear strain during articulation and the effects of lubrication and degeneration.

Methods: Human osteochondral cores from lateral femoral condyles were selected based on surface structure as (1) normal or (2) mildly degenerate. Under video microscopy, pairs of osteochondral blocks from each core were apposed, compressed 15%, and subjected to relative lateral motion with synovial fluid (SF) or phosphate-buffered saline (PBS) as lubricant. When cartilage surfaces began to slide steadily, shear strain (E_{xz}) and modulus (G) were determined overall for the full tissue thickness and also as a function of depth from the surface.

Results: For normal tissue in SF, E_{xz} was highest (0.056) near the articular surface and diminished monotonically with depth, with an overall average E_{xz} of 0.028. For degenerate cartilage in SF, E_{xz} near the surface (0.28) was 5-fold that of normal cartilage and localized there, with an overall E_{xz} of 0.041. In PBS, E_{xz} values near the

articular surface were ~50% higher than that in SF, and overall E_{xz} was 0.045 and 0.062 for normal and degenerate tissue, respectively. Near the articular surface, G was lower with degeneration (0.18 MPa vs. 0.06 MPa). For both normal and degenerate cartilage, G increased with tissue depth to 3-4 MPa, with an overall G of 0.26-0.32 MPa.

Conclusion: During articulation, peak cartilage shear is highest near the articular surface and decreases markedly with depth. With degeneration and diminished lubrication, the markedly increased cartilage shear near the articular surface may contribute to progressive cartilage deterioration and osteoarthritis.

2.2 Introduction

The tissue-scale mechanics of articular cartilage remains to be fully elucidated during the compressive and shear loading of joints with normal movement. After repeated knee bending [11] and running [20], articular cartilage is compressed by ~5-20% of its overall thickness. Within the cartilage tissue of dynamically compressed osteochondral blocks [28], the magnitude of compressive strain is highest near the articular surface and minimal in deeper regions, a pattern consistent with the depth-varying compressive modulus of cartilage [32]. Despite extensive knowledge of cartilage compressive behavior, the overall and depth-varying shear deformation of cartilage during joint movement remains to be elucidated. Theoretical models of articulating joints can predict local cartilage deformation [2, 40] but are highly dependent on assumptions about boundary conditions at articulating surfaces (e.g., friction-less or adherent) and depth-varying mechanical properties [2]. Detailed experimental characterization of apposing cartilage samples sliding relative to each other (Figure 2.1) would further the understanding of cartilage mechanics during joint movement by elucidating the actual boundary condition at the articulating cartilage surface as well as the deformation and properties of cartilage in shear.

Lubrication of articulating cartilage by synovial fluid (SF) facilitates low friction in the boundary mode and may therefore affect the shear deformation of cartilage. When articulating cartilage is tested in a configuration that reveals boundary lubrication effects, SF and lubricant molecules in SF reduce articular surface interaction as indicated by decreased friction [33, 34]. The replacement of SF

lubricant with phosphate buffered saline (PBS) results in an elevation of boundary-mode friction [34]. The dependence of local and overall shear deformation by SF may be important for the maintenance of cartilage health since acute injury or inflammatory arthritis results in the reduced lubricating function of SF and this may be involved in post-injury cartilage degeneration [12].

Cartilage degeneration may also affect the way in which the tissue deforms during joint movement. As cartilage undergoes degeneration, for example with aging [9], articular surfaces become fibrillated and roughened [26]. Concomitantly, cartilage mechanical properties deteriorate for compressive, tensile, and shear loading [36], i.e., cartilage deformation and strain magnitude increase in response to a particular amplitude of applied load. Such mechanical deformation of cartilage affects chondrocyte metabolism, with moderate levels of dynamic compressive and shear strain stimulating matrix synthesis, but excessive levels inhibiting matrix synthesis [31]. Thus, determination of the deformation and strain of articulating cartilage, both with normal and degenerate surfaces, would provide insight into the local mechanical cues that regulate chondrocyte behavior and the consequences of degenerative changes on such cues.

One experimental approach used to elucidate the local strain deformation and strain of cartilage is to track displacement of fiducial markers using a video microscopy system. Previous studies have focused on cartilage deformation and strain when samples were subjected to compression in the absence of applied shear [7, 32, 43]. The depth-dependent compressive behavior of cartilage found in these micro-scale studies were consistent with those in macroscopic tissue explants using MRI

[28], and provided a resolution sufficient to resolve small magnitudes (~1%) of strain. Thus, micro-scale analysis may also provide insight into cartilage shear deformation, both locally and overall. For studying cartilage shear deformation during joint movement (Figure 2.1A), a pair of osteochondral blocks (Figure 2.1B) can be compressed in apposition (Figure 2.1C) and subjected to lateral shearing motion (Figure 2.1D). Such a configuration can be controlled to mimic the biomechanical behavior of articulating cartilage at one scale (full-thickness tissue) and allow elucidation of cartilage deformation at a finer scale (regions of tissue measurements). Combined measurements of strain and stress allow determination of local and overall biomechanical properties such as shear modulus.

Thus, the hypothesis of this study was that during joint articulation, the shear deformation of cartilage is affected by both lubrication and degeneration. To test this, the objectives of this study were (1) to implement a cartilage-on-cartilage sliding test to microscopically observe and analyze cartilage deformation during compression and shear, (2) to use this system to determine the effects of lubrication (by SF versus PBS) and degeneration (normal versus mildly degenerate) on overall and depth-varying shear strain, and (3) to determine the overall and depth-varying shear modulus of normal and mildly degenerate cartilage.

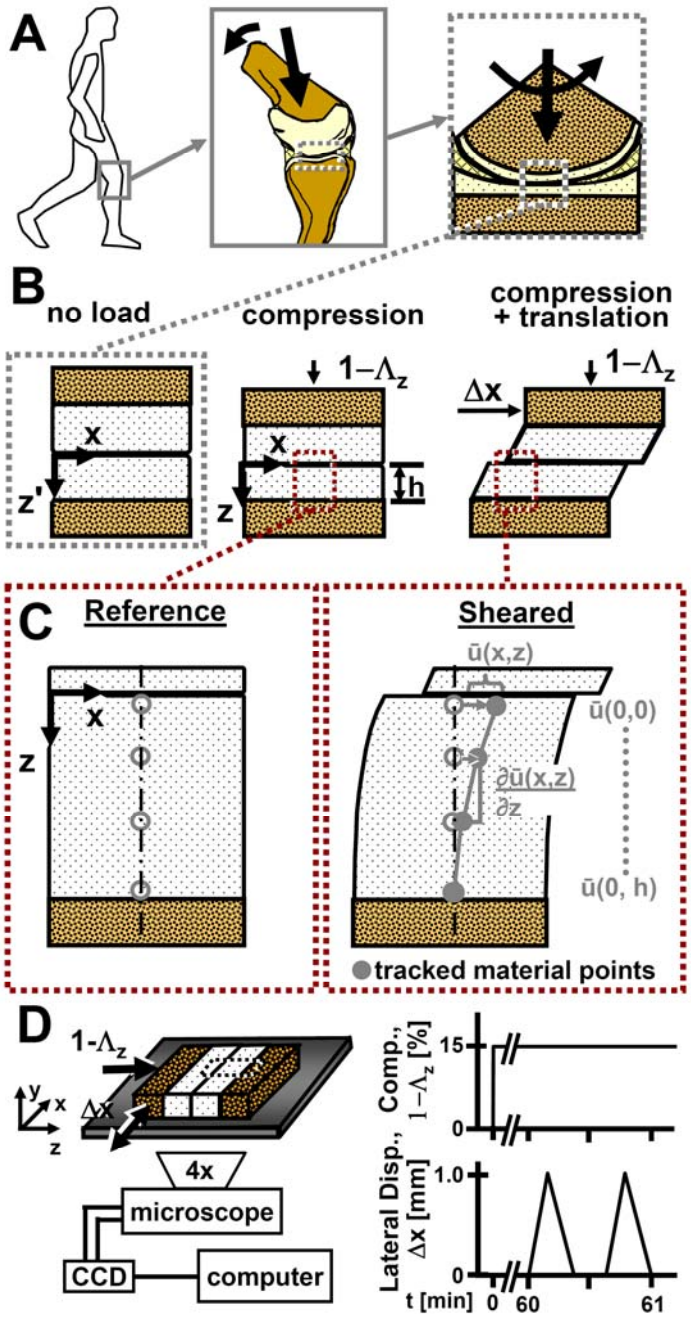

Figure 2.1: Schematic of (**A**) knee joint movements at multiple scales and (**B**) deformation of cartilage under (from left to right) no load, compression, and compression + shear loading. Material points in (**C**) compressed cartilage before and during shear loading were used to determine depth-dependent displacement vectors, ū(x,z'), used to assess intra-tissue deformation. Schematic of (**D**) experimental setup and loading protocol for micro-shear testing.

2.3 Materials and Methods

Sample Isolation

A total of six osteochondral cores (each with a diameter of 10 mm) were isolated, one from each anterior lateral femoral condyle of a single knee block used from each of six fresh cadaveric human tissue donors (Table 2.1). Cores were chosen for this study based on the gross appearance of the articular surface being normal (NL, modified Outerbridge grade of 1 [46], n=3) or mildly degenerate (DGN; grade 3, n=3) from adult age groups of 41-60 yrs and >60 yrs, respectively (Figure 2.2AB). The cores were immersed in phosphate buffered saline (PBS) containing proteinase inhibitors (PI) and stored at -80^{o}C until use.

Experimental Design

On the day of testing, each core was thawed and prepared for testing. The core was scored vertically in the cartilage using a razor blade and cut through the bone using a low-speed saw with a 0.3 mm thick diamond edge blade (Isomet^{TM}, Buehler, Lake Bluff, IL) to yield an osteochondral fragment for histopathologic analysis and two ~rectangular blocks for biomechanical testing. Each of the two blocks had a cartilage surface area of ~3x8 mm^2 and a total thickness of ~7 mm.

Table 2.1: Sample age, thickness, and Mankin-Shapiro scores. Mean ± SEM, n=3

	Normal	Mildly Degenerate
Age (yr)	48 ± 1.7	78 ± 9.2
Thickness (mm)	1.86 ± 0.12	2.08 ± 0.15
Mankin-Shapiro Score	1.89 ± 0.29	9.11 ± 1.24

Histopathology

Histopathologic analysis was performed to assess and confirm the state of degeneration. Samples were fixed in 4% paraformaldehyde in PBS at pH 7.0 for 24 h, decalcified with 18% disodium ethylenediamine tetraacetate in PBS for 7 d, and sectioned to 7 μm using a cryostat. Some sections were stained with Alcian blue to localize sulfated glycosaminoglycans as described previously [35], and other sections were stained with hematoxylin and eosin to highlight cellular detail [30]. Staining of samples resulted in a gradation of intensity (Figure 2.2 CD), reflecting the variation in GAG concentration with depth; thus, the staining method was sufficient to delineate GAG variation, such as loss due to pathology, and allow qualitative scoring. Transmitted light micrographs of the stained sections were obtained and analyzed for histopathology [6] using the Mankin-Shapiro semi-quantitative scale [37]. Briefly, the histopathologic characteristics included structural integrity (surface irregularity and vertical and horizontal clefts), cellularity (cloning and hypocellularity), and glycosaminoglycan loss. A relatively high score represented more degenerate cartilage. Grades from three independent observers were averaged for each sample. Inter-observer errors (standard deviation) for NL and DGN samples were reasonably small, being an average of 1.0 and 2.1, respectively.

Biomechanical Testing

First, samples were first tested by micro-scale shear testing, as described below, with PBS+PI as a lubricant. Then, samples were allowed to re-swell for ~4 h at 4^{o}C.

Next, samples were tested again by micro-scale shear testing, as described below, this time with SF+PI as the lubricant. The SF was pooled from adult bovine knees, stored at -80^{o}C, and characterized previously for boundary lubrication properties [34] and for levels of lubricant molecules (~1 mg/ml of hyaluronan and 0.45 mg/ml of proteoglycan 4 [25]). The same regions of interest were imaged. Then, samples were allowed to re-swell.

Finally, samples were tested in a macro-scale shear system to assess overall mechanical properties of cartilage in shear as described below.

Micro-scale Shear Testing: Each sample, consisting of paired osteochondral blocks, were bathed for ~14-18 h in test lubricant containing PI and propidium iodide (20 μg/ml) to fluorescently highlight cell nuclei at 4^{o}C prior to micro-shear testing.

Each pair of osteochondral blocks (Figure 2.1B,D) was then placed with cartilage in apposition in a custom bi-axial loading chamber mounted onto an epi-fluorescence microscope for digital video imaging [32]. The chamber secured one block at the bone and allowed in-plane movement of the apposing mobile block along the x-directed 8 mm lengths of the samples (Figure 2.1D) with orthogonally positioned plungers interfaced with either a micrometer (for axial displacement; Model 262RL; Starrett Co., Athol, MA) or motion-controller (for lateral displacement; Model MFN25PP; Newport, Irvine, CA). Fluorescence images (Nikon G-2A filter) with a field of view of ~3×2 mm^2 were obtained at 5 frames/s, showing a full-thickness region of cartilage of the secured block and a partial-thickness region of cartilage of the apposing block.

Cartilage deformation was assessed in the secured block during axial and shear loading. First, the reference state (uncompressed) was imaged. Then, an axial displacement was applied (~40 μm/s) by the micrometer to induce 15% compression ($1-\Lambda_z$, where Λ_z is the stretch ratio [15]) of the cartilage tissue (Figure 2.1C), during which time sequential images (~1.5% compression increment/frame) were acquired. Samples were then allowed to stress relax for one hour which was calculated to be sufficient to reach an approximate equilibrium stress based on consideration of characteristic time constant. Experimentally, this duration of stress-relaxation was validated to be sufficient with load decreasing by 130 s to 50% of the peak, and load at one hour being only 3±1% (n=3) higher than the load at 16 hr. Subsequently, lateral motion was applied to the mobile osteochondral block (Figure2.1D). Two sets of lateral displacements (Δx), each consisting of +1 mm and then −1 mm (returning to initial position), were applied at 100 μm/s to the bone portion of the mobile block. The first set, followed by a ~12 s pause, was for preconditioning [34], while the second set was recorded for analysis. The sliding velocity was chosen based on the range of velocities (0-0.1 m/s) occurring during the loading (stance) phase of gait [38, 44]. Before and during the application of lateral displacements (Figure 2.1D), sequential images, with ~10 μm of lateral movement of the mobile block between frames, were taken.

Macro-Scale Shear Testing: To assess the overall compressive and shear biomechanical properties of the cartilage of the secured block, following micro-scale shear tests, each secured block was subjected to a macro-scale test using a bi-axial

mechanical tester (Mach-1^{TM} V500CS, BioSyntech Canada, Montreal) under test conditions chosen to match the mechanical deformation resulting in the micro-shear test but with instrumentation allowing measurement of axial and shear loads. Each sample block was affixed, compressed 15% at a rate of 0.03%/s using a rigid stainless steel platen (~2 μm pore size, providing a no-slip boundary condition), and allowed to stress relax for 1 h to reach equilibrium. With increasing lateral displacement, continuous and monotonically increasing shear load waveforms were observed and confirmed no-slip conditions; a plateau in shear load, which would indicate slip, was not observed. Equilibrium force was recorded and normalized to the 3x8 mm^2 area to yield an estimate of the equilibrium compressive stress. Next, two sets of lateral displacements of the amplitude occurring at the surface at the onset of sliding in micro-shear tests were applied at a rate of 100 μm/s, then held for 10 s while shear load was being recorded, released and followed by a ~12 s pause in PBS+PI. As in the micro-scale tests, the first set was for preconditioning, while the second set was used for analysis. The lateral displacements were then repeated in the reverse direction following a 5 min pause, and shear loads occurring in the last second of the 10 s load-capture period in both directions were averaged. This average shear load was normalized to the 3x8 mm^2 area to yield an estimate of the shear stress (at which sliding occurred in the micro-scale test).

Data Collection and Calculations

Digital micrographs were analyzed to determine the depth-varying and overall strains in cartilage. Images were analyzed in MATLAB 7.0 (Mathworks, Inc., Natick, MA) using software routines similar to those described previously [5, 16, 43]. Briefly, an evenly distributed set of cell nuclei (~250 cell/mm^2), which served as fiducial markers, was selected and tracked by maximizing cross-correlation of regions surrounding each marker to the preceding, and then initial frames. Generally, chondrocyte nuclei for normal tissue were available and chosen in regions up to the true articular surface (defined by a discontinuity in displacement during sliding) while for degenerate tissue, nuclei visible up to ~50-70 μm (~3%) below the true surface due to fibrillation. Local affine mappings of nuclei were used to calculate the displacement ($\bar{u}$) of uniformly-spaced (10 pixel) mesh points in the region of interest (~1 mm × full thickness) during deformation (Figure 2.1D). Displacement gradients ($\frac{\partial \bar{u}}{\partial z}, \frac{\partial \bar{u}}{\partial x}$) were then determined by finite difference approximation, and in turn, used to determine Lagrangian compressive strains (E_{zz}) after axial compression and shear strains (E_{xz}) after lateral shearing, with these Lagrangian strains being appropriate for finite strains as well as small strains [14].

This method was validated, and the inter-observer variability was assessed. Using mathematically transformed images, the calculated strain values deviated less than 0.005 ± 0.005 from the theoretical values, with the error being proportionately smaller in regions exhibiting lower amplitudes of strain. Inter-observer variability, assessed as the average of standard deviation in calculated strain between 3 observers,

was ~0.01 for a subset of data from all sample types (n=4). Here also, the variability was proportionately lower in regions of relatively small shear magnitudes.

The calculated shear strain was interpolated, averaged depth-wise, and plotted as a function of tissue depth, normalized to the cartilage thickness in the compressed state. Shear strain was interpolated linearly at every 0.05 times the normalized tissue thickness near the articular surface (i.e. 0 to 0.3) and 0.1 for remaining regions of the tissue depth (i.e. 0.3 to 1) after applied compression and prior to lateral motion. To consolidate data, strain values were averaged at the same normalized depth (0, surface and 1, tidemark) to yield a depth-profile. Shear strain results were determined when surfaces were sliding, at which time, shear strain was at a peak and no further changes in deformation occurred with additional lateral displacement (i.e., sliding). The overall Lagrangian shear strain was defined as half the lateral surface displacement normalized to the compressed cartilage thickness. Since the shear strain peaked near the articular surface, shear strain occurring at the top 5% was also compared.

Overall cartilage properties were determined from forces recorded during compression and shear. Under compression alone, the compressive modulus of cartilage was defined as the increment in stress divided by the increment in applied compressive strain. The overall shear modulus (G) for each sample was determined as the increment in shear stress (shear load divided by surface area) divided by the increment in shear strain.

The depth-varing shear moduli were estimated from the overall shear modulus and local shear strain for each sample. Since shear modulus is inversely related to shear stain, and with shear stress assumed to be constant at all depths, the local shear

modulus was estimated as the overall shear modulus multiplied by the overall shear strain and divided by the local shear strain. Since these estimates depend on shear strain in the denominator, shear modulus was calculated at every 10% near the articular surface (up to 20%) and every 20% of the tissue depth in the subsequent regions to reduce noise.

Statistical Analysis

Data are reported as mean ± standard error of the mean (SEM), unless noted otherwise. Repeated measures ANOVA was used to determine the effects of normalized tissue depth (0-1, surface-bone), lubricant (PBS, SF), and degeneration (NL, DGN) on tissue shear strain, and to determine the effects of tissue depth and degeneration on shear modulus.

2.4 Results

Histopathology

The overall histopathology scores were consistent with gross (Figure 2.2AB) and histological appearances (Figure 2.2CD) of NL and DGN samples. DGN samples had significantly higher ($p<0.01$) histopathology scores (Table 2.1) than NL samples. For DGN samples, structural (surface irregularity, vertical clefts to transitional zone, and transverse clefts) and cellular (cloning) features exhibited mild degeneration and were ~1-point higher than those for NL samples. In contrast, cellularity and GAG staining scores were similarly low (i.e. normal) between NL and DGN samples. These results confirmed that gross visualization resulted in an appropriate selection of samples, normal and mildly degenerate, for articulation testing.

Compressive Deformation and Properties

The axial compression of cartilage in the secured block resulted in compressive strain (E_{zz}) that varied significantly with depth from the articular surface ($p< 0.001$) but not between NL and DGN groups ($p=0.6$). E_{zz} was relatively high near the articular surface (0.38 ± 0.05) and relatively low in the deepest regions (0.06 ± 0.01). Transverse oriented (E_{xx}) and shear (E_{xz}) strains resulting from the applied compression were low, averaging <0.03 for all samples. The equilibrium compressive modulus (E) for the full-thickness cartilage was not significantly different between sample groups ($p=0.5$), being 0.79 ± 0.13 for NL and 0.61 ± 0.23 MPa for DGN cartilage, respectively.

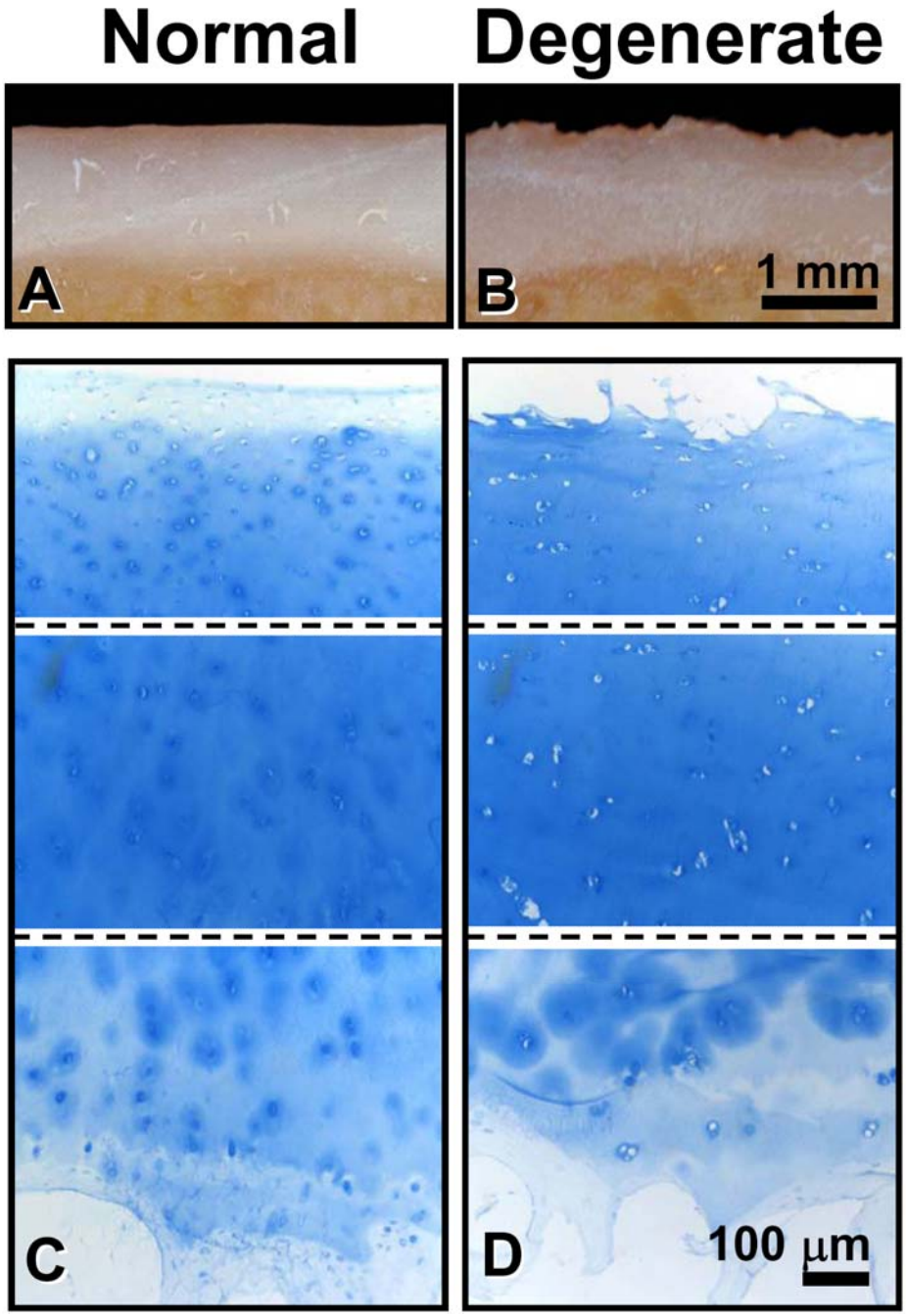

Figure 2.2: **A** and **B**, Photographs of cross-sections of samples of normal and degenerated cartilage. **C** and **D**, Representative micrographs of Alcian blue-stained sections showing structure detail of the superificial (top image), middle (middle image), and deep (bottom image) regions of normal (**C**) and degenerated (**D**) cartilage.

Shear Deformation

Qualitatively, cartilage shear-loading resulted in a sequence of four events. (1) At the onset of applied lateral displacement, cartilage surfaces initially adhered and began to move laterally in unison. (2) With increasing lateral displacement, lateral deformation and hence E_{xz} increased and occurred throughout the tissue depth. (3) Next, lateral deformation and E_{xz} of cartilage peaked just as the surfaces detached and slid relative to each another. (4) With additional lateral displacement, the cartilage deformation and E_{xz} were maintained at steady-state peak.

At the steady state, tissue displacement (bounding boxes, Figure 2.3) and E_{xz} (color map, Figure 2.3) were non-uniform and depth-varying, with high shear magnitudes near the articular surface and low, almost indistinguishable, near the bone. The maximum lateral displacement of apposing surfaces before slipping when lubricated with SF was 115 ± 14 μm and 82 ± 16 μm for NL and DGN tissues, respectively. When lubricated with PBS, NL and DGN maximum lateral displacement was 169 ± 12 μm and 125 ± 18 μm, respectively, before slipping. Differences in shear deformation between normal and degenerate samples were also evident (Figure 2.3A-D). Shear deformation in degenerate samples (Figure 2.3C,D) was concentrated near the surface, while in normal samples, deformation occurred farther into the tissue depth (Figure 2.3A,B).

Quantitatively, E_{xz} of articulating cartilage varied with depth from the articular surface, lubricant, and surface degeneration. In the depth-profile of E_{xz} (Figure 2.4A,B), the highest values were near the articular surface, and E_{xz} decreased

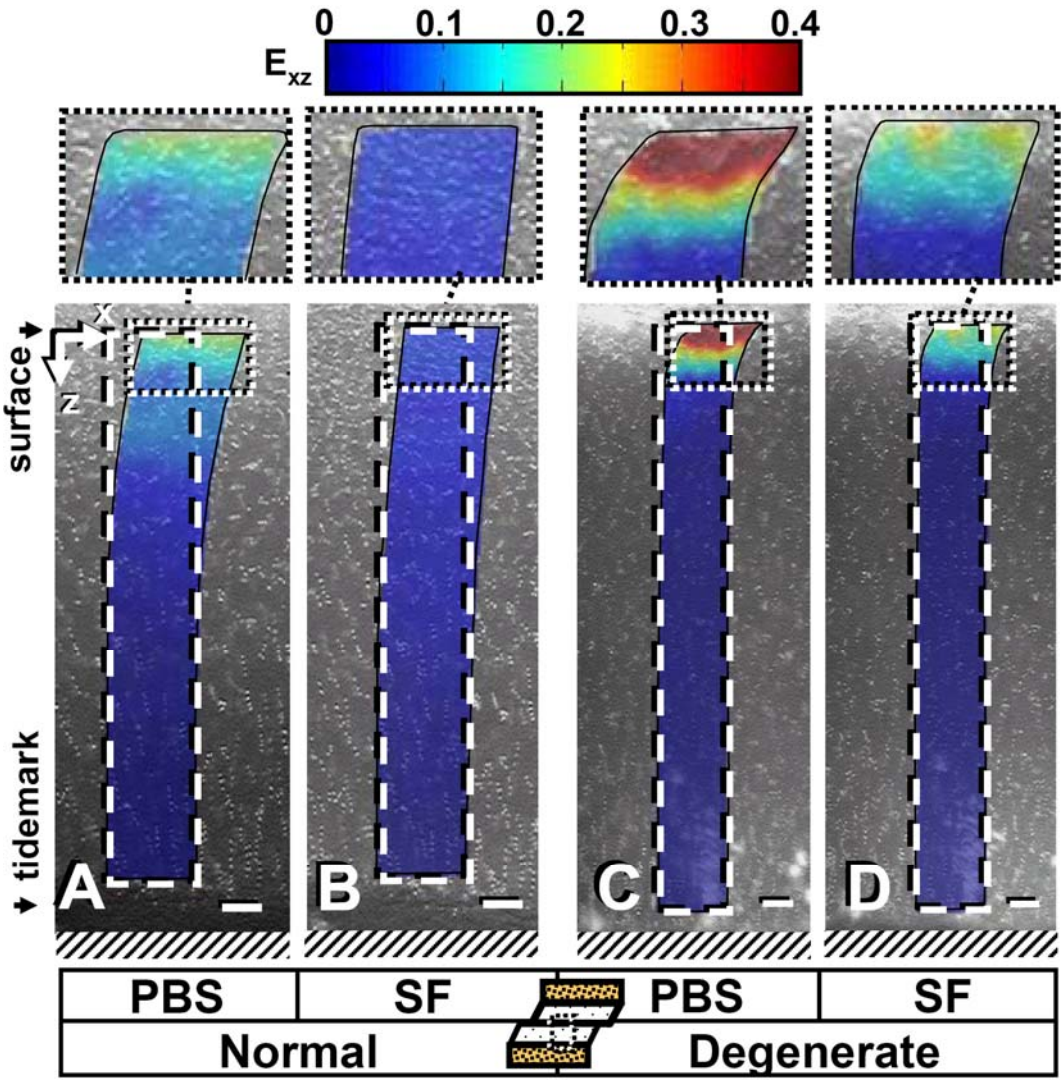

Figure 2.3: Micrographs taken during shear loading of apposing normal (**A,B**) and degenerate (**C,D**) samples lubricated with PBS (**A,C**) or SF (**B,D**), after achieving the maximum shear strain. Cell nuclei tracking method was used to determine maps of shear strain (color maps, **A-D**), magnified above each panel. Dashed lines (– –) encompass the analyzed regions on the undeformed images, while continuous lines encompass the strain maps of the corresponding deformed states. Bars = 100 μm.

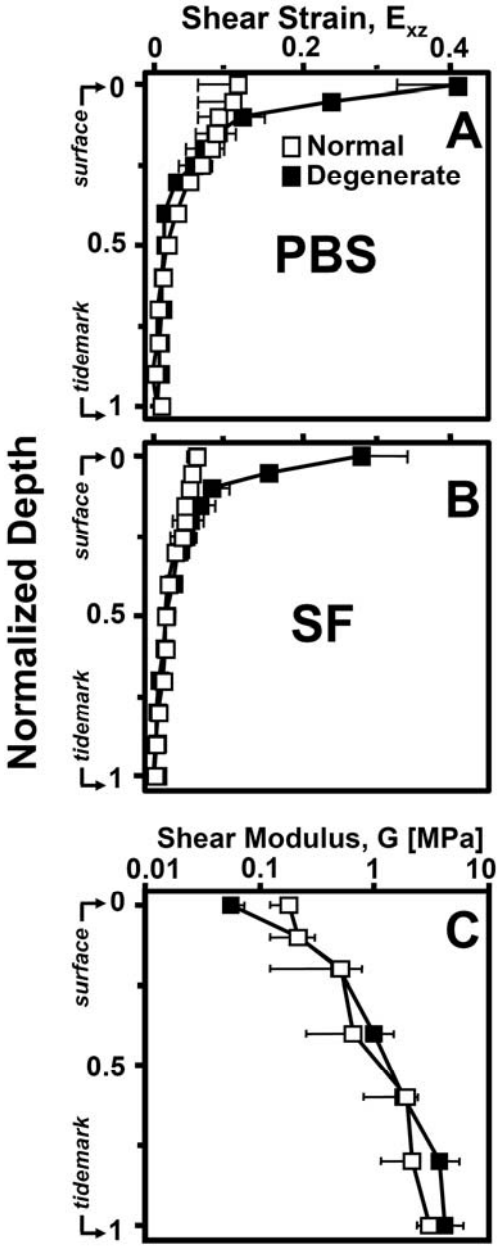

Figure 2.4: Biomechanical measures of adult human articular cartilage in shear. From micro-shear tests, local shear strain, $\mathbf{E_{xz}}$, versus normalized tissue depth for normal (□) and degenerate (■) cartilage. Samples were tested with lubricant of (**A**) phosphate buffered saline (**PBS**) and then (**B**) synovial fluid (**SF**). From macro-scale tests (**C**) local shear modulus, **G**, versus normalized tissue depth for normal (□) and degenerate samples (■).

monotonically with depth ($p<0.001$). The variation of E_{xz} with depth depended on surface degeneration (interaction, $p<0.001$), with E_{xz} decreasing more with depth in the DGN sample. A similar trend was noted with testing in PBS, where E_{xz} decreased at greater rates with depth than when tested in SF (interaction, $p<0.001$) for both NL and DGN samples. The combined effect of depth and degeneration or lubricant on shear strain was evident as varying E_{xz} values near the surface, but similarly low values of E_{xz}, <0.01, in the deep layer of cartilage.

Both peak E_{xz} at the surface (at z=0; Figure 2.5A) and overall E_{xz} (Figure 2.5B) were each significantly affected by both lubricant and degeneration. The peak surface E_{xz} (Figure 2.5A) was ~3-5 times higher with surface degeneration than with normal tissue ($p<0.05$) for both surface lubricants. In PBS, E_{xz} increased from 0.11 (NL) to 0.41 (DGN). In SF, E_{xz} increased from 0.056 (NL) to 0.28 (DGN). In addition, peak surface E_{xz} was ~1.5-2 times lower when tested in SF compared to PBS ($p<0.05$). Overall E_{xz} (Figure 2.5B) was not detectably different between NL and DGN samples ($p=0.10$) tested for a given lubricant. However, overall E_{xz} did vary with lubricant. Overall E_{xz} of NL tissue increased significantly ($p<0.05$) from 0.028 (SF) to 0.045 (PBS), and overall E_{xz} of DGN tissue increased from 0.041 (SF) to 0.062 (PBS).

Shear Properties

To replicate sample shear deformation in micro-scale shear tests, lateral surface displacements in macro-scale shear tests ranging from 70 – 125 μm (measured from micro-shear tests) were applied to NL samples and 120 – 160 μm were applied to

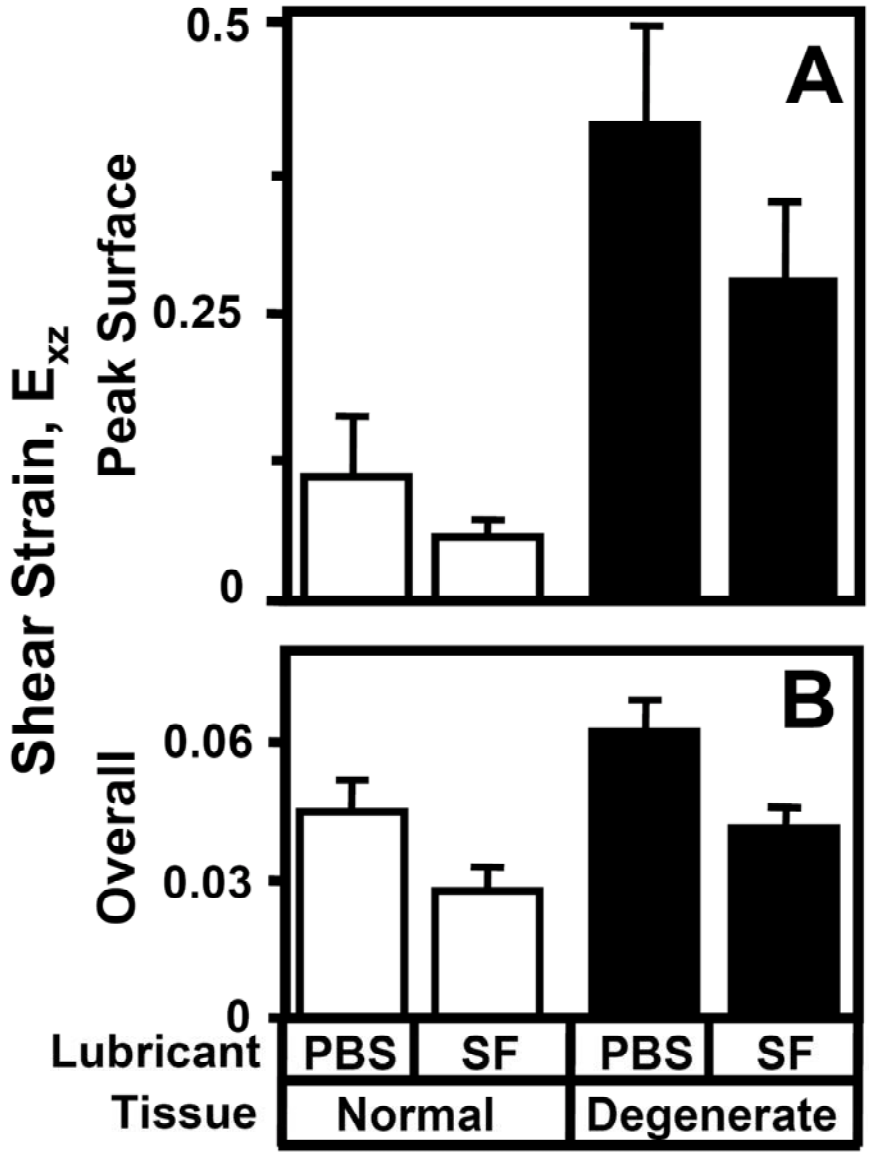

Figure 2.5: Effect on (**A**) peak surface and (**B**) overall shear strain of sample groups, normal and degenerate, and of lubricant, phosphate buffered saline (**PBS**) or synovial fluid (**SF**).

DGN samples. Overall G was not significantly different between normal and mildly degenerate tissue ($p=0.7$), being 0.32 ± 0.09 MPa for NL and 0.26 ± 0.07 MPa for DGN cartilage. G was lowest near the articular surface and increased significantly with tissue depth ($p<0.01$), being 0.2-0.6 and 10-15 times the overall G near the surface and in the deepest region, respectively (Figure 2.4C). G was not significantly different between NL and DGN samples at all depths below the surface ($p>0.5$). Near the articular surface, there was a trend ($p=0.10$) of G being lower with mild surface degeneration, with surface G being 0.18 ± 0.06 MPa and 0.06 ± 0.02 MPa for NL and DGN samples, respectively.

2.5 Discussion

This study elucidated the shear deformation and strain of cartilage during contact and sliding, as well as, the effects of lubrication and mild degeneration, using a micro-scale cartilage-on-cartilage testing system. The present results indicate that cartilage-cartilage articulation results in four sequential events, adherence, adherence and deformation, detachment, and sliding. Peak E_{xz} was highest near the surface and modulated by both lubricant and the condition of the sample itself (Figure 2.4AB). Relative to normal SF as lubricant, E_{xz} increased with PBS as lubricant by ~100% near the surface (Figure 2.5A) and ~55% overall (Figure 2.5B). Also, when degenerate samples were tested, their E_{xz} values near the surface were ~3-5 times higher than those of normal samples (Figure 2.5A).

Osteochondral samples used in this study were prepared from a site that is affected by age-associated degeneration and osteoarthritis. The samples were from the lateral femoral condyle, a load-bearing region where ~22% [10, 17] of arthroscopically-diagnosed chondral defects occur. The biomechanical factors associated with early degeneration in such load-bearing regions may contribute to the progressive degeneration of the articular cartilage. While previously frozen samples were used, a single freeze-thaw cycle does not result in marked changes in compressive properties of normal [39] or degenerate [19] articular cartilage nor its structure [21], and is thus unlikely to have marked effects on shear properties. Although the distal femoral condyle normally apposes the tibial plateau, cartilage

from the femoral condyle was apposed against itself to create a simplified symmetrical loading situation. Future studies could examine cartilage from additional sites.

The testing protocol used in this study provides a mechanical environment mimicking the compression and sliding of articular cartilage during normal joint loading. A knee undergoes a wide range of dynamic compression of up to 5-20% during normal activities [11, 20] and sliding up to ~50 mm (estimated from [38, 44]). The present analysis addresses certain parts of the gait cycle (e.g., contralateral toe-off and heel rise [44]) where compressive loading is high and sliding velocity is low, during which time interaction of opposing tissue surfaces are likely to be initiated. Since samples were allowed to stress-relax for 1 hr, the pattern of cartilage deformation and strain is likely to be representative of that occurring after prolonged cyclic loading and sliding, rather than that which occurs at the onset of cyclic loading. Cartilage gradually depressurizes and reaches an averaged steady-state compression under prolonged cyclic loading. During this time, interstitial fluid pressure diminishes [1], and boundary lubrication becomes increasingly important [34]. The rate-dependence of shear deformation was not assessed; however, shear deformation may not change markedly with rate of lateral displacement since kinetic friction remains fairly constant with sliding velocity [34]. Additional studies may elucidate the time-course of cartilage shear after the onset of loading as well as effects of sliding velocity on shear deformation.

Although edge effects may occur in this shear testing protocol, such effects are likely minimal in the central area of tissue that was analyzed. Boundaries of the analyzed region were ~2 mm away from both the leading and trailing edges of the

samples. Recent studies have shown that intra-tissue deformation (data not shown) and stiffness [4] are affected only ~1-2 mm from vertical boundaries of cartilage. Thus, the results are likely to be representative of the major areas of cartilage contact.

The reduction in E_{xz} with SF as lubricant is consistent with predictions accounting for a variety of past studies on cartilage friction. Friction coefficient decreases with SF as lubricant compared to saline for both cartilage-on-cartilage in the boundary mode [13, 34] and whole joint [22, 24, 45] friction tests. Assuming cartilage material properties (i.e., compressive and shear modulus) are maintained with the uses of SF and PBS, the friction-reducing property of SF would be predicted to result in a lowering of tissue E_{xz}.

The values of overall E_{xz} found in this study are consistent with values estimated during physiologic joint articulation based on previously reported material properties of cartilage, as follows. To provide a first-order estimate of tissue properties, cartilage can be modeled as a linear, homogeneous, isotropic, and elastic tissue. With such assumptions and under small strain conditions, the overall stiffness of cartilage in shear (G) can be related to the Piola-Kirchhoff shear stress (S_{xz}) and the resulting overall Lagrangian E_{xz} [14], finite measures of stress and strain, as follows:

$$G = \frac{S_{xz}}{2E_{xz}} \qquad \text{(Eqn. 1)}$$

In addition, S_{xz} acting on cartilage can be related to the friction coefficient (μ) and the Piola-Kirchhoff normal contact stress (S_n) when surfaces are sliding as follows:

$$S_{xz} = \mu S_n \qquad \text{(Eqn. 2)}$$

Substituting equation 2 into equation 1 and rearranging terms, cartilage E_{xz}, when surfaces are sliding can be expressed as:

$$E_{xz} = \frac{\mu S_n}{G} \qquad \text{(Eqn. 3)}$$

Using the reported values of μ ~0.01 [41], S_n ~2 MPa [29], and overall G ~0.2-0.4 MPa found in this study, the estimated overall E_{xz} is 0.02-0.05 when surfaces are sliding. The estimate of E_{xz} is consistent within the range of overall E_{xz} determined in this study (Figure 2.5B). Conversely, this suggests that an overall E_{xz} ranging from 0.01 to 0.1 may be suitable for biomimetic *in vitro* simulation of physiologic shear loading, for example during mechanical evaluation and mechanical stimulation for tissue engineering of cartilage.

The increased E_{xz} with degeneration, particularly near the surface (Figure 2.5B) with SF as lubricant, appears to be due to both increased friction between sliding surfaces and a reduction in tissue shear modulus. Roughened surfaces have local asperities that can cause increased interaction and adherence between tissue surfaces, increasing friction during sliding. Since boundary lubricants modulate friction, higher E_{xz} in degenerate cartilage when tested in PBS indicates that friction between degenerate surfaces is higher than that between normal surfaces (Figure 2.5A). Additionally with degeneration, cartilage mechanical properties, such as G, become impaired [36]. Diminished G would result in increased cartilage E_{xz} for the same magnitude of S_{xz} (equation 3), i.e. even if friction coefficient was similar. Since surface E_{xz} increased with degeneration with SF lubricant, and G near the surface tended to diminish with degeneration, the elevated E_{xz} at the surface in mildly

degenerate tissue is likely a result of both increased μ and reduced G (Equation 3 and Figure 2.5A).

Depth-variations in E_{xz} and G of the present cartilage samples provide additional information on the depth-varying biomechanical properties of articular cartilage. Compressive strain is depth-varying in both statically [32] and dynamically [28] compressed cartilage, decreasing monotonically with depth from the articular surface. E_{xz} found in this study was similarly depth-varying, being highest near the surface and lowest near the tidemark (Figure 2.4A,B). Compressive modulus, deduced from the overall compressive stress and local strain, was reflective of the depth-varying strain magnitudes, with cartilage increasing in stiffness with increasing depth [32]. Similarly, G was lowest near the articular surface and increased monotonically to a maximum in the deepest region (20%) (Figure 2.4C). While G near the surface only tended to decrease with degeneration, the lack of statistical correspondence was likely due to the calculation from two measurements, shear stress and strain (each having variability), as well as donor variability. The overall unconfined compressive modulus at equilibrium found in this study (E = 0.79 MPa) is consistent with previously reported values for human cartilage (E = 0.58 MPa) [18]. The overall shear properties of human cartilage have yet to be reported; however, overall G can be estimated from Poisson's ratio (ν) and the aggregate modulus (H_A) reported in indentation tests, using the relationship $G = \frac{H_A(1+\upsilon)(1-2\upsilon)}{2(1+\upsilon)(1-\upsilon)}$ [14, 27]. The overall G found in this study (0.32 MPa) is consistent with that estimated from indentation tests (G = 0.2-0.4 MPa) [3]. Thus, in compression, the deformation and mechanical properties are consistent

with previous studies, while in shear, the newly described depth-varying strain and shear properties are within values predicted for full-thickness human cartilage.

With cartilage degeneration, the tissue structure and low cellularity may affect the analysis and interpretation of deformation and strain. Degenerate cartilage contains clefts and areas of erosion [37], both of which result in material discontinuities within cartilage. Thus, continuum assumptions are not strictly valid. Also, compatibility conditions [14] are not maintained when fibrillated tissues overlap during deformation. Nevertheless, the present samples were only mildly degenerate and relatively intact except at the surface. And, while the surface of the present degenerate samples exhibited few visible cells, cells near the surface (3-5% depth) were able to be tracked. From a linear extrapolation, this may have resulted in a slight (~15%) underestimation of the absolute magnitude of the superficial shear strains.

The present results suggest changes in E_{xz} magnitudes and shear behavior may contribute to cartilage degeneration and pathogenesis. While samples were tested with a common overall compressive strain in this study, marked differences in E_{xz} between groups occurred even with this conservative testing protocol. Under common loads instead of overall strain, softer tissues (i.e. degenerate cartilage) would exhibit larger compressive and shear strains, excessive levels of which can contribute to cartilage degeneration. Excessive magnitudes of compressive strain result in mechanical injury to cells [8, 23] and matrix [8, 42], leading to reduced cartilage remodeling, maintenance, and repair. Likewise, high E_{xz} that results from degenerated matrix, along with deficient lubrication, may lead to additional degeneration. Cell death and matrix damage may spread with continued exposure to high E_{xz}, reducing local

mechanical properties of cartilage in both compression and shear. Cartilage E_{xz} may then further increase and further the changes in tissue structure, resulting in a self-propagating cycle of degeneration. Such mechanical effects may also induce changes in surrounding joint tissues and the biochemical environment which can supplement cartilage deterioration.

2.6 Acknowledgments

We like to thank co-authors Dr. Won C. Bae, June Chun, Kenneth Gratz, and Dr. Martin Lotz for their contributions to this work. We also thank the many residents and staff of the Lotz Lab of the Scripps Research Institute of La Jolla for harvesting and providing the human tissue used in this study, and Barbara Schumacher for guidance on histopathological processing. This work was supported by the San Diego Fellowship for Benjamin L. Wong and the NIH and Howard Hughes Medical Institute through the Professors Program Grant to UCSD for Dr. Robert L. Sah.

2.7 References

1. Armstrong CG, Lai WM, Mow VC: An analysis of the unconfined compression of articular cartilage. *J Biomech Eng* 106:165-73, 1984.

2. Ateshian GA, Lai WM, Zhu WB, Mow VC: An asymptotic solution for the contact of two biphasic cartilage layers. *J Biomech* 27:1347-60, 1994.

3. Athanasiou KA, Rosenwasser MP, Buckwlter JA, Malinin TI, Mow VC: Interspecies comparisons of in situ intrinsic mechanical properties of distal femoral cartilage. *J Orthop Res* 9:330-40, 1991.

4. Bae WC, Law AW, Amiel D, Sah RL: Sensitivity of indentation testing to step-off edges and interface integrity in cartilage repair. *Ann Biomed Eng* 32:360-9, 2004.

5. Bae WC, Lewis CW, Levenston ME, Sah RL: Indentation testing of human articular cartilage: effects of probe tip geometry and indentation depth on intra-tissue strain. *J Biomech* 39:1039-47, 2006.

6. Bae WC, Temple MM, Amiel D, Coutts RD, Niederauer GG, Sah RL: Indentation testing of human cartilage: sensitivity to articular surface degeneration. *Arthritis Rheum* 48:3382-94, 2003.

7. Chahine NO, Wang CC, Hung CT, Ateshian GA: Anisotropic strain-dependent material properties of bovine articular cartilage in the transitional range from tension to compression. *J Biomech* 37:1251-61, 2004.

8. Chen C-T, Bhargava M, Lin PM, Torzilli PA: Time, stress, and location dependent chondrocyte death and collagen damage in cyclically loaded articular cartilage. *J Orthop Res* 21:888-98, 2003.

9. Clark JM, Simonian PT: Scanning electron microscopy of "fibrillated" and "malacic" human articular cartilage: technical considerations. *Microsc Res Tech* 37:299-313, 1997.

10. Curl WW, Krome J, Gordon ES, Rushing J, Smith BP, Poehling GG: Cartilage injuries: a review of 31,516 knee arthroscopies. *Arthroscopy* 13:456-60, 1997.

11. Eckstein F, Lemberger B, Stammberger T, Englmeier KH, Reiser M: Patellar cartilage deformation in vivo after static versus dynamic loading. *J Biomech* 33:819-25, 2000.

12. Elsaid KA, Jay GD, Warman ML, Rhee DK, Chichester CO: Association of articular cartilage degradation and loss of boundary-lubricating ability of

synovial fluid following injury and inflammatory arthritis. *Arthritis Rheum* 52:1746-55, 2005.

13. Forster H, Fisher J: The influence of loading time and lubricant on the friction of articular cartilage. *Proc Inst Mech Eng [H]* 210:109-19, 1996.

14. Fung YC. A First Course in Continuum Mechanics. 2nd ed. Englewood Cliffs: Prentice-Hall; 1977.

15. Fung YC. Biomechanics: Mechanical Properties of Living Tissues. 2nd ed. New York: Springer-Verlag; 1993.

16. Gratz KR, Sah RL: Experimental measurement and quantification of frictional contact between biological surfaces experiencing large deformation and slip. *J Biomech* 41:1333-40, 2008.

17. Hjelle K, Solheim E, Strand T, Muri R, Brittberg M: Articular cartilage defects in 1,000 knee arthroscopies. *Arthroscopy* 18:730-4, 2002.

18. Jurvelin JS, Buschmann MD, Hunziker EB: Mechanical anisotropy of the human knee articular cartilage in compression. *Proc Inst Mech Eng [H]* 217:215-9, 2003.

19. Kempson GE, Spivey CJ, Swanson SA, Freeman MA: Patterns of cartilage stiffness on normal and degenerate human femoral heads. *J Biomech* 4:597-609, 1971.

20. Kersting UG, Stubendorff JJ, Schmidt MC, Bruggemann GP: Changes in knee cartilage volume and serum COMP concentration after running exercise. *Osteoarthritis Cartilage* 13:925-34, 2005.

21. Kiefer GN, Sunbdy K, McAllister D, Shrive NG, Frank CB, Lam T, Schachar NS: The effect of cryopreservation on the biomechanical behavior of bovine articular cartilage. *J Orthop Res* 7:494-501, 1989.

22. Linn FC: Lubrication of animal joints. II. the mechanism. *J Biomech* 1:193-205, 1968.

23. Loening A, Levenston M, James I, Nuttal M, Hung H, Gowen M, Grodzinsky A, Lark M: Injurious mechanical compression of bovine articular cartilage induces chondrocyte apoptosis. *Arch Biochem Biophys* 381:205-12, 2000.

24. Mabuchi K, Tsukamoto Y, Obara T, Yamaguchi T: The effect of additive hyaluronic acid on animal joints with experimentally reduced lubricating ability. *J Biomed Mater Res* 28:865-70, 1994.

25. Mazzucco D, Scott R, Spector M: Composition of joint fluid in patients undergoing total knee replacement and revision arthroplasty: correlation with flow properties. *Biomaterials* 25:4433-45, 2004.

26. Meachim G, Emery IH: Quantitative aspects of patello-femoral cartilage fibrillation in Liverpool necropsies. *Ann Rheum Dis* 33:39-47, 1974.

27. Mow VC, Hayes WC, eds. Basic Orthopaedic Biomechanics. 2nd ed. New York: Raven Press; 1997.

28. Neu CP, Hull ML, Walton JH: Heterogeneous three-dimensional strain fields during unconfined cyclic compression in bovine articular cartilage explants. *J Orthop Res* 23:1390-8, 2005.

29. Raimondi MT, Pietrabissa R: Contact pressures at grafted cartilage lesions in the knee. *Knee Surg Sports Traumatol Arthrosc* 13:444-50, 2005.

30. Ross MH, Kaye GI, Pawlina W. Histology: A Text and Atlas. 4th ed. Philadelphia, PA: Lippincott Williams & Wilkins; 2003.

31. Sah RL, Grodzinsky AJ, Plaas AHK, Sandy JD: Effects of static and dynamic compression on matrix metabolism in cartilage explants. In: *Articular Cartilage and Osteoarthritis,* ed. by KE Kuettner, Schleyerbach R, Peyron JG, Hascall VC, Raven Press, New York, 1992, 373-92.

32. Schinagl RM, Gurskis D, Chen AC, Sah RL: Depth-dependent confined compression modulus of full-thickness bovine articular cartilage. *J Orthop Res* 15:499-506, 1997.

33. Schmidt TA, Gastelum NS, Nguyen QT, Schumacher BL, Sah RL: Boundary lubrication of articular cartilage: role of synovial fluid constituents. *Arthritis Rheum* 56:882-91, 2007.

34. Schmidt TA, Sah RL: Effect of synovial fluid on boundary lubrication of articular cartilage. *Osteoarthritis Cartilage* 15:35-47, 2007.

35. Scott JE, Dorling J: Differential staining of acid glycosaminoglycans (mucopolysaccharides) by alcian blue in salt solutions. *Histochemie* 5:221-33, 1965.

36. Setton LA, Elliott DM, Mow VC: Altered mechanics of cartilage with osteoarthritis: human osteoarthritis and an experimental model of joint degeneration. *Osteoarthritis and Cartilage* 7:2-14, 1999.

37. Shapiro F, Glimcher MJ: Induction of osteoarthrosis in the rabbit knee joint. Histologic changes following menisectomy and meniscal lesions. *Clin Orthop Rel Res* 147:287-95, 1980.

38. Shelburne KB, Torry MR, Pandy MG: Muscle, ligament, and joint-contact forces at the knee during walking. *Med Sci Sports Exerc* 37:1948-56, 2005.

39. Swann AC, Seedhom BB: The stiffness of normal articular cartilage and the predominant acting stress levels: implications for the aetiology of osteoarthrosis. *Br J Rheum* 32:16-25, 1993.

40. Swanson SAV: Friction, wear, and lubrication. In: *Adult Articular Cartilage,* ed. by MAR Freeman, Pitman Medical, Tunbridge Wells, England, 1979, 415-60.

41. Tanaka E, Kawai N, Tanaka M, Todoh M, van Eijden T, Hanaoka K, Dalla-Bona DA, Takata T, Tanne K: The frictional coefficient of the temporomandibular joint and its dependency on the magnitude and duration of joint loading. *J Dent Res* 83:404-7, 2004.

42. Thibault M, Poole AR, Buschmann MD: Cyclic compression of cartilage/bone explants in vitro leads to physical weakening, mechanical breakdown of collagen and release of matrix fragments. *J Orthop Res* 20:1265-73, 2002.

43. Wang CC, Deng JM, Ateshian GA, Hung CT: An automated approach for direct measurement of two-dimensional strain distributions within articular cartilage under unconfined compression. *J Biomech Eng* 124:557-67, 2002.

44. Whittle M. Gait Analysis: An Introduction. 3rd ed. Oxford; Boston: Butterworth-Heinemann; 2002.

45. Wright V, Dowson D: Lubrication and cartilage. *J Anat* 121:107-18, 1976.

46. Yamada K, Healey R, Amiel D, Lotz M, Coutts R: Subchondral bone of the human knee joint in aging and osteoarthritis. *Osteoarthritis Cartilage* 10:360-9, 2002.

CHAPTER 3

SHEAR DEFORMATION KINEMATICS DURING CARTILAGE ARTICULATION: EFFECT OF LUBRICATION, DEGENERATION, AND STRESS RELAXATION

3.1 Abstract

Objective: During joint articulation, the biomechanical behavior of cartilage not only facilitates load-bearing and low-friction, but also provides regulatory cues to chondrocytes. Elucidation of cartilage kinematics under combined compression and shearing conditions clarifies these cues in health and disease. The objectives of this study were to elucidate the effects of lubricant, tissue degeneration, and stress relaxation duration on cartilage shear kinematics during articulation.

Methods: Human osteochondral cores with normal and mildly degenerate surface structures were isolated. Paired blocks from each core were apposed, compressed, allowed to stress relax for 5 or 60 min, and shear tested with a micro-scale video microscopy system using phosphate-buffered saline (PBS) or synovial fluid as lubricant. During applied lateral motion, local and overall shear strain (E_{xz}) of articular

cartilage were determined. The applied lateral displacement at which E_{xz} reached 50% of the peak ($\Delta x_{1/2}$) was also determined.

Results: Quantitatively, surface E_{xz} increased at the onset of lateral motion and peaked just as surfaces detached and slid. With continued lateral motion, surface E_{xz} was maintained. After short stress relaxation, effects of lubrication on E_{xz} and $\Delta x_{1/2}$ were not apparent. With prolonged stress relaxation, E_{xz} and $\Delta x_{1/2}$ near the articular surface increased markedly when PBS was used as lubricant. Similar patterns were observed for overall E_{xz} and $\Delta x_{1/2}$. With degeneration, surface E_{xz} was consistently higher for all cases after the onset of lateral motion.

Conclusion: Thus, cartilage shear kinematics is markedly affected by lubricant, cartilage degeneration, and loading duration. Changes in these factors may be involved in the pathogenesis of osteoarthritis.

3.2 Introduction

Articular cartilage is a deformable, low-friction, and wear-resistant connective tissue that bears repeated loading and sliding during normal joint movement. After daily activities such as repeated knee bending [4] and running [9], overall cartilage thickness compresses ~5-20%. The compression of cartilage at equilibrium is depth-varying, being highest near the articular surface and minimal in the deeper regions for dynamically compressed osteochondral blocks [15]. Similarly, for compressed and sliding apposing osteochondral blocks, cartilage shear strain is highest near the articular surface and negligible near the tidemark, with cartilage shearing ~2-5% overall after surfaces detached and slide [22]. While recent investigations have elucidated the shear behavior of cartilage after achieving a steady state (i.e. after surfaces detach and slide), shear kinematics (i.e. prior to and after surface detachment and sliding) of cartilage articulation remains to be determined. Further characterization of apposing cartilage samples sliding relative to each other (Figure 3.1A,B) would further elicit the understanding of cartilage contact mechanics during joint loading by elucidating the changing boundary conditions at the articulating surface as well as the shear deformation of cartilage with applied lateral-loading, as opposed to after reaching a steady-state peak.

Lubrication of cartilage surfaces by pressurized interstitial fluid or boundary lubricants facilitate low friction during joint movement and may therefore affect the shear kinematics and sliding of articulating cartilage. At the onset of loading and/or motion, interstitial fluid within cartilage becomes pressurized and is forced between

articulating surfaces to bear normal load and reduce interaction between contacting surfaces, facilitating low friction [1]. After compression and stress relaxation to allow dissipation of hydrostatic pressure, the effects of boundary lubrication on articulating cartilage have been elucidated; synovial fluid (SF) and boundary lubricant molecules in SF reduce articular surface interaction as indicated by decreased friction [17, 18] and reduced surface shear strain (E_{xz}) [22]. In contrast, the replacement of SF lubricant with phosphate buffered saline (PBS) results in an elevation of boundary-mode friction [18] and surface E_{xz} [22]. Collectively, these studies suggest local and overall shear kinematics depends on both duration of loading (i.e., the time after onset and the extent of prolonged loading) and surface lubricant.

Cartilage degeneration may also affect shear deformation kinematics during joint movement. As cartilage undergoes degeneration, articular surfaces become fibrillated and roughened [14], which may lead to increased surface interaction between articulating cartilage surfaces. For articulating osteochondral blocks, peak cartilage E_{xz} near the surface increases with degeneration, while shear stiffness near the articular surface tends to decrease [22]. While shear deformation increases with degeneration, whether increased friction or deteriorating shear properties are responsible for such changes in shear mechanics remain unclear. By characterizing shear kinematics during cartilage articulation for both normal and degenerate tissues, the mechanism by which degeneration increases shear deformation may be further elucidated.

Tracking of fiducial markers using a video microscopy system provides an approach to elucidate local and overall shear deformation and strain of cartilage

during lateral-loading. Previously, a pair of osteochondral blocks were compressed in apposition and subjected to lateral shearing motion (Figure 3.1A) within physiologic range to mimic and study the biomechanical behavior of articulating cartilage at a micro-scale level after shear deformation reached a peak [22]. Samples were allowed to stress relax for 1 hour to replicate deformation and strain that likely occurs after prolonged cyclic loading and sliding, rather than that which occurs at the onset of cyclic loading. However with this configuration, shear deformation and strain can be captured during lateral-loading, as opposed to after reaching a peak. In addition, short stress-relaxation durations can be implemented to capture shear deformation that is likely representative of that occurring at the onset of cyclic loading. Thus, micro-scale analysis may be used to elucidate shear kinematics, locally and overall, during cartilage articulation near the onset or after prolonged cyclic loading.

Thus, the governing hypothesis of this study was that the shear kinematics of cartilage during joint articulation is affected by lubrication, cartilage degeneration, and stress relaxation duration. The specific objective of this study was to determine the effects of (1) lubrication (PBS versus SF), (2) degeneration (normal versus mildly degenerate), and (3) stress relaxation (5 min versus 60 min) on the shear deformation (tissue displacement) and shear strain (local and overall) of cartilage after compression and during applied lateral-loading in a cartilage-on-cartilage micro-scale shear test.

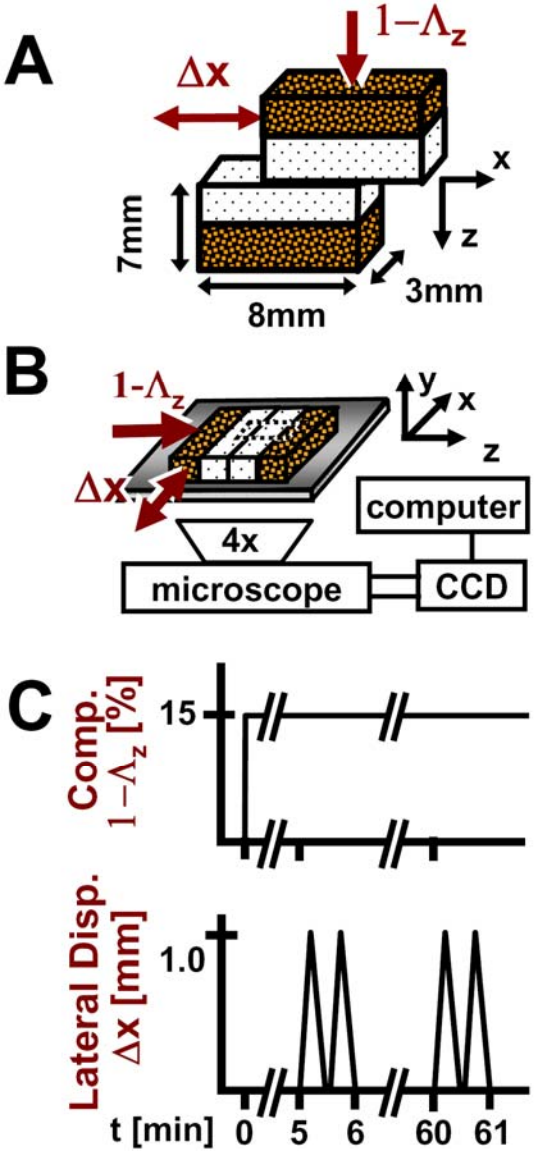

Figure 3.1: Schematics of (**A**) sample and testing configuration, (**B**) micro-shear test setup, and (**C**) loading protocol.

3.3 Materials and Methods

Sample Isolation

As previously described [22], 10 mm diameter osteochondral cores (n=6) were isolated, one each, from the anterior lateral femoral condyles of six fresh cadaveric human donors. Cores with grossly normal (NL, modified Outerbridge grade of 1 [23], n=3) or mildly degenerate (DGN; grade 3, n=3) surfaces were chosen from adult age groups of 41-60 yrs and >60 yrs, respectively. The cores were immersed in phosphate buffered saline (PBS) containing proteinase inhibitors (PI) and stored at -70^{o}C until use.

On the day of testing, each core was thawed in PBS+PI and prepared for testing. The cartilage of each core was scored vertically using a razor blade, and the bone was cut using a low-speed saw with a 0.3 mm thick diamond edge blade (Isomet^{TM}, Buehler, Lake Bluff, IL) to yield two rectangular blocks for micro-scale shear testing (Figure 3.1A). Each of the two blocks had a cartilage surface area of ~3x8 mm^2 and a total thickness of ~7 mm. From macroscopic images, thickness measurements were made at three separate locations and averaged to a yield a full cartilage thickness measurement for each sample.

Samples used in this study were characterized previously for histopathology [22], which confirmed the gross characterization of samples and the appropriate selection of NL and DGN samples for articulation testing. DGN samples exhibited structural (surface irregularity, vertical clefts to transitional zone, and transverse clefts) and cellular (cloning) features reflective of mild degeneration, while cellularity

and glycoaminoglycan staining were normal and similar between NL and DGN samples.

Experimental Design

Micro-scale shear testing was conducted as previously described [22]. First, samples were tested, as described below, with PBS+PI as a lubricant. Then, samples were allowed to re-swell in PBS+PI for ~4 h at 4^{o}C. Next, samples were tested again by micro-scale shear testing, this time with SF+PI as the lubricant. The SF was pooled from adult bovine knees, stored at -80^{o}C, and characterized previously for boundary lubrication properties [18] and for levels of lubricant molecules (~1 mg/ml of hyaluronan and 0.45 mg/ml of proteoglycan 4 [12]). The same regions of interest were imaged and analyzed.

Micro-scale Shear Testing:

Each sample consisted of paired osteochondral blocks and was mechanically tested as previously described [22]. Samples were bathed for ~14-18 h in test lubricant containing PI and propidium iodide (20 μg/ml) to fluorescently highlight cell nuclei at 4^{o}C prior to micro-shear testing.

Each pair of osteochondral blocks (Figure 3.1B) was then placed in a custom bi-axial loading chamber mounted onto an epi-fluorescence microscope for digital video imaging [3, 16] with cartilage surfaces in apposition. The bone of one block was secured while the apposing mobile block was allowed in-plane movement with orthogonally positioned plungers interfaced with either a micrometer (for axial

displacement; Model 262RL; Starrett Co., Athol, MA) or motion-controller (for lateral displacement; Model MFN25PP; Newport, Irvine, CA). Fluorescence images (Nikon G-2A filter) with a field of view of ~3×2 mm^2 were obtained at 5 frames/s, showing a full-thickness region of cartilage of the secured block and a partial-thickness region of cartilage of the apposing block.

Cartilage deformation was assessed similarly in the secured block during shear loading as previously described [22]. An axial displacement was applied (~40 μm/s) by the micrometer to induce 15% compression ($1-\Lambda_z$, where Λ_z is the stretch ratio [7]) of the overall cartilage tissue thickness (Figure 3.1B,C). After 5 minutes of stress relaxation, lateral motion was applied to the mobile osteochondral block (Figure 3.1B,C). Two sets of lateral displacements (Δx), each consisting of +1 mm and then −1 mm (returning to initial position), were applied at 100 μm/s to the bone portion of the mobile block. The first set, followed by a ~12 s pause, was for preconditioning [18], while the second set was recorded for analysis. The sliding velocity was chosen based on the range of velocities (0-0.1 m/s) occurring during the loading (stance) phase of gait [19, 21]. Subsequently, samples were then allowed to stress relax for a total of 60 minutes, and after, the two sets of lateral displacements were reapplied with shear deformation being recorded during the second set (Figure 3.1C). Experimentally, this duration of stress-relaxation was validated to be sufficient to reach a compressive equilibrium with load decreasing by 130 s to 50% of the peak, and load at one hour being only 3±1% (n=3) higher than the load at 16 hr. Before and during the application of lateral displacements (Figure 3.1B,C), sequential images,

with ~10 μm of lateral movement of the mobile block between frames, were taken to capture the shear deformation and sliding during cartilage articulation.

Data Analysis

Digital micrographs were analyzed to determine the depth-varying and overall shear strains (E_{xz}) in cartilage as previously described [22] during cartilage articulation and lateral-loading. Briefly, images were analyzed in MATLAB 7.0 (Mathworks, Inc., Natick, MA) using image routines developed previously [8]. First, an evenly distributed set of cell nuclei (~250 cell/mm^2), which served as fiducial markers, were selected and tracked by maximizing cross-correlation of regions surrounding each marker to the preceding, and then initial frames. Local affine mappings of nuclei at each captured frame were used to calculate the displacement of uniformly-spaced (10 pixel) mesh points in the region of interest (~1 mm × full thickness) during deformation. For each recorded image frame, displacement gradients were then determined by finite difference approximation, and in turn, used to determine Lagrangian shear strains (E_{xz}) after applied axial compression and during lateral shearing [6].

During applied lateral displacement (Δx), the calculated intra-tissue displacement (u) and shear strain (E_{xz}) were consolidated by first averaging and then interpolating values depth-wise. For each sample, u and E_{xz} at the same normalized depth (0, surface and 1, tidemark) were averaged and then interpolated linearly at every 0.05 times the normalized tissue thickness near the articular surface (i.e. 0 to 0.3) and 0.1 for remaining regions of the tissue depth (i.e. 0.3 to 1) after applied

compression and during lateral motion. To consolidate data further, u and E_{xz} values were averaged among samples to yield an average depth-profile during applied lateral displacement.

From depth-averaged intra-tissue displacements and shear strains, u and E_{xz} near the articular surface, overall E_{xz}, and Δx at 50% peak surface and overall E_{xz} were determined and used for further comparisons. Surface E_{xz} and u were defined as that occurring at the top 5% of the cartilage thickness. The overall Lagrangian E_{xz} was determined as half u near the articular surface (u_s) normalized to the compressed cartilage thickness. Surface and overall E_{xz} and u_s were determined at Δx increments of 0.1 mm (Δx ranging between 0 to 0.8 mm) to assess the kinematics of cartilage shear deformation during articulation. To assess and compare rates at which surface and overall E_{xz} reached equilibrium, Δx when surface or overall E_{xz} reached 50% the peak value were determined for all experimental cases.

Statistical Analysis

Data are reported as mean ± standard error of the mean (SEM), unless noted otherwise. Repeated measures ANOVA was used to determine the effects of stress relaxation (5, 60 min), applied lateral displacement (0-0.8 mm), lubricant (PBS, SF), and degeneration (NL, DGN) on tissue displacement and shear strain.

3.4 Results

Sample Characteristics

NL cores exhibited a glassy cartilage appearance with a smooth intact surface and had an average total tissue thickness of 1.86 ± 0.12 mm. Contrastingly, DGN cartilage appeared opaque with the surface being rough and fibrillated, and such samples had a slightly higher average tissue thickness of 2.08 ± 0.15 mm.

Cartilage Shear Deformation

As previously described [22], shear-loading resulted in a sequence of four events during cartilage articulation for all cases. (1) Initially at the onset of Δx, cartilage surfaces adhered and began to displace (color map boundaries, Figure 3.2) laterally in unison, initiating E_{xz} (color map, Figure 3.2) near the articular surface (Figure 3.2A-D, I-II). (2) With increasingly Δx, u and E_{xz} increased (Figure 3.2A-D, II). (3) Next, just as surfaces detached and slid relative to each another, cartilage u and E_{xz} peaked (Figure 3.2A-D, III). (4) With additional Δx, cartilage u and E_{xz} were maintained at steady-state peak (Figure 3.2A-D, IV). Effects of lubrication and degeneration on u_s (Figure 3.2A-D, i-iv) and E_{xz} (local and overall) were most apparent from these micrographs (Figure 3.2A-D, I-IV), and therefore, compared further.

Tissue displacement near the articular surface varied with Δx and was affected by degeneration, stress relaxation, and lubrication. With increasing Δx, magnitudes of

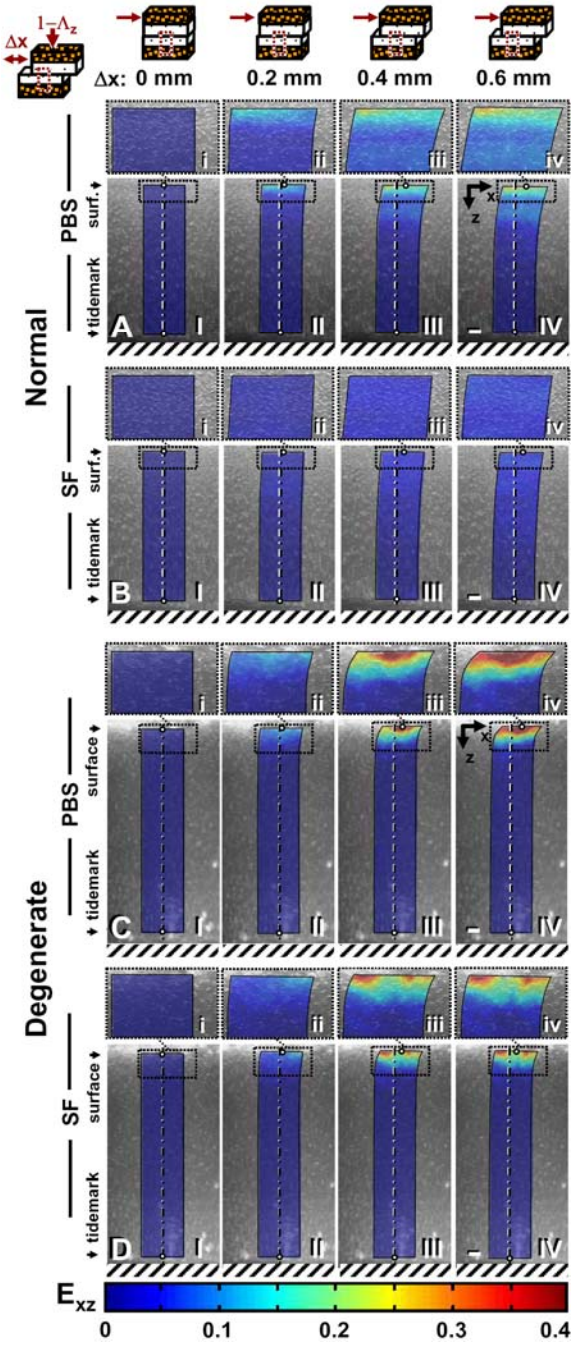

Figure 3.2: Micrographs taken during shear loading of apposing (**A,B**) normal and (**C,D**) degenerate samples lubricated with PBS (**A,C**) or SF (**B,D**) after 60 minutes of stress relaxation and (**I**) 0, (**II**) 0.2, (**III**) 0.4, and (**IV**) 0.6 mm of applied lateral displacement (Δx). Cell nuclei tracking method was used to determine (**I-IV**) maps of shear strain (color maps) with (**i-iv**) magnified views of the surface above. Bars = 150 mm.

u_s increased markedly ($p<0.001$), eventually reaching a maximum peak ranging from 50-125 μm and 120-170 μm for NL and DGN samples, respectively, for all experimental conditions (Figure 3.3). With degeneration, u_s was markedly higher ($p<0.05$) during lateral-loading for both test lubricants and stress relaxation durations. After a short 5 min stress relaxation period, differences due to lubrication in u_s were not apparent (Figure 3.3A) during shear-loading. While after 60 min of stress relaxation, u_s became significantly higher (interaction, $p<0.05$) when samples were tested in PBS than when tested with SF (Figure 3.3B) during applied lateral displacement (Δx) for both NL and DGN samples.

Cartilage E_{xz} during articulation varied with Δx and normalized tissue depth for both 5 and 60 min of stress relaxation. After 5 min of stress relaxation, E_{xz} was negligible throughout tissue depth when Δx is zero (Figure 3.4A). With increasing Δx, E_{xz} increased and became increasingly depth-varying (Figure 3.4B,C). At higher magnitudes of Δx, E_{xz} was highest near the articular surface and decreased monotonically with depth, becoming negligible near the tidemark (Figure 3.4D). Similar trends for cartilage E_{xz} were noted after 60 min of stress relaxation (Figure 3.4E-H). However, differences in depth-varying E_{xz} due to degeneration, lubrication, and stress relaxation became most apparent at higher magnitudes of applied lateral displacement.

Both surface and overall E_{xz} varied markedly with Δx and each was significantly affected by degeneration, lubrication, and/or stress relaxation. Similarly to u_s, surface E_{xz} increased significantly ($p<0.001$) with Δx for all cases, eventually

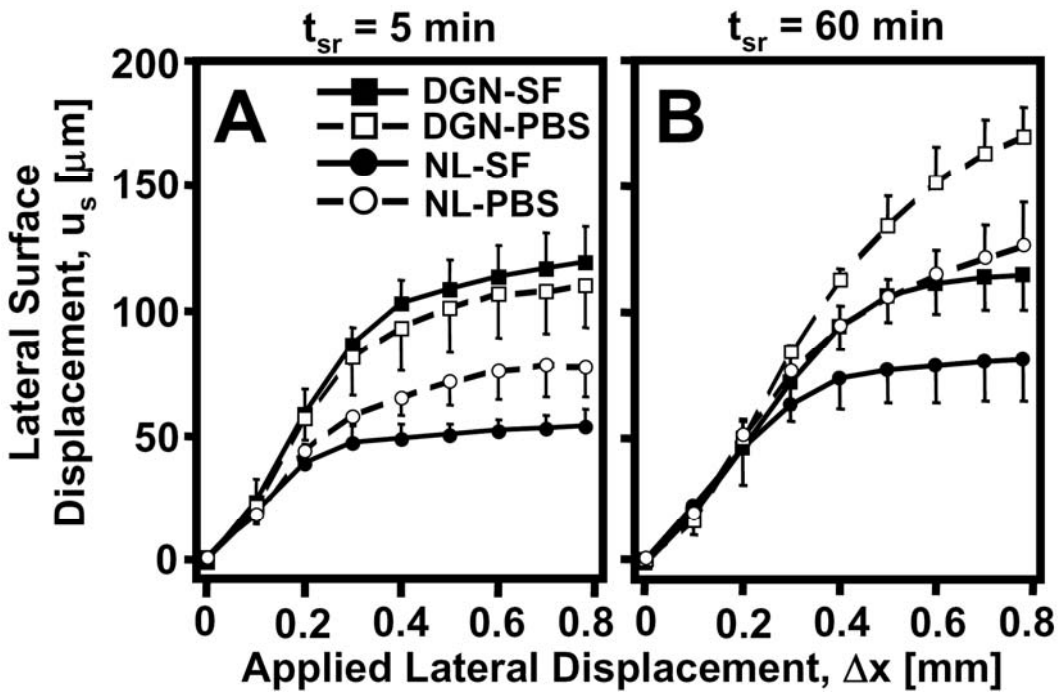

Figure 3.3: Lateral surface displacement (u_s) versus applied lateral displacement (Δx) for normal (NL: ●,○) and degenerate (DGN: ■,□) cartilage after (**A**) 5 and (**B**) 60 minutes of stress relaxation time (t_{sr}). Samples were tested with phosphate buffered saline (PBS: ○,□) and synovial fluid (SF: ●,■).

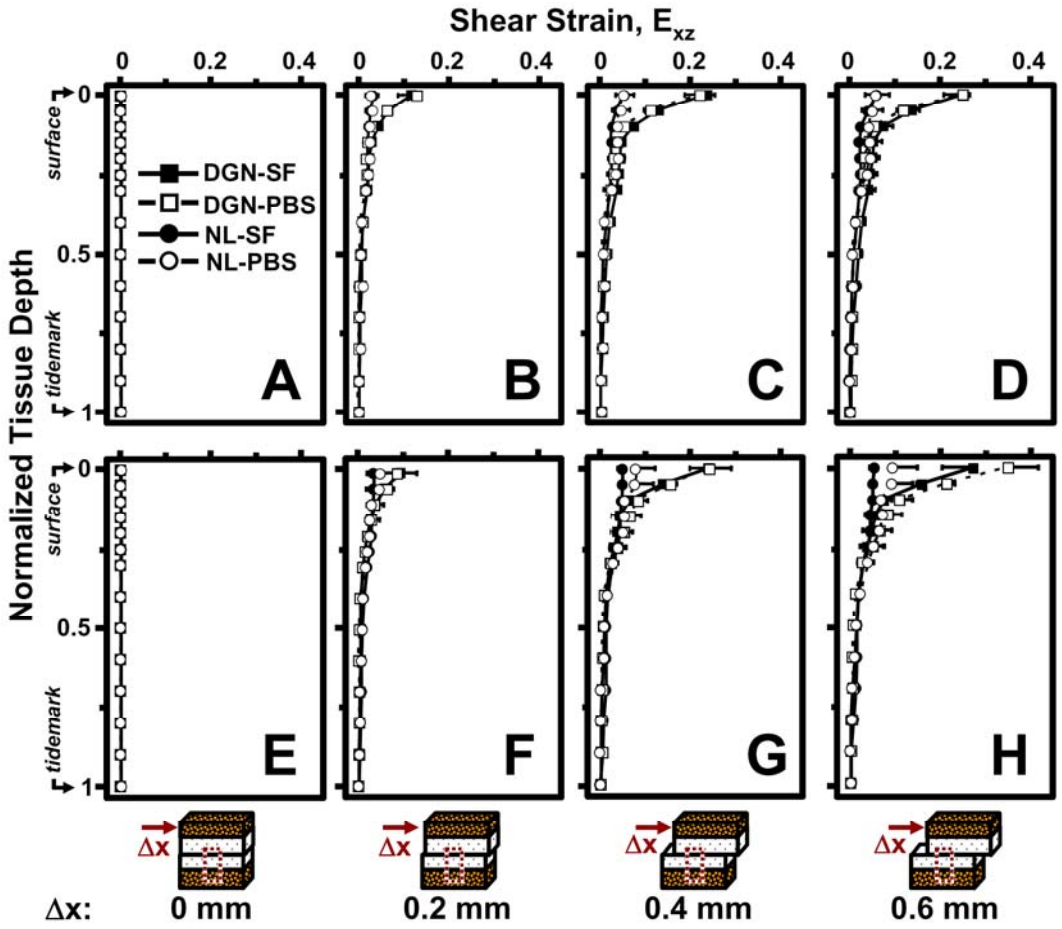

Figure 3.4: Local shear strain, E_{XZ}, versus normalized tissue depth for normal (NL: ●,○) and degenerate (DGN: ■,□) cartilage after 5 (**A-D**) and 60 (**E-H**) minutes of stress relaxation and (**A,E**) 0, (**B,F**) 0.2, (**C,G**) 0.4, and (**D,H**) 0.6 mm of applied lateral displacement (Δx). Samples were tested with phoshate buffered saline (PBS: ○,□) and synovial fluid (SF: ●,■).

reaching a peak maximum (Figure 3.5A,B). During shear-loading, the E_{xz} near the articular surface for DGN samples was significantly higher ($p<0.05$) than NL samples for all lubricant (PBS, SF) and stress relaxation (5, 60 min) conditions. After 5 min of stress relaxation, differences in surface E_{xz} during lateral-loading due to lubrication were not apparent for both NL and DGN samples (Figure 3.5A). However, after 60 min of stress relaxation, surface E_{xz} during articulation was markedly higher when PBS was used as a lubricant than when SF, for both NL and DGN samples (interaction, $p<0.001$). Overall E_{xz} showed similar trends, increasing significantly with Δx ($p<0.001$) and when samples were tested with PBS as a lubricant and were allowed to stress relax for 60 min (interaction, $p<0.001$) (Figure 3.5C,D). However, overall E_{xz} was not detectably different between NL and DGN samples during shear-loading ($p=0.2$) for all cases.

To assess the rate at which surface and overall E_{xz} reached their peaks during articulation, Δx at 50% peak E_{xz} ($\Delta x_{1/2}$) were determined and significantly varied with lubricant and stress relaxation. Differences in $\Delta x_{1/2}$ for surface ($p=0.5$) and overall ($p=0.4$) E_{xz} were not apparent between NL and DGN samples for all lubricant and stress relaxation conditions (Figure 3.6A-D). However, $\Delta x_{1/2}$ for surface E_{xz} markedly increased with PBS as lubricant in a stress-relaxation dependent manner (interaction, $p<0.05$). After 5 min of stress relaxation, surface $\Delta x_{1/2}$ was not detectably different ($p=0.4$) when samples were tested with PBS or SF as lubricant (Figure 3.6A). However after 60 min of stress relaxation, surface $\Delta x_{1/2}$ was 30-50% higher ($p<0.01$) with PBS than with SF as a lubricant (Figure 3.6B). Similar trends were also observed

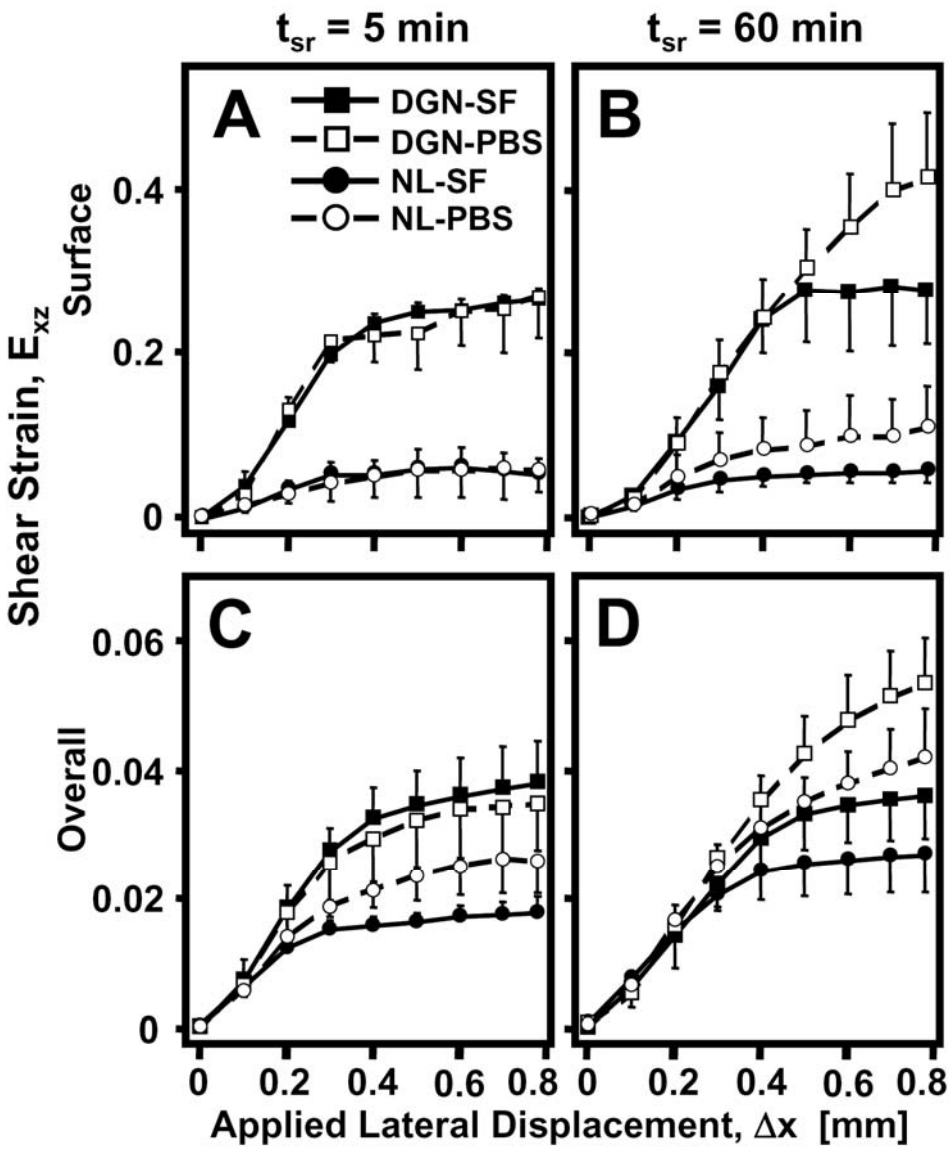

Figure 3.5: (**A,B**) Surface and (**C,D**) overall shear strain, E_{xz}, versus applied lateral displacement (Δx) for normal (NL: ●,○) and degenerate (DGN: ■,□) cartilage after (**A,C**) 5 and (**B,D**) 60 minutes of stress relaxation time (t_{sr}). Samples were tested with phoshate buffered saline (PBS: ○,□) and synovial fluid (SF: ●,■).

for overall $\Delta x_{1/2}$ (Figure 3.6C,D). When PBS lubricant was used, $\Delta x_{1/2}$ for overall E_{xz} was significantly higher than with SF in a stress-relaxation dependent-manner (interaction, $p<0.01$), being 25-40% greater ($p<0.05$) with PBS than SF after 60 min of stress relaxation (Figure 3.6D).

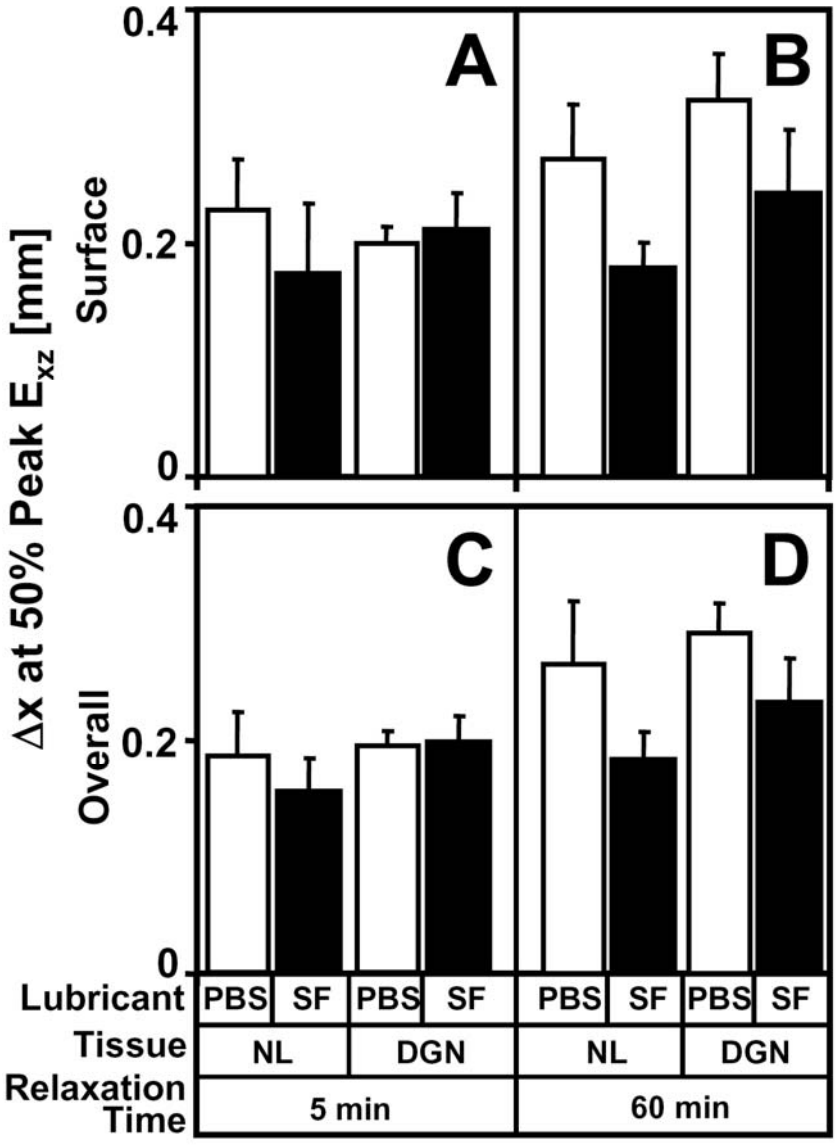

Figure 3.6: Effect of lubricant (synovial fluid and PBS), degeneration (normal and degenerate), and stress relaxation time (5 and 60 minutes) on (**A**) surface and (**B**) overall $\Delta x_{1/2}$ at 50% peak E_{xz} ($\Delta x_{1/2}$).

3.5 Discussion

This study elucidated the shear kinematics of cartilage-on-cartilage compression and sliding and suggests that during cartilage-on-cartilage articulation four sequential events occur (Figure 3.7). Initially when apposing cartilage layers are compressed against one another, adherence between articulating surfaces develops (Figure 3.7 A-I, B-I). With applied lateral displacement, the surfaces remain adhered; and as a result, the two cartilage layers behave as one contiguous tissue layer, and shear deformation increases in both cartilage layers (Figure 3.7 A-II, B-II). With continued applied lateral displacement, shear deformation continues to increase and eventually peaks just as the cartilage surfaces detach (Figure 3.7 A-III, B-III). With further applied lateral displacement, the articular surfaces slide across one another and peak shear deformation is maintained in both layers as the apposing cartilage layers undergo relative motion at the articular surfaces (Figure 3.7 A-IV, B-IV).

The effects of lubrication, mild degeneration, and stress relaxation on shear kinematics of cartilage-on-cartilage articulation were also found to be marked. With increasing Δx, u_s and E_{xz} increased and peaked when surfaces began to slide, indicated by a plateau in E_{xz} despite increasing Δx (Figure 3.7B). The effect of lubrication was not apparent on shear deformation during lateral-loading after 5 min of stress relaxation (Figure 3.5A,C; 3.6A,C). However, after 60 min of stress relaxation, peak E_{xz} and $\Delta x_{1/2}$ increased with PBS as lubricant by ~100% and ~30-50% near the surface (Figure 3.5B; 3.6B) and ~55% and ~25-40% overall (Figure 3.5D; 3.6D), respectively. When DGN samples were tested, E_{xz} near the surface was consistently higher than NL

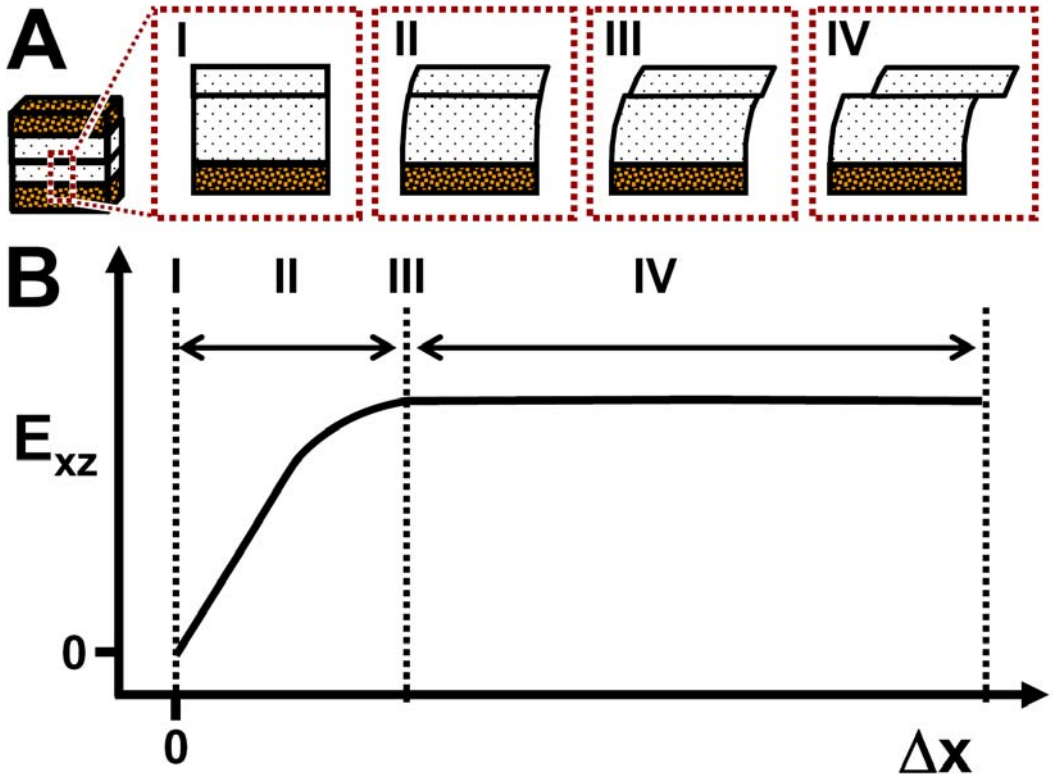

Figure 3.7: Four sequential events, (**I**) adherence, (**II**) adherence and shear deformation, (**III**) detachment as shear deformation peaks, and (**IV**) sliding with maintenance of shear deformation, that occurs during cartilage-on-cartilage articulation. (**A**) Schematic and (**B**) where these events occur in a representative shear strain (E_{xz}) versus applied lateral displacement (Δx) diagram.

samples during lateral motion and were ~3-5 times higher at peak, being independent of stress relaxation duration and lubricant (Figure 3.5A,B).

The testing protocol used in this study mimics certain aspects of the compression and sliding of articular cartilage during normal joint loading. Cartilage within the knee undergoes a wide range of dynamic compression (5-20%) during normal activities [4, 9] and sliding up to ~50 mm (estimated from [19, 21]). The loading parameters used in this study mimic the high compressive loading and low sliding velocity events of gait, such as contralateral toe-off and heel rise [21]. During such time, interaction of opposing articular surfaces is likely to be initiated and high. At the onset of cyclic loading, interstitial fluid within cartilage pressurizes and bears the majority of the load [1]. After prolonged cyclic loading, cartilage gradually depressurizes and reaches an averaged steady-state compression [15]. In this study, samples were allowed to stress-relax for both 5 and 60 minutes. As a result, the pattern of cartilage deformation and strain for short and prolonged stress-relaxation times are likely to be representative of that occurring near the onset and after prolonged cyclic loading, respectively.

The interactive effects of lubrication and stress relaxation time on cartilage shear kinematics is consistent with a transition in the dominating lubrication mode from interstitial fluid pressurization to boundary-mode during loading. Near the onset of compression, pressurized interstitial fluid between articular surfaces bears normal loads and offers little resistance to shear loads [1]. As a result, cartilage E_{xz} will be low regardless of lubricant near the onset of compression (Figure 3.5A,C). With prolonged compression, hydrostatic pressure of cartilage and the interstitial fluid

between articular surfaces dissipates [10]. At this point, direct surface-to-surface contact increases and bears a greater share of the normal load, and thus, resistance to shear loads becomes increasingly dependent on the presence/absence of boundary lubricants [13]. Therefore, cartilage E_{xz} would be predicted to increase with the use of PBS, which is devoid of boundary lubricants, after prolonged compression, being consistent with the present results.

The reduction in E_{xz} with SF as lubricant after prolonged compression is consistent with predictions that account for past studies on cartilage boundary-mode friction. Synovial fluid decreases boundary-mode friction between articulating cartilage surfaces compared to saline[17, 18], and thus, reduces interaction between surfaces during articulation. As a result, cartilage surfaces would be predicted to slide at lower magnitudes of Δx with SF as lubricant than saline and result in a reduced peak tissue E_{xz}. After prolonged stress relaxation, $\Delta x_{1/2}$ was significantly lower for SF than PBS (Figure 3.6B,D), indicating tissue E_{xz} reached a peak sooner when SF was a lubricant. In addition, peak tissue E_{xz} was markedly decreased with SF at this time (Figure 3.5B,D). Collectively, such results suggest that surfaces slid sooner when SF was used as lubricant once hydrostatic pressure dissipated, which resulted in lowering tissue E_{xz}.

The increase in E_{xz} with degeneration, particularly near the articular surface (Figure 3.5A,B) with SF as a lubricant, is likely due to a reduction in tissue shear stiffness (modulus) and less likely due to an increase in cartilage friction. Magnitudes of E_{xz} near the articular surface were consistently greater in DGN than NL cartilage for each applied lateral displacement (Figure 3.5A,B). Such results would suggest a

reduction in shear modulus near the articular surface, which agree with previously reported results [22], because shear modulus is estimated as an increment in shear load divided by an increment in E_{xz}.. While roughened surfaces may lead to greater shear deformation by increasing surface interaction and thus friction, greater shear with roughened surfaces may occur only if roughened surfaces slide at greater applied lateral loads than smooth surfaces. The present results indicate no apparent differences in $\Delta x_{1/2}$ between DGN and NL cartilage (Figure 3.6), suggesting DGN and NL cartilage slid at approximately the same point during lateral motion. Thus, friction was likely similar between the DGN and NL surfaces and did not contribute to increasing cartilage shear.

While the present results indicate the increase in shear deformation for DGN samples was due to a loss in shear stiffness, the cause (i.e., relative roles of friction and reduced shear modulus) of elevated shear with degeneration remains to be elucidated. Immediately following cartilage injury or wear, surface irregularities, such as chondral lesions, cracks, and focal defects, may result without any signs of fibrillation and apparent changes to the mechanical stiffness of cartilage. At this time, however, surface irregularities may increase roughness, and thus friction, causing surfaces to slide later than normal smooth surfaces which lead to elevated shear deformation. With continued loading over time (on the order of years), fibrillation may eventually develop that changes matrix structure and result in a decrease in mechanical stiffness and elevate shear deformation. Samples used in the present study were mildly degenerate, characterized by surface roughening and fibrillation, which likely is a result of years of loading following initial wear or injury. Thus, for DGN

samples in this study, increased shear deformation was likely a result of decreased shear stiffness, while if DGN samples were taken immediately following injury or wear, elevated shear deformation would likely result from increased friction.

Collectively, this study provides insight into the effects of lubrication, degeneration, and stress relaxation on the shear kinematics of cartilage during joint articulation and its implications for cartilage degeneration. The present results suggest with prolonged loading, boundary lubricants modulate shear deformation by regulating when surfaces slide (sooner or later) during lateral motion. This is particularly important since SF's boundary-lubricating function is markedly reduced in acute injury [5], which could cause surfaces to detach later during lateral movement and lead to elevated shear strain. In addition, degeneration results in increased shear strain despite normal SF lubricant function and duration of loading. Excessive magnitudes of compressive strain result in mechanical injury to cells [2, 11] and matrix [2, 20], which is likely similar for high E_{xz} magnitudes, predisposing cartilage to osteoarthritis and wear. Thus, development of treatments that not only restore mechanical integrity, but also restore SF lubricant function, may be critical in preventing shear-induced cartilage degradation and accelerated wear.

3.6 Acknowledgments

We like to thank co-authors Dr. Won C. Bae and Kenneth Gratz for their contributions to this work. We thank the many residents and staff of the Lotz Lab of the Scripps Research Institute of La Jolla for harvesting and providing the human tissue used in this study. This work was supported by the San Diego Fellowship for Benjamin L. Wong and the NIH and Howard Hughes Medical Institute through the Professors Program Grant to UCSD for Dr. Robert L. Sah.

3.7 References

1. Ateshian GA, Mow VC: Friction, lubrication, and wear of articular cartilage and diarthrodial joints. In: *Basic Orthopaedic Biomechanics and Mechano-Biology,* ed. by VC Mow, Huiskes R, Lippincott Williams & Wilkins, Philadelphia, 2005, 447-94.

2. Chen C-T, Bhargava M, Lin PM, Torzilli PA: Time, stress, and location dependent chondrocyte death and collagen damage in cyclically loaded articular cartilage. *J Orthop Res* 21:888-98, 2003.

3. Chen SS, Falcovitz YH, Schneiderman R, Maroudas A, Sah RL: Depth-dependent compressive properties of normal aged human femoral head articular cartilage: relationship to fixed charge density. *Osteoarthritis Cartilage* 9:561-9, 2001.

4. Eckstein F, Lemberger B, Stammberger T, Englmeier KH, Reiser M: Patellar cartilage deformation in vivo after static versus dynamic loading. *J Biomech* 33:819-25, 2000.

5. Elsaid KA, Jay GD, Warman ML, Rhee DK, Chichester CO: Association of articular cartilage degradation and loss of boundary-lubricating ability of synovial fluid following injury and inflammatory arthritis. *Arthritis Rheum* 52:1746-55, 2005.

6. Fung YC. A First Course in Continuum Mechanics. 2nd ed. Englewood Cliffs: Prentice-Hall; 1977.

7. Fung YC. Biomechanics: Mechanical Properties of Living Tissues. 2nd ed. New York: Springer-Verlag; 1993.

8. Gratz KR, Sah RL: Experimental measurement and quantification of frictional contact between biological surfaces experiencing large deformation and slip. *J Biomech* 41:1333-40, 2008.

9. Kersting UG, Stubendorff JJ, Schmidt MC, Bruggemann GP: Changes in knee cartilage volume and serum COMP concentration after running exercise. *Osteoarthritis Cartilage* 13:925-34, 2005.

10. Krishnan R, Kopacz M, Ateshian GA: Experimental verification of the role of interstitial fluid pressurization in cartilage lubrication. *J Orthop Res* 22:565-70, 2004.

11. Loening A, Levenston M, James I, Nuttal M, Hung H, Gowen M, Grodzinsky A, Lark M: Injurious mechanical compression of bovine articular cartilage induces chondrocyte apoptosis. *Arch Biochem Biophys* 381:205-12, 2000.

12. Mazzucco D, Scott R, Spector M: Composition of joint fluid in patients undergoing total knee replacement and revision arthroplasty: correlation with flow properties. *Biomaterials* 25:4433-45, 2004.

13. McCutchen CW: Boundary lubrication by synovial fluid: demonstration and possible osmotic explanation. *Fed Proceedings* 25:1061-8, 1966.

14. Meachim G, Emery IH: Quantitative aspects of patello-femoral cartilage fibrillation in Liverpool necropsies. *Ann Rheum Dis* 33:39-47, 1974.

15. Neu CP, Hull ML, Walton JH: Heterogeneous three-dimensional strain fields during unconfined cyclic compression in bovine articular cartilage explants. *J Orthop Res* 23:1390-8, 2005.

16. Schinagl RM, Gurskis D, Chen AC, Sah RL: Depth-dependent confined compression modulus of full-thickness bovine articular cartilage. *J Orthop Res* 15:499-506, 1997.

17. Schmidt TA, Gastelum NS, Nguyen QT, Schumacher BL, Sah RL: Boundary lubrication of articular cartilage: role of synovial fluid constituents. *Arthritis Rheum* 56:882-91, 2007.

18. Schmidt TA, Sah RL: Effect of synovial fluid on boundary lubrication of articular cartilage. *Osteoarthritis Cartilage* 15:35-47, 2007.

19. Shelburne KB, Torry MR, Pandy MG: Muscle, ligament, and joint-contact forces at the knee during walking. *Med Sci Sports Exerc* 37:1948-56, 2005.

20. Thibault M, Poole AR, Buschmann MD: Cyclic compression of cartilage/bone explants in vitro leads to physical weakening, mechanical breakdown of collagen and release of matrix fragments. *J Orthop Res* 20:1265-73, 2002.

21. Whittle M. Gait Analysis: An Introduction. 3rd ed. Oxford; Boston: Butterworth-Heinemann; 2002.

22. Wong BL, Bae WC, Chun J, Gratz KR, Sah RL: Biomechanics of cartilage articulation: effects of lubrication and degeneration on shear deformation. *Arthritis Rheum* 58:2065-74, 2008.

23. Yamada K, Healey R, Amiel D, Lotz M, Coutts R: Subchondral bone of the human knee joint in aging and osteoarthritis. *Osteoarthritis Cartilage* 10:360-9, 2002.

CHAPTER 4

CARTILAGE MECHANICS DURING TIBIO-FEMORAL ARTICULATION: LOCAL AND OVERALL COMPRESSIVE AND SHEAR DEFORMATION AND PROPERTIES

4.1 Abstract

Objective: During knee movement, femoral cartilage articulates against cartilage from the tibial plateau, and the resultant mechanical behavior has yet to be fully characterized. The objectives of this study were to determine 1) the overall and depth-varying axial and shear strains, and 2) the associated moduli, of femoral and tibial cartilage during the compression and shearing of apposing tibial and femoral samples.

Methods: Osteochondral blocks from human lateral femoral condyles (LFC) characterized as normal and donor-matched lateral tibial plateau (LTP) were apposed, compressed 13%, and subjected to relative lateral motion. When surfaces began to slide, axial ($-E_{zz}$) and shear (E_{xz}) strains and compressive (E) and shear (G) modulus, overall and as a function of depth, were determined for both LFC and LTP.

Results: For LFC and LTP, $-E_{zz}$ was greatest near the surface and decreased monotonically with depth. LTP $-E_{zz}$ was 2-fold that of LFC near the surface and

overall. Similarly, E_{xz} was greatest near the surface and decreased with depth. Near the articular surface, E_{xz} of LTP was 8-fold higher than LFC, while overall E_{xz} for LTP was 4-fold higher. E for LFC was 1.7-fold greater than LTP, both near the surface (0.40 versus 0.24MPa) and overall (0.76 versus 0.47MPa). Similarly, G was 7-fold greater for LFC (0.22MPa) than LTP near the surface (0.03MPa) and 3-fold higher for LFC (0.38MPa) than LTP (0.13MPa) overall.

Conclusion: These results indicate that tibial cartilage deforms and strains more axially and in shear than the apposing femoral cartilage during tibio-femoral articulation, reflecting their respective moduli.

4.2 Introduction

Articular cartilage articulates against each other in the knee to biomechanically facilitate joint movement [15]. During knee movement, cartilage lining the femoral condyle contacts, compresses, and slides against tibial cartilage (Figure 4.1A). To reveal cartilage mechanical properties and deformation in response to loading, cartilage samples are typically tested *in vitro* and against non-biologic counter-platens in confined [16, 20] and unconfined compression [5, 12], torsion [33], and shear [4]. Since physiologically, cartilage articulates against cartilage, and resultant deformation may depend upon the mechanical behavior of the counter-articulating surface, mechanical tests that load physiologically apposing cartilage surfaces (i.e. femoral against tibial cartilage) would be useful to elucidate cartilage deformation, and its associated mechanical properties, that occurs during joint loading.

In response to physiologic loading, knee cartilage deforms, and resultant magnitudes vary with joint location and tissue depth. Following various physical activities such as knee bending, impact loading, and running, cartilage compresses ~3-20% of the overall thickness [6, 13, 27] with compression typically being higher in tibial than femoral cartilage [6, 13]. Such differences in deformation between cartilage regions reflect differences in stiffness, with femoral cartilage being stiffer than tibial cartilage [14]. Moreover, cartilage stiffness varies across the surface of the femoral [2, 24] and tibial [15] joint. During cartilage-on-cartilage articulation, axial and shear deformation varies with depth, being highest near the surface and becoming minimal near the tidemark [30, 31]. Collectively, these results suggest deformation of femoral

and tibial cartilage is markedly different, overall and locally, during tibio-femoral articulation.

Recently, cartilage deformation during cartilage-on-cartilage articulation was elucidated [30, 31] using video microscopy [21] and image correlation to track the displacement of fidicial markers [10, 28]. With this experimental approach, a pair of osteochondral blocks were compressed in apposition and subjected to lateral shearing motion to mimic the biomechanical environment during joint movement. Resultant compressive and shear strains of cartilage were determined locally and overall with a resolution sufficient to resolve small magnitudes (~1%) of strain. In addition, measurements of strain and stress were combined to determine local and overall shear modulus. However, such studies examined articulation mechanics in a simplified geometry, with the apposing cartilage samples being from the femoral condyle. Using this configuration, osteochondral samples from the tibia and femoral condyle can be apposed (Figure 4.1B) and tested to examine the mechanics of tibio-femoral articulation (Figure 4.1C) to extend previous findings and further the understanding of cartilage mechanics during joint movement.

Thus, the hypothesis of this study was that during tibio-femoral articulation, the deformation, and its associated properties, of tibial cartilage is markedly different from femoral cartilage. To test this hypothesis, the objectives of this study were to determine the overall and depth-varying axial and shear strains, as well as the associated overall and depth-varying moduli, of tibial and femoral cartilage during compression and shear.

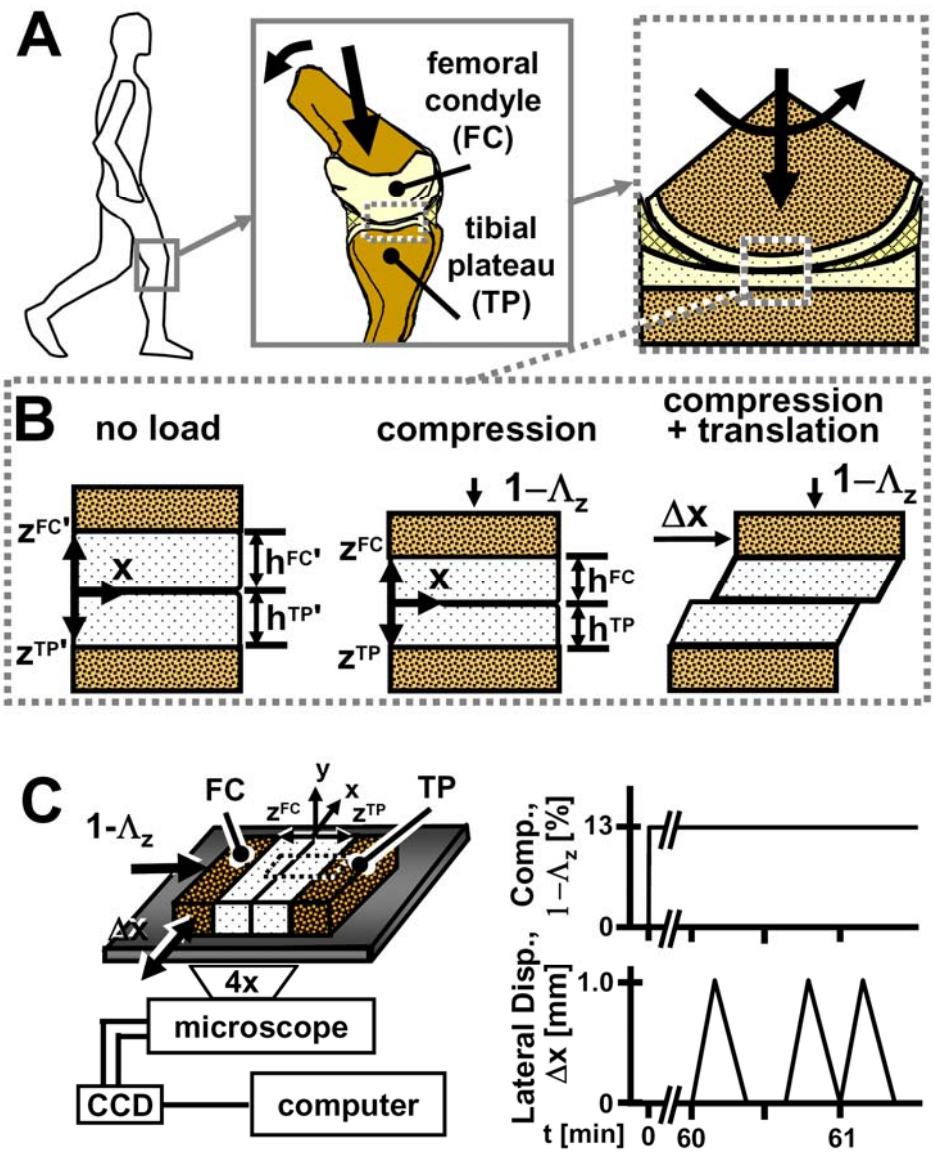

Figure 4.1: Schematic of (**A**) knee joint movements at multiple scales and (**B**) deformation of cartilage under (from left to right) no load, compression, and compression + shear loading. Schematic of (**C**) experimental setup and loading protocol for micro-scale testing.

4.3 Materials and Methods

Sample Isolation

Six osteochondral cores (each with a 10mm diameter) were isolated, one each, from the anterior lateral femoral condyle (LFC) of six fresh cadaveric human donors (mean±SEM: 46±1.5 yrs). Additionally, six osteochondral blocks (each with a chondral area of ~1cm^2) were harvested from the region of the donor-matched lateral tibial plateau (LTP) not covered by the meniscus. LFC cores with grossly normal surfaces (modified Outerbridge grade of 1 [32]) were selected, while all donor-matched LTP blocks displayed mild surface fibrillation and were grades 2-3. The specimens were immersed in phosphate buffered saline (PBS) containing proteinase inhibitors (PI) [7] and stored at -70^{o}C until use.

Experimental Design

On the day of testing, the osteochondral specimens were thawed and further processed. The LFC core and LTP block were each trimmed as previously [30] using a low-speed saw (Isomet^{TM}, Buehler, Lake Bluff, IL) to yield an osteochondral fragment for histopathologic analysis and one ~rectangular block for biomechanical testing. Each rectangular block had a cartilage surface area of ~3x8mm^2 and a total thickness of ~1cm. Samples of paired one LFC and one donor-matched LTP block were created with the 8mm lengths being parallel to the direction of joint articulation.

Histopathology

Histopathologic analysis was utilized to confirm macroscopic assessments as previously described [30]. Briefly, LFC and LTP fragments were fixed in 4% paraformaldehyde (USB Corporation, Cleveland, OH) in phosphate buffered saline (PBS) at pH 7.0 for 24 h, decalcified with 18% disodium ethylenediamine tetraacetate in (Fisher Scientific, S311-500) PBS for 7 d, and sectioned to 7 μm using a cryostat. To highlight cellular detail, some sections were stained with hematoxylin and eosin [18], while others were stained with Alcian blue [23] to localize sulfated glycosaminoglycans. Transmitted light micrographs of stained sections were obtained and analyzed for histopathology [3] using the Mankin-Shapiro semi-quantitative scale [25]. Briefly, the histopathologic characteristics included structural integrity (surface irregularity and vertical and horizontal clefts), cellularity (cloning and hypocellularity), and glycosaminoglycan loss. Relatively high scores represented more degenerated cartilage. For each sample, grades from three independent observers were averaged. Inter-observer errors (standard deviation) for LFC and LTP samples were reasonably small, being an average of 0.65 and 1.22, respectively.

Biomechanical Testing

Samples were first tested by micro-scale testing with PBS+PI as lubricant. Following re-swelling at 4^{o}C for ~16h, samples were then tested in a macro-scale system to assess overall cartilage mechanical properties.

Micro-scale Shear Testing Each sample was micro-scale tested as previously described [30]. Briefly, samples were first bathed for ~14-18h at 4^{o}C in PBS+PI and

propidium iodide (20μg/ml) to fluorescently highlight cell nuclei. Each sample was then secured in a custom bi-axial loading chamber mounted onto an epi-fluorescence microscope for digital video (Figure 4.1C). The chamber secured the LTP block at the bone and allowed in-plane movement of the apposing LFC block with orthogonally positioned plungers.

Cartilage deformation was assessed separately in both the LFC and LTP blocks during axial and shear loading. First, an axial displacement was applied (~40μm/s) to induce 13% compression ($1-\Lambda_z$, where Λ_z is the stretch ratio [9]) of the overall cartilage thickness (Figure 4.1B,C), during which time sequential fluorescence images were acquired (~1.5% compression increment/frame). Then, samples were allowed to stress relax for 1h which was confirmed to be sufficient to reach an approximate equilibrium stress for the current sample geometries [30]. Subsequently, three sets of lateral displacements (Δx), each consisting of +1mm and then −1mm (returning to initial position), were applied (100μm/s) to the bone portion of the LFC block. The first set was for preconditioning [22], while the second and third sets were recorded for viewing the LTP and LFC blocks, respectively. Deformation during the application of lateral displacements (Figure 4.1C) was captured with sequential fluorescence images at 3 frames/s.

Macro-Scale Shear Testing: The overall compressive and shear properties of LFC and LTP cartilage were assessed independently by subjecting each block to macro-scale tests as described previously [30]. Test conditions were chosen to match the mechanical deformation resulting in micro-scale tests but with instrumentation

allowing measurement of axial and shear loads. Each block was affixed in a bi-axial mechanical tester (Mach-1^{TM} V500CS, BioSyntech Canada, Montreal) in PBS+PI, compressed to a magnitude (0.03 %/s) matching that in micro-scale tests using a rigid stainless steel platen (~2μm pore size, providing a no-slip boundary condition), and allowed to stress relax for 1h. Resultant equilibrium force was recorded and used to yield an estimate equilibrium compressive stress. Next, three sets of lateral displacements of the surface amplitude during sliding in micro-scale tests were applied (100μm/s), held for 10s, and then released. Similar to micro-scale tests, the first set was for preconditioning, while the third set was for analysis. The lateral displacements were then repeated in the reverse direction, and shear loads occurring in the last second of load-capture in both directions were averaged and used to yield an estimate shear stress.

Data Collection and Calculations

Digital micrographs from micro-scale tests were analyzed as previously described [10, 30] to determine the depth-varying and overall strains in cartilage. During deformation, evenly distributed cell nuclei (~250 cells/mm^2) served as fiducial markers and were tracked to calculate the displacement and displacement gradients of uniformly-spaced (10 pixel) mesh points in the region of interest (~1mm × full thickness). From this data, Lagrangian compressive strains ($-E_{zz}$) at compressive equilibrium, and shear strains relative to the compressed (E_{xz}) and uncompressed cartilage thickness ($E_{xz'}$) at compressive equilibrium and during relative lateral motion were determined [8].

To assess depth-variation and compare strains, local strains were averaged depth-wise and plotted as a function of tissue depth. Sample thickness was normalized and divided into 8 intervals, with 4 intervals being 0.083 times the normalized thickness near the articular surface (i.e. 0 to 0.333) and 0.167 times for the remaining tissue depth (i.e. 0.333 to 1). To reduce noise and consolidate data, strains were averaged at the same normalized depth interval to yield a depth-profile.

Overall axial and shear strains as well as the overall compressive (E) and shear modulus were determined as previously described [30]. For this study, shear moduli were determined relative to the compressed (G_1) and uncompressed (G_0) cartilage thickness. In addition, the depth-varing compressive and shear moduli were also estimated from the overall respective moduli and local strain for each sample [30].

Statistical Analysis

Data are reported as mean ± standard error of the mean (SEM). Repeated measures ANOVA was used to determine the effects of normalized tissue depth (0-1, surface-bone) and location (LFC, LTP) on tissue strain and modulus. Planned pair-wise comparisons were used to assess differences between LFC and LTP groups for strains and moduli near the surface and overall. Modulus data were log transformed before analysis to adjust for sample variances that were proportional to amplitude.

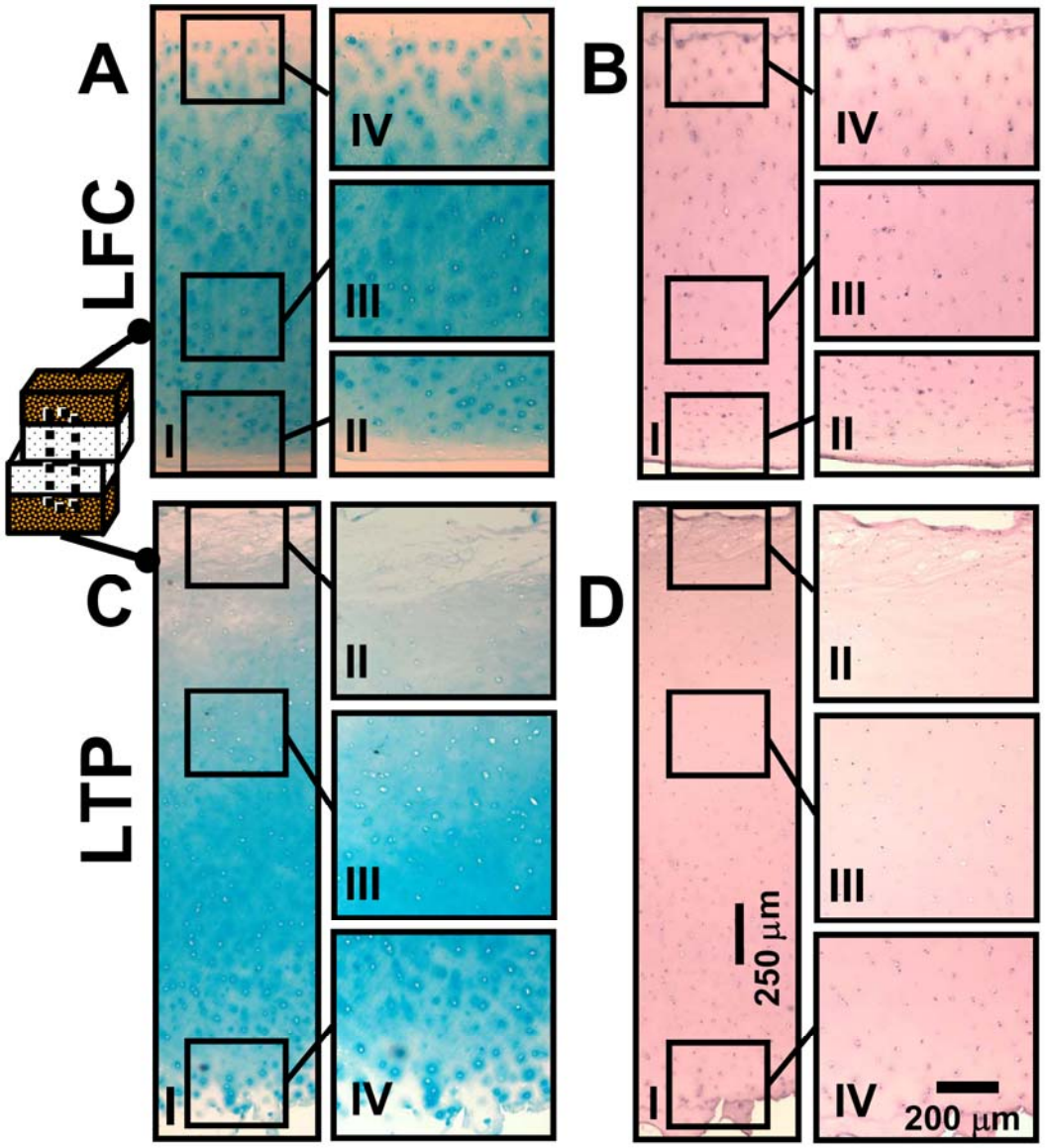

Figure 4.2: Representative micrographs of LFC (**A, B**) and LTP (**C**, **D**) cartilage in apposition and stained with Alcian blue (**A**, **C**) and H&E (**B**, **D**) showing structural and cellular detail of the full thickness (**I**), superificial (**II**), middle (**III**), and deep (**IV**) regions.

4.4 Results

Sample Thickness and Histopathology

Cartilage in LTP samples was generally thicker than LFC, and the overall histopathology scores were consistent with their gross and histological appearances (Figure 4.2). LTP cartilage had an average thickness of 2.88 ± 0.53mm, while LFC cartilage was 2.20 ± 0.15mm in thickness. The histopathology score of 6.44 ± 0.72 for LTP samples was significantly higher ($p<0.01$) than the LFC score of 1.83 ± 0.39. For LTP samples, structural features (surface irregularity and transverse clefts) exhibited mild degeneration and GAG loss was apparent, which resulted in scores being ~1-point higher than those for LFC samples. In contrast, cellularity and cloning scores were similarly low (i.e. normal) between LFC and LTP samples.

Deformation: Axial Strains

At compressive equilibrium, $-E_{zz}$ decreased significantly with depth from the articular surface ($p<0.001$) for both locations (Figure 4.3A,B,D,E) and was lower in magnitude in the LFC (Figure 4.3A,B) than LTP cartilage (Figure 4.3D,E). The axial displacements of the articular surface relative to the tidemark was on average 507 ± 92 and 169 ± 17μm for LTP and LFC samples, respectively. This translated to compression near the articular surface being relatively high and decreasing markedly from 0.38 to 0.02 in the deepest regions for LTP cartilage, and from 0.22 to 0.01 for LFC samples (Figure 4.4A). Near the articular surface, $-E_{zz}$ was ~2x higher ($p<0.01$) in

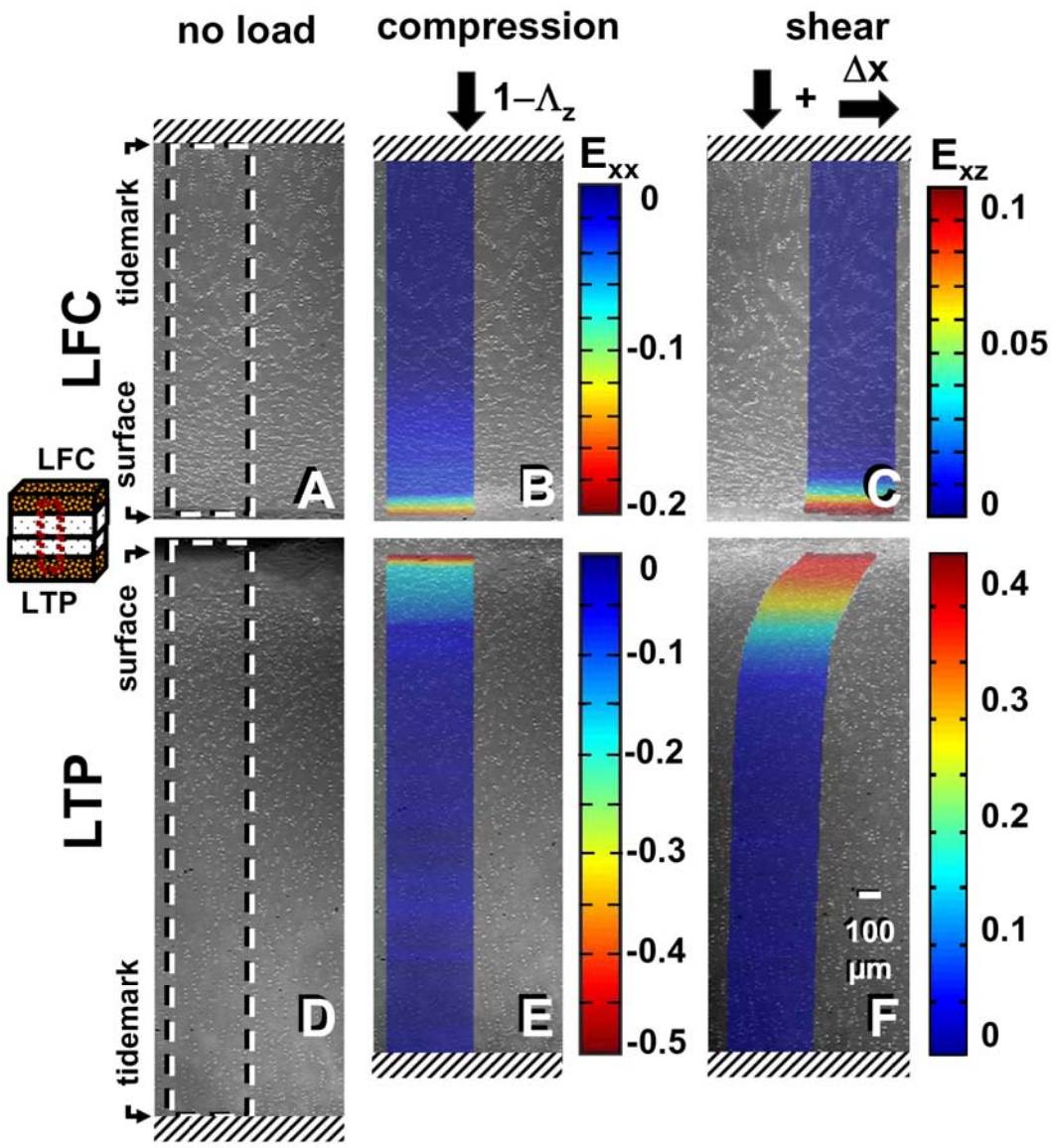

Figure 4.3: Micrographs with superimposed strain colormaps taken of apposing LFC (**A-C**) to LTP (**D-F**) samples when unloaded (**A, D**), after axial compression (**B, E**), and during lateral shear (**C, F**). Maps of compressive strain relative to the unloaded thickness (color maps: **B, E**) and shear strain relative to the compressed thickness (color maps, **C**, **F**) after achieving surface sliding were determined. Dashed lines (**– –**) encompass the analyzed regions on the undeformed images, while strain map boundaries encompass the corresponding deformed states.

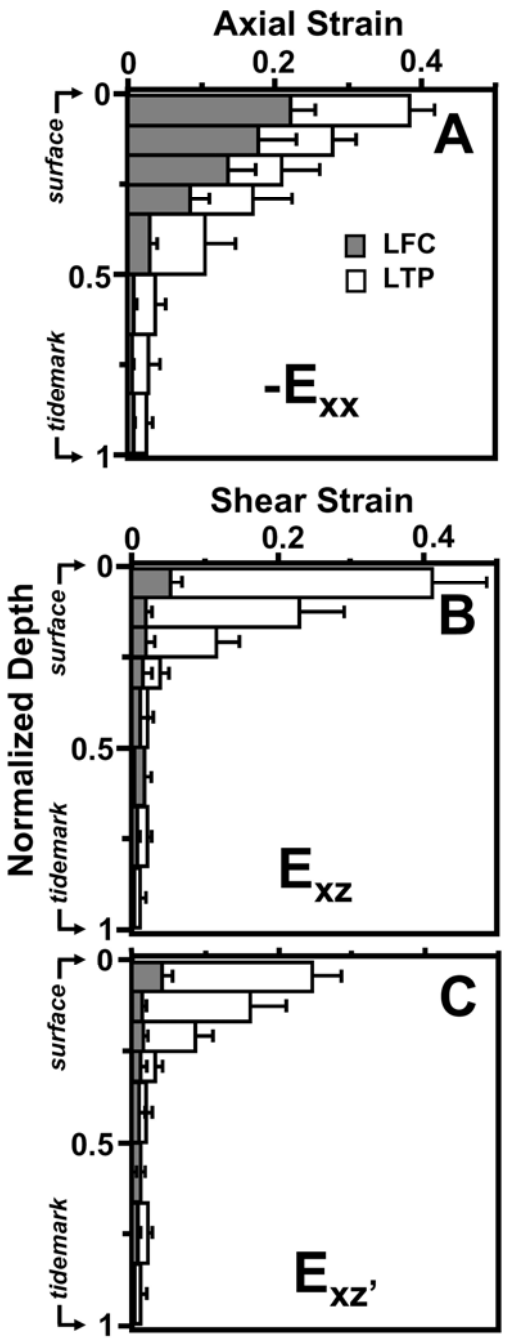

Figure 4.4: Local axial strain ($-E_{ZZ}$) relative to the unloaded cartilage thickness versus normalized tissue depth under applied compression alone (**A**) for both LFC and LTP cartilage. Local shear strain relative to the compressed cartilage thickness (E_{XZ} in **B**) and to the unloaded cartilage thickness (E_{XZ}' in **C**) under compression and during shear. Values are mean ± SEM.

LTP (0.38) than LFC (0.22) cartilage (Figure 4.5A). Similarly, overall $-E_{zz}$ of LTP (0.16 ± 0.02) was twice that of LFC (0.07 ± 0.02) cartilage (Figure 4.5D). Lateral (E_{xx}) and shear (E_{xz}) strains resulting from the applied compression were low, averaging <0.03 for all samples, while E_{xx} and $-E_{zz}$ did not apparently change following lateral motion (<1%) (data not shown).

Deformation: Shear Strain

As described previously [31], shear loading of apposing cartilage surfaces results in surface sliding with maintenance of peak shear deformation (Figure 4.3C,F), and at this time, E_{xz} varied markedly with depth from the articular surface for both locations ($p<0.01$) and between LFC (Figure 4.3C) and LTP (Figure 4.3F) cartilage ($p<0.01$). On average, the resultant lateral displacement at the surface of LTP and LFC cartilage was 398 ± 38 and 81 ± 9μm, respectively. As a result, E_{xz} decreased significantly ($p<0.001$) and monotonically from 0.41 and 0.05 near the articular surface, to very low magnitudes (≤0.01) near the tidemark for LTP and LFC cartilage, respectively (Figure 4.4B). Near the articular surface, E_{xz} was ~8x higher ($p<0.01$) in LTP than LFC cartilage (Figure 4.5B), while overall E_{xz} was ~4x higher ($p<0.01$) for LTP (0.09 ± 0.01) than LFC (0.02 ± 0.01) samples (Figure 4.5E). Effects of depth ($p<0.01$) and tissue location ($p<0.01$) on local (Figure 4.4C, 5C) and overall (Figure 4.5F) E_{xz}, were similar to those found for E_{xz}; however, values were lower in magnitude.

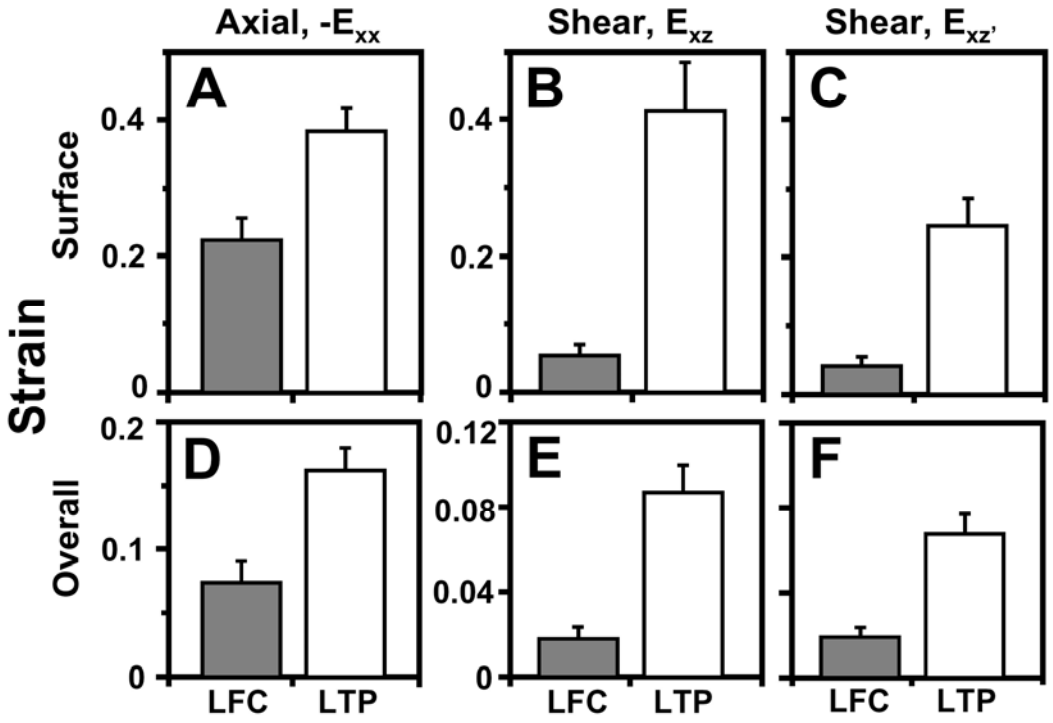

Figure 4.5: Comparison of peak compressive ($-E_{ZZ}$) surface (**A**) and overall strains (**D**) relative to the unloaded cartilage thicknesses between LFC and LTP sample groups. Peak surface (**B, C**) and overall (**E, F**) shear strains relative to either the compressed cartilage thickness (E_{XZ} in **B, E**) or the unloaded cartilage thickness (E_{XZ}' in **C, F**).

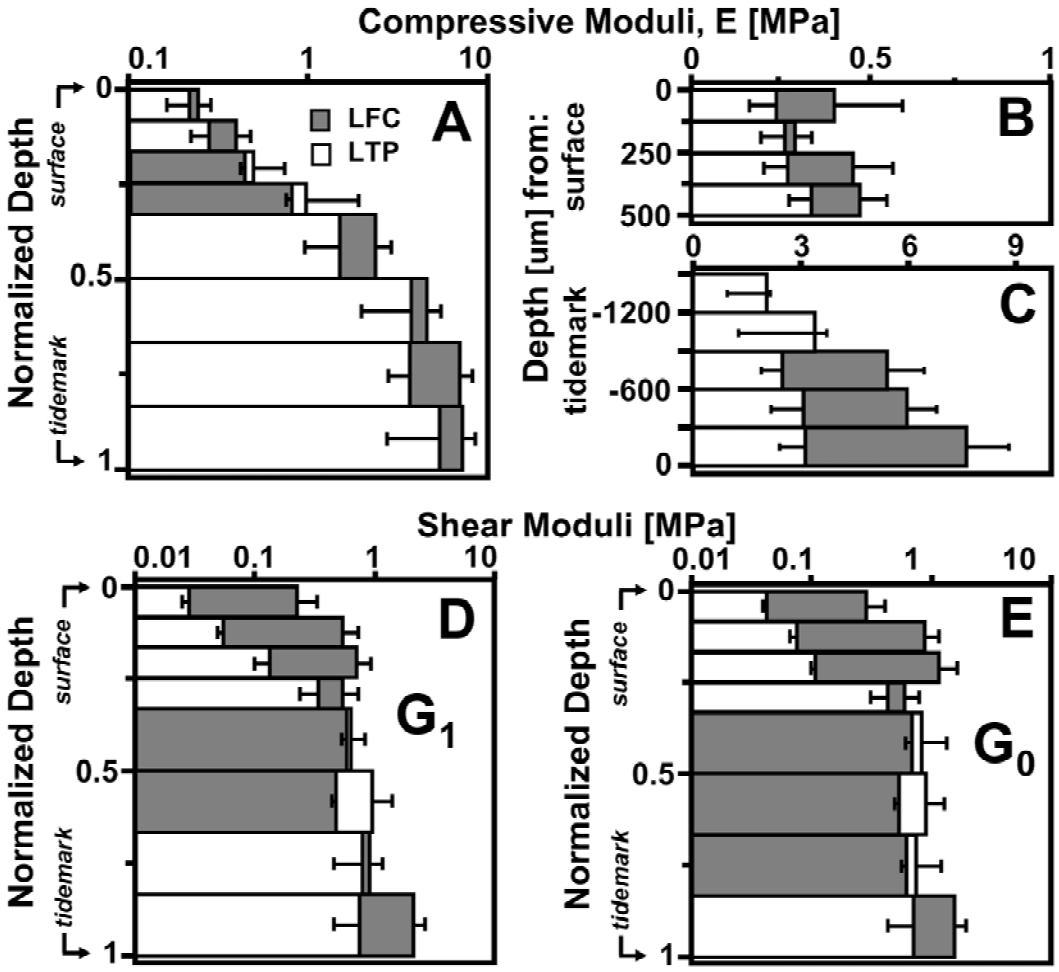

Figure 4.6: Local compressive modulus (E) relative to the unloaded cartilage thickness versus normalized tissue depth (**A**) and absolute depth from the articular surface (**B**) and tidemark (**C**) under applied compression alone for both LFC and LTP cartilage. Local shear modulus versus normalized tissue depth relative to the compressed cartilage thickness (G_1 in **D**) and to the unloaded cartilage thickness (G_0 in **E**) under compression and during shear. Values are mean ± SEM.

Tissue Properties: Compressive

To estimate compressive loads during micro-scale tests, axial compression for each cartilage layer (LFC, LTP) in micro-scale shear tests was replicated by applying axial displacements measured in micro-scale tests (reported above) to LFC and LTP cartilage in macro-scale tests. Local E markedly increased ($p<0.001$) with increasing depth from the articular surface for all cases, being 25-30 times higher near the tidemark than the surface (Figure 4.6A). As a function of normalized tissue depth, E was not apparently different between locations at all depths ($p=0.11$) and near the articular surface ($p=0.17$). Since cartilage thickness was generally greater in LTP samples, each normalized depth interval was thicker for LTP cartilage, and comparisons of E may be more appropriate between similar thickness depth regions. When determined as a function of absolute tissue depth, E also increased with increasing distance from the articular surface (Figure 4.6B) and decreased significantly ($p<0.001$) with increasing distance from the tidemark (Figure 4.6C). Within the top 125 μm of the articular surface (Figure 4.7A), E was 0.40 ± 0.19 MPa for LFC cartilage, being markedly higher ($p<0.05$) than that of LTP samples (0.24 ± 0.08 MPa). Similarly, overall E was markedly higher ($p<0.01$) for LFC (0.76 ± 0.13 MPa) than LTP cartilage (0.47 ± 0.08 MPa) (Figure 4.7D).

Tissue Properties: Shear

Similarly for measurement of shear loads, resultant shear deformation of each cartilage layer (LFC, LTP) in micro-scale tests was replicated in macro-scale tests by applying resultant lateral surface displacement measured from micro-scale tests

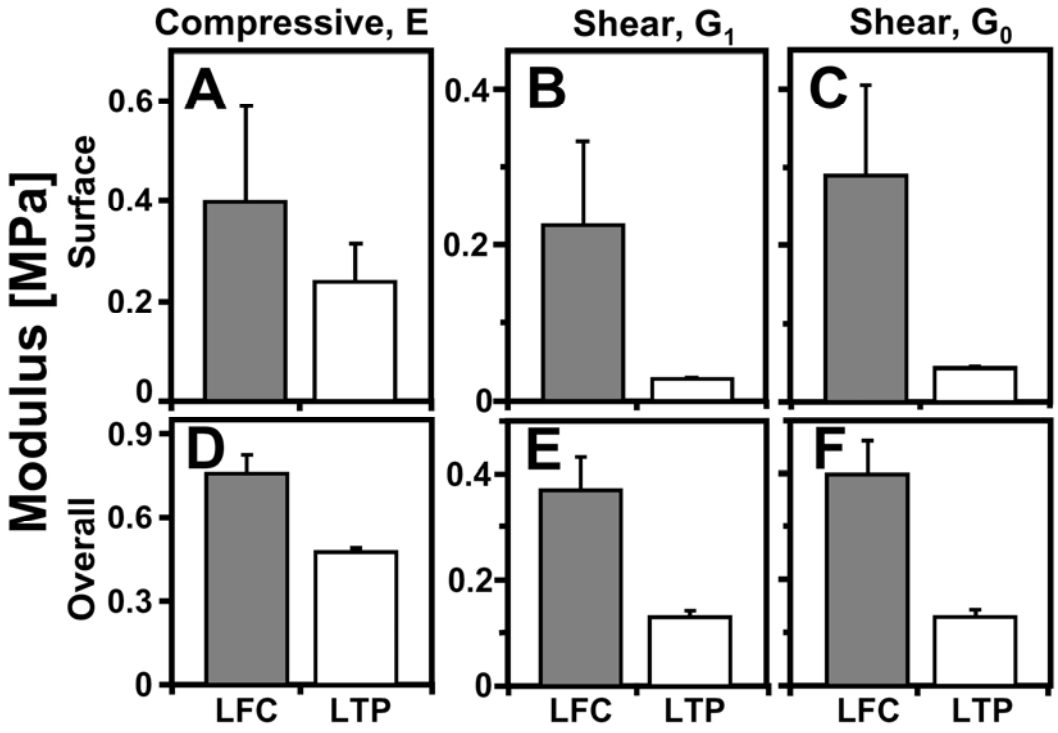

Figure 4.7: Comparison of peak compressive (E) surface (**A**) and overall modulii (**D**) relative to the unloaded cartilage thicknesses between LFC and LTP sample groups. Peak surface (**B, C**) and overall (**E, F**) shear modulii relative to either the compressed cartilage thickness (G_1 in **B, E**) or the unloaded cartilage thickness (G_0 in **C, F**).

(reported above) to LFC and LTP cartilage. With increasing tissue depth, local G_1 increased significantly ($p<0.001$) for both cartilage layers, and differences between LFC and LTP samples were marked ($p<0.01$) (Figure 4.6D). Near the articular surface, G_1 was 9- and 27-fold lower than the modulii near the tidemark for LFC and LTP cartilage, respectively. For LFC cartilage, G_1 near the surface was 0.22 ± 0.11 MPa, which was 7-fold higher ($p<0.05$) than the surface G_1 of LTP cartilage (0.03 ± 0.003 MPa) (Figure 4.7B). Overall G_1 was markedly higher ($p<0.001$) in LFC (0.38 ± 0.06 MPa) than LTP cartilage (0.13 ± 0.01 MPa) (Figure 4.7E). Effects of tissue depth and location on local (Figure 4.6D, 7C) and overall (Figure 4.7G) G_0 were found to be similar to G_1, with G_0 increasing with tissue depth ($p<0.001$) and being markedly higher in LFC cartilage near the surface ($p<0.01$) and overall ($p<0.001$). In all cases, values of G_0 were slightly higher in magnitudes than that of G_1.

4.5 Discussion

This study utilized a micro-scale cartilage-on-cartilage testing system to elucidate cartilage strain during tibio-femoral articulation as well as the mechanical properties of femoral and tibial cartilage. The present results indicate that during axial and lateral loading of tibial against femoral cartilage (Figure 4.8A), tibial cartilage deforms and strains markedly more in both compression and shear than femoral cartilage (Figure 4.8B), and such trends are a result of femoral cartilage being stiffer in compression and shear. Under axial displacement, $-E_{zz}$ for LTP, near the articular surface and overall, was 50% higher than that of LFC. During lateral motion, E_{xz} was dramatically higher in LTP than LFC cartilage, being ~80% higher near the surface and overall. In addition, E near the surface and overall for LFC were both ~40% higher than that of LTP. Analogously, G_1 and G_0 were greater in magnitude for LFC than LTP, being 80% higher near the surface and 65% overall.

The experimental approach utilized in the present study mimics the compression and sliding between femoral and tibial cartilage that occurs during physiologic tibio-femoral joint articulation. Samples were taken from the lateral femoral condyle and donor-matched tibial plateau, where such surfaces appose and articulate against each other within the joint [15]. Such regions are load-bearing, and tibio-femoral cartilage experiences a wide range of compression (3-20%) [6, 13, 27] and sliding (up to ~50 mm) during normal activities (estimated from refs [29] and [26]). The present study addresses certain physiologic loading parameters

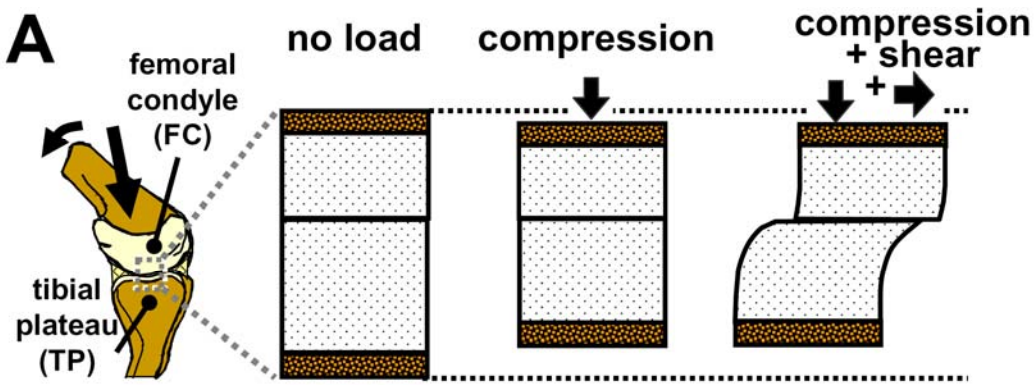

B

location	strain			
femoral condyle	$-E_{zz}$	—	+	+
	E_{xz}	—	—	+
tibial plateau	$-E_{zz}$	—	+++	+++
	E_{xz}	—	—	+++

Figure 4.8: Schematic of cartilage compressive and shear deformation of femoral cartilage apposing tibial cartilage when unloaded, compressed, and compressed and sheared. (**B**) Table of relative magnitudes for compressive ($-E_{ZZ}$) and shear strain (E_{XZ}) for both femoral and tibial cartilage when they are unloaded, compressed, and compressed and sheared in apposition.

(i.e high compressive loading and low sliding velocity during contralateral toe-off and heel rise [29]) as well as the relative loading and sliding of physiologically articulating cartilage surfaces. Although synovial fluid (SF) normally lubricates surfaces physiologically and reduces absolute magnitudes of E_{xz} during articulation in the boundary mode [30, 31], the present study used PBS as lubricant to allow sufficient lateral displacements in LFC samples so that G_1 could be appropriately estimated. However, relative differences in strain and modulus between regions should be consistent, although measured E_{xz} would likely be reduced (~50%) if SF had been used [30]. Future studies could be conducted to assess the effect of lubricant on cartilage deformation during tibio-femoral articulation.

Depth-variations in $-E_{zz}$, E_{xz}, E, and G_1 for the cartilage used in this study is consistent with those previously reported. In both compressed tibial [16] and patella-femoral cartilage [20], $-E_{zz}$ was depth-varying, decreasing monotocially with increasing depth from the articular surface. During lateral articulation, E_{xz} was also highest at articular surface and lowest near the tidemark [30, 31] in femoral cartilage. For the present study, both $-E_{zz}$ and E_{xz} of LFC and LTP cartilage exhibited similar depth-varying trends (Figure 4.4), decreasing markedly with increasing depth. Reflective of the depth-variation in strain, cartilage stiffness in compression [20] and shear [30] for patella-femoral and femoral cartilage, respectively, increased with increasing depth. Similarly, E and G_1 for LFC and LTP cartilage both increased with increasing depth, being ~1.5-2x lower near the surface and 5-10x higher near the tidemark than the overall values (Figure 4.5).

The magnitudes of E and G_1 reported in this study for cartilage from human femoral condyles and tibial plateau are consistent with those previously reported. From indentation tests, overall E was estimated to be 0.47 and 0.68 MPa for cartilage from the lateral aspects of the tibial plateau and femoral condyle, respectively, [14] being similar to those found in the current study (LTP: 0.47 MPa, LFC: 0.76 MPa). Analogous to E, overall G_1 for femoral cartilage reported for this study (0.38 MPa) was also consistent with those previously reported (0.32 MPa) [30]. Thus, for human tibio-femoral cartilage, mechanical properties in compression and shear were similar to those previously described.

The tissue deformation being greater in cartilage from the tibia than the femoral condyle is consistent with *in vivo* tibio-femoral deformation and predictions accounting for past studies on tibial and femoral tissue stiffness. Following impact loading, tibial cartilage deformation was observed with MRI to be significantly higher than that of femoral cartilage [6]. In addition, indentation stiffness for femoral cartilage was ~1.2-1.5 times greater than tibial cartilage in human joints [14], being consistent with trends (1.5-2 times) found in this study. As a result, femoral cartilage would be predicted to deform less than tibial cartilage during articulation because it is relatively stiffer. In addition to the intrinsic structural differences between regions [1], differences in deformation, and associated stiffness, may be partly attributed to the mild degeneration observed in LTP cartilage (Figure 4.2).

This study further elucidates cartilage mechanics by providing insight into the cartilage deformation of articulating surfaces during tibio-femoral joint articulation. Collectively, the present results suggest cartilage deformation in compression and

shear are asymmetric between cartilage surfaces, locally and overall, during tibio-femoral articulation, being markedly higher in femoral cartilage than tibial cartilage, and are reflected by differences in mechanical stiffness. Cell metabolism and matrix synthesis, and as result tissue structure, are markedly regulated by mechanical deformation [11, 17, 19]. Thus, relative differences in deformation between articulating surfaces may be a biomechanical stimulus that regulates the regional variations in cartilage stiffness within the physiologic knee joint.

4.6 Acknowledgments

This work was supported by NIH and Howard Hughes Medical Institute through the Professors Program Grant to UCSD for Dr. Robert L. Sah. We thank the many residents and staff at Dr. Lotz's Laboratory at the Scripps Research Institute for harvesting and providing the human tissue used in this study, and Chris Kim and Dr. Won Bae for their help in the histopathology assessments..

4.7 References

1. Arokoski JP, Hyttinen MM, Helminen HJ, Jurvelin JS: Biomechanical and structural characteristics of canine femoral and tibial cartilage. *J Biomed Mater Res* 48:99-107, 1999.

2. Athanasiou KA, Rosenwasser MP, Buckwlter JA, Malinin TI, Mow VC: Interspecies comparisons of in situ intrinsic mechanical properties of distal femoral cartilage. *J Orthop Res* 9:330-40, 1991.

3. Bae WC, Temple MM, Amiel D, Coutts RD, Niederauer GG, Sah RL: Indentation testing of human cartilage: sensitivity to articular surface degeneration. *Arthritis Rheum* 48:3382-94, 2003.

4. Buckley MR, Gleghorn JP, Bonassar LJ, Cohen I: Mapping the depth dependence of shear properties in articular cartilage. *J Biomech* 41:2430-7, 2008.

5. Chahine NO, Wang CC, Hung CT, Ateshian GA: Anisotropic strain-dependent material properties of bovine articular cartilage in the transitional range from tension to compression. *J Biomech* 37:1251-61, 2004.

6. Eckstein F, Hudelmaier M, Putz R: The effects of exercise on human articular cartilage. *J Anat* 208:491-512, 2006.

7. Frank EH, Grodzinsky AJ, Koob TJ, Eyre DR: Streaming potentials: a sensitive index of enzymatic degradation in articular cartilage. *J Orthop Res* 5:497-508, 1987.

8. Fung YC. A First Course in Continuum Mechanics. 2nd ed. Englewood Cliffs: Prentice-Hall; 1977.

9. Fung YC. Biomechanics: Mechanical Properties of Living Tissues. New York: Springer-Verlag; 1981.

10. Gratz KR, Sah RL: Experimental measurement and quantification of frictional contact between biological surfaces experiencing large deformation and slip. *J Biomech* 41:1333-40, 2008.

11. Jin M, Frank EH, Quinn TM, Hunziker EB, Grodzinsky AJ: Tissue shear deformation stimulates proteoglycan and protein biosynthesis in bovine cartilage explants. *Arch Biochem Biophys* 395:41-8, 2001.

12. Jurvelin JS, Buschmann MD, Hunziker EB: Mechanical anisotropy of the human knee articular cartilage in compression. *Proc Inst Mech Eng [H]* 217:215-9, 2003.

13. Kersting UG, Stubendorff JJ, Schmidt MC, Bruggemann GP: Changes in knee cartilage volume and serum COMP concentration after running exercise. *Osteoarthritis Cartilage* 13:925-34, 2005.

14. Lyyra T, Kiviranta I, Vaatainen U, Helminen HJ, Jurvelin JS: In vivo characterization of indentation stiffness of articular cartilage in the normal human knee. *J Biomed Mater Res* 48:482-7, 1999.

15. Mow VC, Gu WY, Chen FH: Structure and Function of Articular Cartilage and Meniscus. In: *Basic Orthopaedic Biomechanics and Mechano-Biology,* ed. by VC Mow, Huiskes R, Lippincott Williams & Wilkins, Philadelphia, 2005, 720.

16. Neu CP, Hull ML, Walton JH: Heterogeneous three-dimensional strain fields during unconfined cyclic compression in bovine articular cartilage explants. *J Orthop Res* 23:1390-8, 2005.

17. Nugent GE, Aneloski NM, Schmidt TA, Schumacher BL, Voegtline MS, Sah RL: Dynamic shear stimulation of bovine cartilage biosynthesis of proteoglycan 4 (PRG4). *Arthritis Rheum* 54:1888-96, 2006.

18. Ross MH, Kaye GI, Pawlina W. Histology: A Text and Atlas. 4th ed. Philadelphia, PA: Lippincott Williams & Wilkins; 2003.

19. Sah RL, Kim YJ, Doong JH, Grodzinsky AJ, Plaas AHK, Sandy JD: Biosynthetic response of cartilage explants to dynamic compression. *J Orthop Res* 7:619-36, 1989.

20. Schinagl RM, Gurskis D, Chen AC, Sah RL: Depth-dependent confined compression modulus of full-thickness bovine articular cartilage. *J Orthop Res* 15:499-506, 1997.

21. Schinagl RM, Ting MK, Price JH, Sah RL: Video microscopy to quantitate the inhomogeneous equilibrium strain within articular cartilage during confined compression. *Ann Biomed Eng* 24:500-12, 1996.

22. Schmidt TA, Sah RL: Effect of synovial fluid on boundary lubrication of articular cartilage. *Osteoarthritis Cartilage* 15:35-47, 2007.

23. Scott JE, Dorling J: Differential staining of acid glycosaminoglycans (mucopolysaccharides) by alcian blue in salt solutions. *Histochemie* 5:221-33, 1965.

24. Setton LA, Mow VC, Muller FJ, Pita JC, Howell DS: Mechanical properties of canine articular cartilage are significantly altered following transection of the anterior cruciate ligament. *J Orthop Res* 12:451-63, 1994.

25. Shapiro F, Glimcher MJ: Induction of osteoarthrosis in the rabbit knee joint. Histologic changes following menisectomy and meniscal lesions. *Clin Orthop Rel Res* 147:287-95, 1980.

26. Shelburne KB, Torry MR, Pandy MG: Muscle, ligament, and joint-contact forces at the knee during walking. *Med Sci Sports Exerc* 37:1948-56, 2005.

27. Van de Velde SK, Bingham JT, Gill TJ, Li G: Analysis of tibiofemoral cartilage deformation in the posterior cruciate ligament-deficient knee. *J Bone Joint Surg Am* 91:167-75, 2009.

28. Wang CC, Deng JM, Ateshian GA, Hung CT: An automated approach for direct measurement of two-dimensional strain distributions within articular cartilage under unconfined compression. *J Biomech Eng* 124:557-67, 2002.

29. Whittle M. Gait Analysis: An Introduction. 3rd ed. Oxford; Boston: Butterworth-Heinemann; 2002.

30. Wong BL, Bae WC, Chun J, Gratz KR, Sah RL: Biomechanics of cartilage articulation: effects of lubrication and degeneration on shear deformation. *Arthritis Rheum* 58:2065-74, 2008.

31. Wong BL, Bae WC, Gratz KR, Sah RL: Shear deformation kinematics during cartilage articulation: effect of lubrication, degeneration, and stress relaxation. *Mol Cell Biomech* 5:197-206, 2008.

32. Yamada K, Healey R, Amiel D, Lotz M, Coutts R: Subchondral bone of the human knee joint in aging and osteoarthritis. *Osteoarthritis Cartilage* 10:360-9, 2002.

33. Zhu W, Mow VC, Koob TJ, Eyre DR: Viscoelastic shear properties of articular cartilage and the effects of glycosidase treatment. *J Orthop Res* 11:771-81, 1993.

CHAPTER 5

CARTILAGE SHEAR KINEMATICS DURING TIBIO-FEMORAL ARTICULATION: EFFECT OF ACUTE JOINT INJURY & HYALURONAN SUPPLEMENTATION ON SYONVIAL FLUID LUBRICATION

5.1 Abstract

Objective: To characterize the effects of acute injury and tribosupplementation by hyaluronan (HA) on synovial fluid (SF) function to modulate cartilage shear during tibio-femoral articulation.

Methods: Human osteochondral blocks from the lateral femoral condyle (LFC) and tibial plateau (LTP) were apposed, compressed 13%, and subjected to sliding under video microscopy. Tests were conducted with equine SF from a normal joint (NL-SF), SF from contra-lateral acutely injured joint (AI-SF), and AI-SF to which HA was added (AI-SF+HA). Local and overall shear strain (E_{xz}) and the applied lateral displacement (Δx) at which E_{xz} reached 50% of the peak ($\Delta x_{1/2}$) were determined.

Results: During articulation, LFC and LTP cartilage E_{xz} increased with Δx and peaked when surfaces slid, with peak E_{xz} being maintained during sliding. With AI-SF as lubricant, surface and overall $\Delta x_{1/2}$ were ~40% and ~20% higher than values with NL-SF and AI-SF+HA as lubricant, respectively. Also with AI-SF as lubricant, peak E_{xz} was markedly higher than with NL-SF as lubricant both near the surface (~80%) and overall (50-200%). Following HA supplementation to AI-SF, E_{xz} was reduced from values with AI-SF alone by 30-50% near the surface and 20-30% overall. Magnitudes of surface and overall E_{xz} were markedly (~50-80%) higher in LTP cartilage than LFC cartilage for all lubricants.

Conclusion: Acute injury impairs SF function, elevating cartilage E_{xz} markedly during tibio-femoral articulation, a consequence which may contribute to post-injury associated cartilage degeneration. Tribosupplementation with HA partially restores the function of AI-SF, and tribosupplements could potentially slow or prevent E_{xz} induced secondary osteoarthritis.

5.2 Introduction

Within the knee joint, articular cartilage lining the femoral condyle articulates against articular cartilage from the tibial plateau (Figure 1A) to facilitate diarthrodial joint movement [15]. Following various physical activities such as knee bending, impact loading, and running, cartilage compresses ~3-20% of the overall thickness [4, 12, 31], with compression typically being higher in cartilage from the tibial plateau than the femoral condyle [4, 12]. Under such magnitudes of physiologic compression, tibio-femoral cartilage compression and shear are depth-varying, being highest near the surface and decreasing monotonically with increasing depth, and greater in tibial cartilage than femoral cartilage [36]. However, the shear kinematics as well as the effects of synovial fluid lubrication remains to be elucidated for physiologically apposed cartilage surfaces. Such characterization would further the understanding of cartilage contact mechanics during joint loading by elucidating the changing boundary conditions at the surface and shear deformation during applied lateral-loading for physiologically apposing cartilage surfaces (i.e. femoral against tibial cartilage).

In healthy joints, synovial fluid (SF) is present between articulating cartilage surfaces and facilitates the low-friction tribological properties of cartilage by functioning as an effective boundary lubricant. The main constituents of SF identified to interact and absorb to the articular surface are lubricant molecules hyaluronan (HA) [16], proteoglycan 4 (PRG4) [10, 27], and surface-active phospholipids (SAPLs) [22]. In a configuration to reveal boundary lubrication effects, the surface interaction, as indicated by friction [26], and shear deformation [34, 35] of articulating cartilage, are

reduced by SF relative to interactions with phosphate buffered saline (PBS). The SF lubricant molecules, PRG4 and HA, contribute, both independently and in combination, to reducing articulating cartilage friction under boundary lubrication conditions [25]. Thus, altered lubricant molecule concentrations may diminish the boundary lubrication function of SF and cause elevated shear deformation, predisposing cartilage to accelerated wear and degradation.

Following acute injury, the friction-reducing function of SF is compromised and may be caused by reduced HA concentrations. In acutely injured equine joints, HA concentration decreased markedly (~0.3 mg/ml to 0.2 mg/ml), while PRG4 and SAPL concentrations increased (~4 times) compared to SF from the contra-lateral normal joints [1]. When SF was tested between articulating cartilage surfaces to reveal boundary mode lubrication, friction was markedly higher with SF from the acutely injured joints (AI-SF) than that from the contra-lateral normal joints (NL-SF). When AI-SF was reconstituted with HA (AI-SF+HA), friction reduced towards normal magnitudes and was within the range found for NL-SF, suggesting lowered HA concentrations reduced SF function. Though friction for AI-SF was relatively higher than that for NL-SF, absolute magnitudes were low (~0.04) compared to PBS (~0.24). Whether such alterations in the friction-reducing function of SF following acute injury actually results in increased shear deformation, and whether exogenous HA restores shear deformation during tibio-femoral cartilage articulation remains to be elucidated. Since tissue deformation markedly regulates matrix metabolism [21], such information would further elucidate the consequences of altered SF function

following acute injury in cartilage degeneration and pathogenesis by determining its effect on cartilage shear deformation.

Recently, femoral and tibial cartilage deformation during tibio-femoral cartilage articulation was elucidated [36] using video microscopy [24] to track the displacement of fluorescently-labeled cells [9]. With this experimental approach, osteochondral samples from the tibia and femoral condyle were lubricated with PBS, compressed with the cartilage surfaces in apposition, and subjected to lateral shearing motion to mimic the biomechanical environment during tibio-femoral joint articulation (Figure 1B). Resultant compressive and shear strains of cartilage were determined locally and overall with a resolution sufficient to resolve small magnitudes (~1%) of strain. Using such a configuration, mechanical tests can be performed using other surface lubricants. Thus, microscale analysis can be used to assess the effects of synovial fluid lubrication on local and overall shear deformation of femoral and tibial cartilage during tibio-femoral cartilage articulation.

The hypothesis of this study was that during tibio-femoral articulation, cartilage lubrication by AI-SF elevates tissue shear deformation, while lubrication by AI-SF with reconstituted HA returns shear deformation near normal magnitudes. To test this hypothesis, the objectives of this study were to determine, during tibio-femoral cartilage articulation, (1) the effects of acute injury on SF lubricant function and (2) the ability of HA addition to AI-SF to restore lubricant function, with lubricant function assessed as peak cartilage shear deformation during sliding motion.

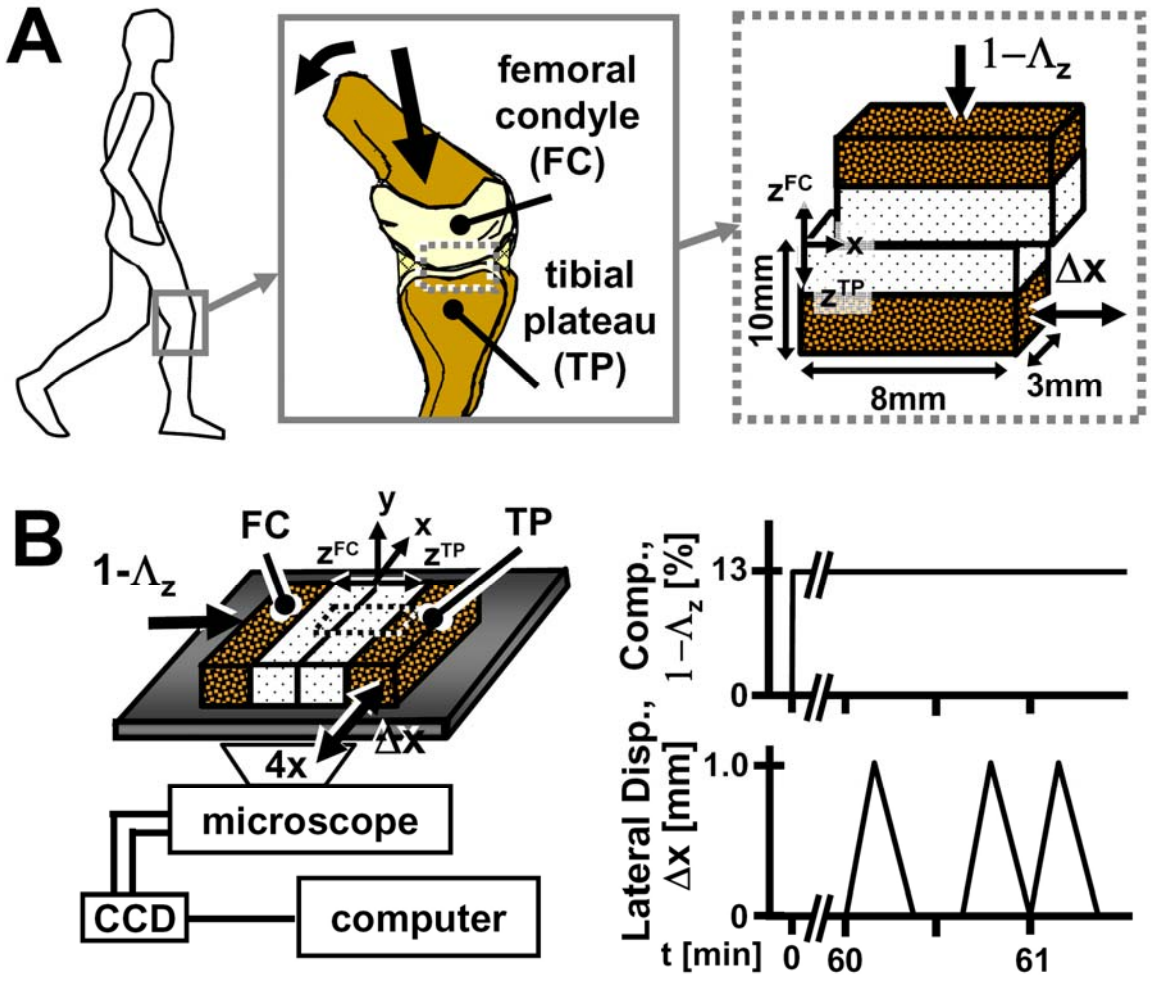

Figure 5.1: Schematic of (**A**) knee joint movements at multiple scales and (**B**) of experimental setup and loading protocol for micro-shear testing.

5.3 Materials and Methods

Sample Isolation and Preparation

Six osteochondral cores, each with a 10 mm diameter, were isolated, one from each anterior lateral femoral condyle (LFC) of six fresh cadaveric human male (n=3) and female (n=3) donors (mean ± SEM age of 46 ± 1.5 yrs). In addition, six osteochondral blocks (each with a chondral surface area of ~1 cm^2) were harvested from the region of the donor-matched lateral tibial plateau (LTP) not covered by the meniscus. LFC cores with grossly normal surfaces (modified Outerbridge grade of 1 [37]) were selected, while all donor-matched LTP blocks displayed mild surface fibrillation and were modified Outerbridge grades of 2-3 [37]. The harvested specimens were immersed in phosphate buffered saline (PBS) containing proteinase inhibitors (PI) [6] and stored at -70^oC until use.

The osteochondral specimens were thawed and further processed on the day of testing. The LFC core and LTP block were each trimmed using a low-speed saw with a 0.3 mm thick diamond edge blade (Isomet^{TM}, Buehler, Lake Bluff, IL) to yield one ~rectangular block for biomechanical testing. Each rectangular block had a cartilage surface area of ~3x8 mm^2 and a total thickness of ~1 cm. Blocks were created such that their 8 mm lengths were parallel to the direction of articulation in the joint from which they were isolated from (Figure 1A). Samples consisted of one LFC and one donor-matched LTP block and were each vigorously rinsed in ~15 ml of PBS+PI overnight to deplete the articular surface of residual SF prior to mechanical testing [25].

From macroscopic images [36], thickness measurements of the present samples were made at three separate locations and averaged to a yield a full cartilage thickness measurement. For the LTP samples, cartilage thickness was 2.88 ± 0.53 mm and somewhat thicker than the cartilage thickness of the LFC samples (2.20 ± 0.15 mm). In addition, samples used in this study were characterized for histopathology [36], confirming the characteristics of LFC and LTP samples. LFC cartilage was normal, with both LFC and LTP cartilage exhibiting normal cellularity and an absence of cell cloning. LTP cartilage exhibited typical features of mild degeneration, with mild surface irregularity, occasional transverse clefts, and mildly-reduced glycosaminoglycan staining.

Lubricants

Soon after an acute injury (within 3 weeks), synovial fluid (SF) was aspirated from joints of six mature (2-4yr old) horses (with IACUC approval) during arthroscopic surgery by one of the authors (CWM). SF was aspirated from the injured joint (AI-SF) as well as the contralateral uninjured joint (NL-SF) which showed no clinical signs of injury. Collected samples were cleared of cells and debris by centrifugation (3,000 g, 30 min) and resultant supernatants were frozen at -70^{o}C until mechanical testing.

The synovial fluid samples were characterized for boundary lubrication properties of lubricant molecules, confirming NL-SF and AI-SF were characteristic of SF from normal and acutely injured joints, respectively. For lubricant samples used in this study, coefficient of kinetic friction was 0.040 ± 0.003 for AI-SF and 0.022 ±

0.001 for NL-SF. Levels of HA were lower in AI-SF (0.19 ± 0.05 mg/ml) than NL-SF (0.31 ± 0.11 mg/ml) samples, while SAPL and proteoglycan 4 concentrations were higher in AI-SF than NL-SF lubricants, differences that are distinctive of synovial response to injury. Lubricant samples used in this study were (1) SF from the contralateral non-injured joint (NL-SF), (2) SF from the injured joint (AI-SF), and (3) AI-SF to which hyaluronan (HA) was added (AI-SF+HA). For AI-SF+HA lubricant samples, high molecular weight (800kDa) HA (SUPARTZ®, Seikagaku Corporation, Tokyo, Japan) was added to AI-SF to create a final concentration of supplemented HA to be 1 mg/ml. All lubricant samples in the present study had PI added prior to mechanical testing.

Experimental Design

To assess the effect of acute injury on SF function in terms of cartilage shear deformation, lubricants were tested on cartilage samples in microshear tests described below. In particular, each of the lubricant samples (AI-SF, AI-SF+HA, NL-SF) from one equine animal were paired and tested sequentially between cartilage tissue from one human donor to reduce donor-donor variability of lubricant and tissue. Prior to mechanical testing, cartilage was completely immersed in ~0.5 ml of test lubricant containing PI and propidium iodide (20 mg/ml) at 4^{o}C for 12-16 h to lubricate surfaces and fluorescently highlight cell nuclei. Subsequently, AI-SF, AI-SF+HA, and then NL-SF were tested sequentially in microscale shear tests. Inbetween lubricant bathing and mechanical testing, cartilage samples were rinsed, allowed to reswell, and reincubated in PBS+PI for ~4 h at 4^{o}C.

Micro-scale Shear Testing:

Samples were tested in shear with microscale analysis of tissue shear stain as described previously [36]. Briefly, each LFC and LTP pair was secured, with cartilage surfaces in apposition (Figure 1B), in a custom bi-axial loading chamber mounted onto an epi-fluorescence microscope for digital video imaging [23]. The chamber secured the LFC block at the bone and allowed in-plane movement of the apposing mobile LTP block with orthogonally positioned plungers interfaced with either a micrometer (for axial displacement; Model 262RL; Starrett Co., Athol, MA) or motion-controller (for lateral displacement; Model MFN25PP; Newport, Irvine, CA). Subsequently, an axial displacement was applied (~40 μm/s) to the bone portion of the LFC sample to induce 13% compression ($1-\Lambda_z$, where Λ_z is the stretch ratio [8]) of the overall (i.e. LFC and LTP) cartilage thickness (Figure 1B) determined from gross images. Samples were then allowed to stress relax for 1h which was confirmed to be sufficient to reach an approximate equilibrium stress for the current sample geometries [34].

Following axial compression, cartilage deformation was assessed separately in the LFC and LTP tissue during shear loading as previously described [36]. Three sets of applied lateral displacements (Δx), each consisting of +1 mm and then −1 mm (returning to initial position) was applied to the bone portion of the LFC block (Figure 1B) to induce relative lateral motion. The first set of sliding motion was for preconditioning [26], while tissue motions during the second and third set were recorded for the LTP and LFC cartilage, respectively, for analyses. Before and during

the application of lateral displacements, sequential fluorescence (Nikon G-2A filter) images were taken separately for LFC and LTP cartilage at increments of 33 μm to capture the shear deformation and sliding during tibio-femoral cartilage articulation. Resultant images with a field of view of ~3×2 mm^2 encompassed the entire cartilage thickness of the LFC (or LTP) and a partial view of the apposing surface. The identical regions of interest were imaged and analyzed for each of the three lubricant conditions.

Data Collection and Calculations

Digital fluorescence images from microscale tests were analyzed as described previously [9, 34] in MATLAB 7.0 (Mathworks, Inc., Natick, MA) to determine the depth-varying and overall shear deformation in cartilage. Briefly, an evenly distributed set of cell nuclei (~250 cells/mm^2) was selected to serve as fiducial markers and tracked by maximizing cross-correlation of regions surrounding each marker to the preceding, and then initial frames. For each recorded image, local affine mappings of nuclei were used to calculate the displacement of uniformly-spaced (10 pixel) mesh points in the region of interest (~1 mm × full thickness) during deformation. Subsequently, displacement gradients were determined by finite difference approximation, from which, Lagrangian shear strains (E_{xz}) relative to the compressed cartilage thickness at compressive equilibrium were determined for both LFC and LTP cartilage during lateral shearing [7].

Local and overall E_{xz} as well as the Δx at 50% peak surface and overall E_{xz} were determined separately for LFC and LTP samples. For each image frame, Exz of

the LFC and Exz of the LTP were consolidated by interpolating values depth-wise and averaging. At the same normalized depth (0, surface and 1, tidemark) for each sample, E_{xz} was first averaged. Then, E_{xz} was interpolated linearly at every 0.05 times the normalized tissue thickness near the articular surface (i.e. 0 to 0.3) and 0.1 for remaining regions of the tissue depth (i.e. 0.3 to 1). To consolidate data further, E_{xz} values were averaged among samples to yield an average depth-profile for every 0.1 mm increment (every 3rd acquired image frame) of applied lateral displacement. Surface E_{xz} was defined as that occurring at the top 5% of the cartilage thickness. The overall Lagrangian E_{xz} was determined as half the lateral tissue displacement near the articular surface normalized to the compressed cartilage thickness. Surface and overall E_{xz} were determined at Δx increments of 0.1 mm (Δx ranging between 0 to 0.8 mm) to assess the kinematics of cartilage shear deformation during articulation. To assess and compare rates at which surface and overall E_{xz} reached equilibrium, Δx when surface and overall E_{xz} reached 50% the peak value were determined for all experimental cases.

Statistical Analysis

Data are reported as mean ± standard error of the mean (SEM), unless noted otherwise. Repeated measures ANOVA was used to determine the effects of joint location (LFC, LTP) and lubricant (AI-SF, AI-SF+HA, NL-SF) on local and overall E_{xz}. $\Delta x_{1/2}$ data were log transformed prior to analysis to account for sample variances being approximately proportional to the amplitude of the data. When significant interactions were found between joint location and lubricant, Dunett post-hoc

comparisons were made between lubricant groups (AI-SF versus NL-SF, AI-SF+HA versus NL-SF) for a given joint location. Systat 10.2.05 (Systat Software, Richmond, CA) and Microsoft Office Excel 2003 (Microsoft Corporation, Redmond, WA) were used to perform all statistical analyses.

5.4 Results

Shear Deformation Kinematics

Similar to previous qualitative [34] and quantitative [35] descriptions of cartilage-on-cartilage articulation, tibio-femoral cartilage articulation resulted in a sequence of four main events for all experimental conditions during shear loading. Qualitatively at compressive equilibrium, (1) LFC and LTP surfaces adhered and began to move laterally in unison to initiate E_{xz} in both apposing tissues near the onset of Δx. (2) With increasing Δx, LFC and LTP E_{xz} increased while surfaces remained adhered. (3) Eventually with sufficient Δx, LFC and LTP E_{xz} reached a peak just as their respective surfaces detached and slid relative to each other. (4) With additional Δx, cartilage E_{xz} in both LFC and LTP tissues maintained a relatively steady-state peak.

During shear loading, cartilage E_{xz}, near the articular surface and overall, increased markedly with Δx and was significantly higher for LTP than LFC cartilage. For both LFC and LTP cartilage, E_{xz} near the surface and overall increased markedly ($p<0.001$) with increasing Δx, eventually reaching a maximum that was maintained with additional Δx for all lubricant cases (Figure 2). These quantitative trends are consistent with the qualitative observations described above. When AI-SF was used as the lubricant, the resultant E_{xz} near the articular surface of LFC samples reached a peak value during articulation that was higher than that when samples were tested with AI-SF+HA and NL-SF as lubricants (Figure 2A). Analogously, overall E_{xz} of LFC cartilage also reached a higher peak magnitude for AI-SF as lubricant than AI-SF+HA

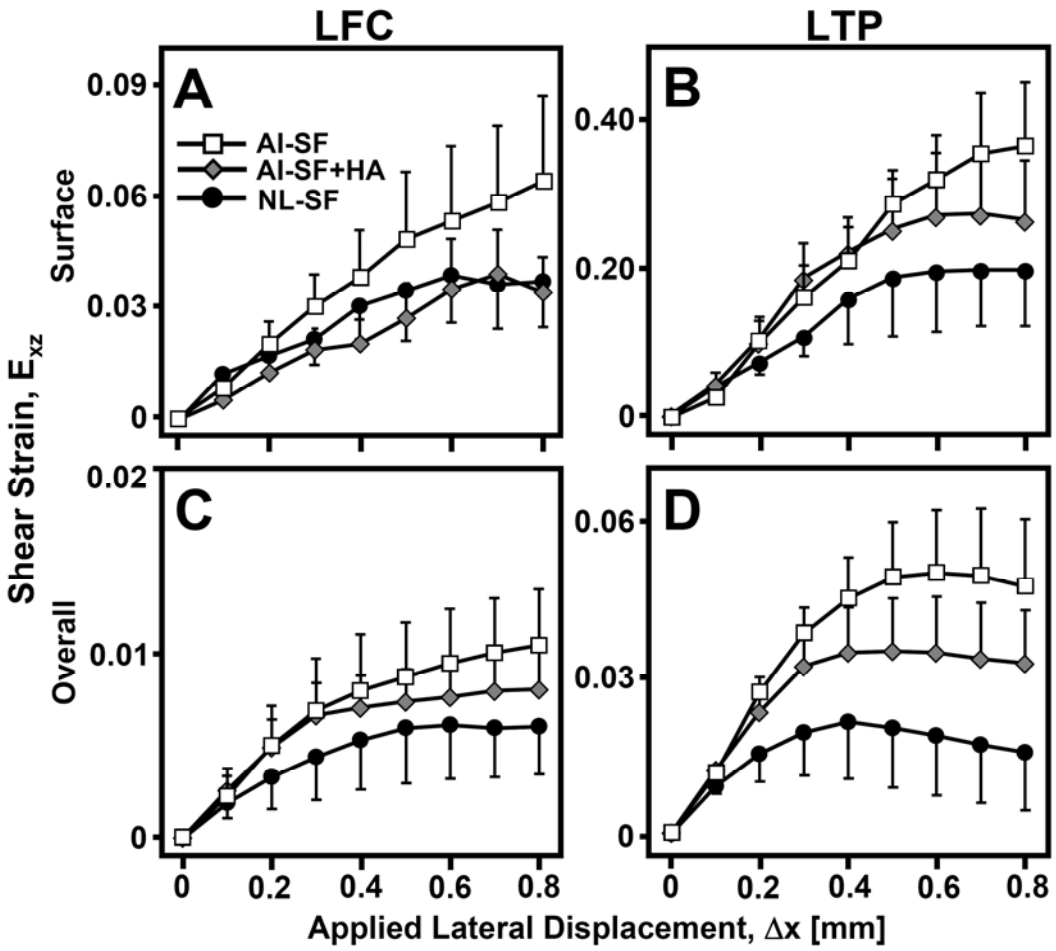

Figure 5.2: Surface (**A,B**) and overall (**C,D**) shear strain (E_{XZ}) versus applied lateral displacement (Δx) for (**A,C**) the lateral femoral condyle (LFC) and (**B,D**) tibial plateau (LTP) cartilage tested with acutely injured SF (AI-SF), acutely injured SF supplemented with HA (AI-SF+HA), and contra-lateral normal SF (NL-SF).

and NL-SF as lubricants (Figure 2C). Typically, E_{xz} near the surface and overall of LFC samples reached peak values that were highest, 2nd highest, and lowest during articulation when AI-SF, AI-SF+HA, and NL-SF, respectively, were used as the lubricant. Similar trends in LTP E_{xz} during tibio-femoral articulation were found; however, the E_{xz} magnitudes of LTP cartilage were markedly higher near the articular surface ($p<0.01$) and overall ($p<0.05$) than those of the LFC samples (Figure 2B,D). For all cases, E_{xz} reached a steady-state peak at a Δx of 0.8 mm. Thus, effects of lubrication on tissue E_{xz} were further compared at this point as described below (***Peak shear deformation***).

To assess the rate at which surface and overall E_{xz} reached their peak values during articulation, Δx at 50% peak E_{xz} ($\Delta x_{1/2}$) near the surface and overall were determined and were significantly dependent upon lubricant. Differences in $\Delta x_{1/2}$ near the surface ($p=0.5$) and overall ($p=0.10$) were not statistically significant between LFC and LTP cartilage for all cases (Figure 3). Near the articular surface, $\Delta x_{1/2}$ was markedly affected by lubricant ($p<0.05$), tending to be higher when samples were tested with AI-SF ($p=0.13$) and AI-SF+HA ($p=0.07$) as lubricant than NL-SF (Figure 3A). Overall $\Delta x_{1/2}$ was also markedly affected by lubricant ($p<0.05$), increasing significantly with AI-SF as lubricant ($p<0.05$) compared to NL-SF as lubricant (Figure 3B). However, when samples were tested with AI-SF+HA as lubricant, overall $\Delta x_{1/2}$ was not significantly different than $\Delta x_{1/2}$ when NL-SF was used as lubricant ($p=0.7$).

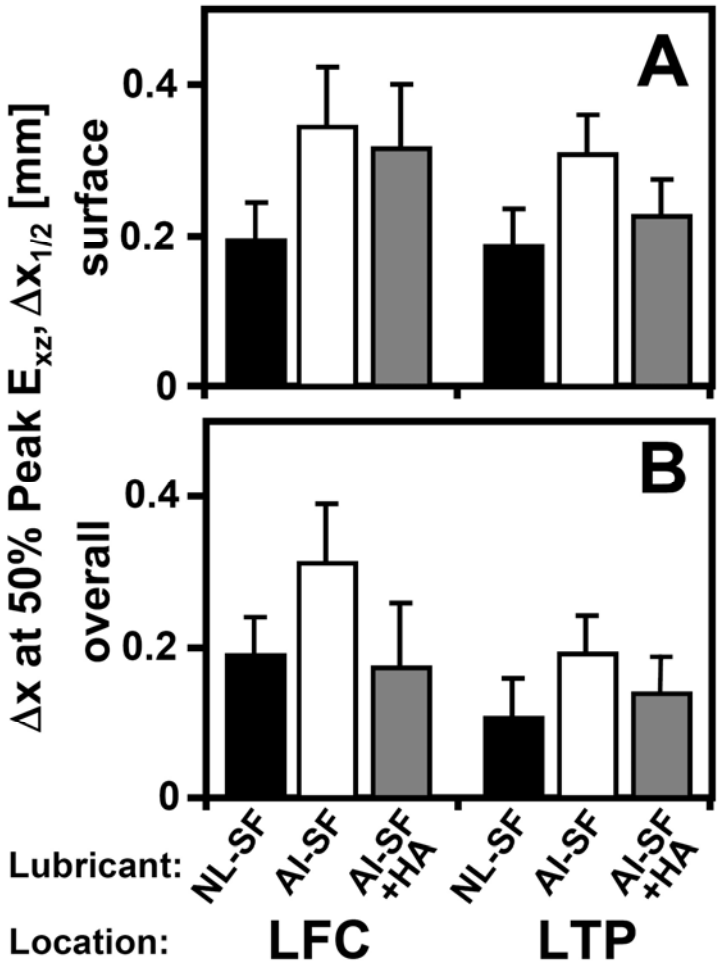

Figure 5.3: Effect of acute injury lubrication on Δx at 50% peak ($\Delta x_{1/2}$) (**A**) surface and (**B**) overall shear strain for lateral femoral condyle (LFC) and tibial plateau (LTP) samples.

Peak Shear Deformation

When tibio-femoral surfaces were sliding and E_{xz} was at a peak, lateral tissue displacements and deformation were depth-varying, being highest near the articular surface and lowest (almost negligible) near the tidemark for LFC and LTP cartilage (Figure 4A-C). For LFC cartilage, the maximum lateral displacement (mean ± SEM) was 31 ± 11 μm when tibio-femoral surfaces were lubricated with NL-SF, and increased to 48 ± 13 μm ($p=0.4$) and 41 ± 6 μm ($p=0.7$) when lubricated with AI-SF and AI-SF+HA, respectively. Similarly for LTP cartilage, the maximum lateral displacement was 76 ± 48 μm when tibio-femoral surfaces were lubricated with NL-SF, and increased to 193 ± 63 μm ($p<0.05$) when lubricated with AI-SF, but only to 143 ± 48 μm ($p=0.06$) when lubricated with AI-SF+HA. Differences in shear deformation between LFC and LTP cartilage were also apparent, with shear deformation of LFC (Figure 4A-C; top images) cartilage being much lower than LTP shear deformation (Figure 4A-C; bottom images) during tibio-femoral articulation.

Peak E_{xz} varied with tissue depth, lubricant, and joint location (Figure 4D). With tissue depth, E_{xz} markedly ($p<0.001$) decreased monotonically with increasing depth from the articular surface for all experimental conditions. There was an apparent interactive effect between lubricant and tissue depth ($p<0.001$) on LFC and LTP E_{xz}, as indicated by the differences in E_{xz} between lubricant conditions being greatest near the surface and lowest (almost indistinguishable) in the deeper regions. A similar interactive effect between cartilage location and depth on E_{xz} was also evident

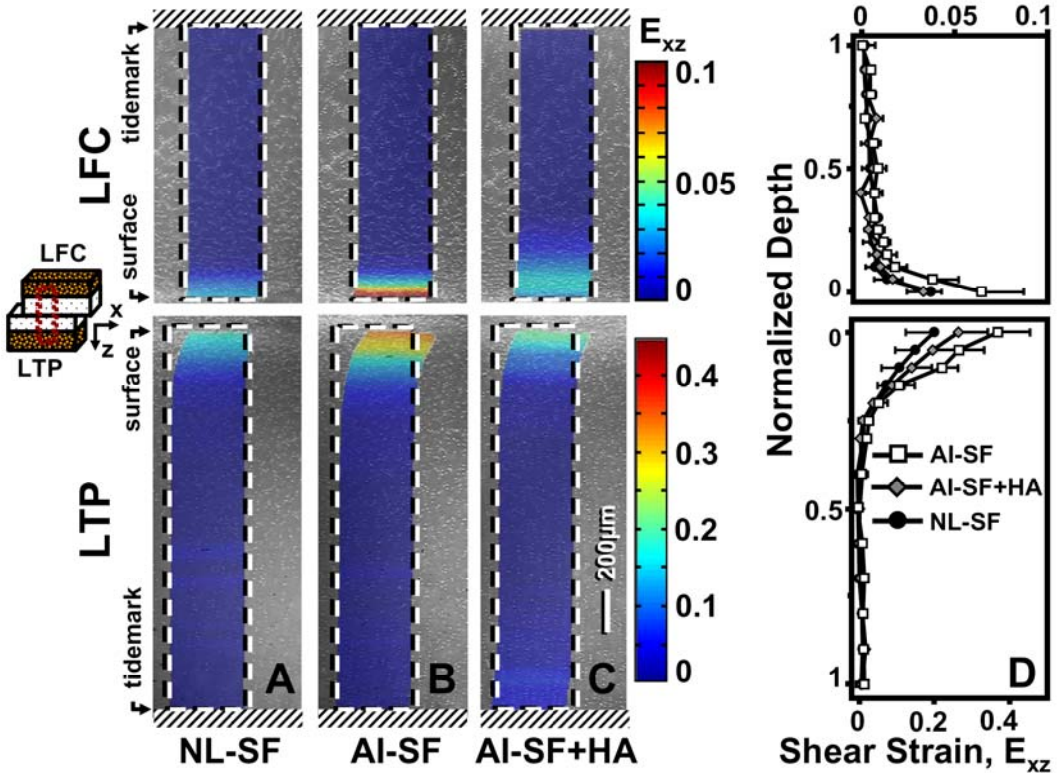

Figure 5.4: **A-C**, Representative micrographs with superimposed colormaps of shear strain taken of apposing LFC (top images) to LTP (bottom images) samples after achieving maximum shear strain with NL-SF (**A**), AI-SF (**B**), and AI-SF+HA (**C**) as lubricants. Cell nuclei tracking method was used to determine maps of shear strain (color maps, **A-C**). Dashed lines (– –) encompass the analyzed regions on the undeformed images, while strain map boundaries encompass the corresponding deformed states. **D**, Local shear strain (E_{XZ}) averaged depth-wise versus normalized tissue depth for LFC (top graph) and LTP (bottom graph) samples. Values are mean ± SEM.

($p<0.001$) for all lubricant cases, with LTP E_{xz} being markedly higher in magnitude than LFC E_{xz} near the surface and being similarly low to LFC E_{xz} near the tidemark.

Depending on the joint location (LFC or LTP) from which cartilage samples were isolated, peak E_{xz} near the surface and overall were each significantly affected by lubrication, increasing with acute injury and reducing towards normal with HA supplementation. Near the surface and overall, interactive effects between joint location and lubrication on E_{xz} were marked ($p<0.05$); and thus, effects of lubricant were further assessed within each joint location (LFC, LTP). For LTP cartilage, E_{xz} near the surface was 0.2 when tibio-femoral surfaces were lubricated with NL-SF and markedly increased ($p<0.05$) to 0.37 when surfaces were lubricated with AI-SF (Figure 5A). When AI-SF was supplemented with HA (AI-SF+HA), surface E_{xz} of LTP cartilage reduced to 0.26 during tibio-femoral articulation, and the resultant shear strain was statistically indistinguishable ($p=0.5$) from the magnitudes for normal lubricant (NL-SF) conditions. Analogous to surface E_{xz}, overall E_{xz} of LTP cartilage was 0.02 when tibio-femoral surfaces were lubricated with NL-SF and markedly increased ($p<0.05$) to 0.05 when surfaces were lubricated with AI-SF (Figure 5B). When the AI-SF lubricant was supplemented with HA (AI-SF+HA), overall E_{xz} of LTP cartilage reduced to 0.03, and the resultant shear strain was statistically indisguishable ($p=0.3$) from the magnitudes for normal lubricant (NL-SF) conditions. For LFC cartilage, surface and overall E_{xz} were tended to be lowest for NL-SF, highest for AI-SF, and 2nd highest for AI-SF+HA surface lubricants. However, differences were relatively small (<0.01) and not statistically significant for surface ($p=0.2$) and overall ($p=0.25$) E_{xz} of LFC cartilage.

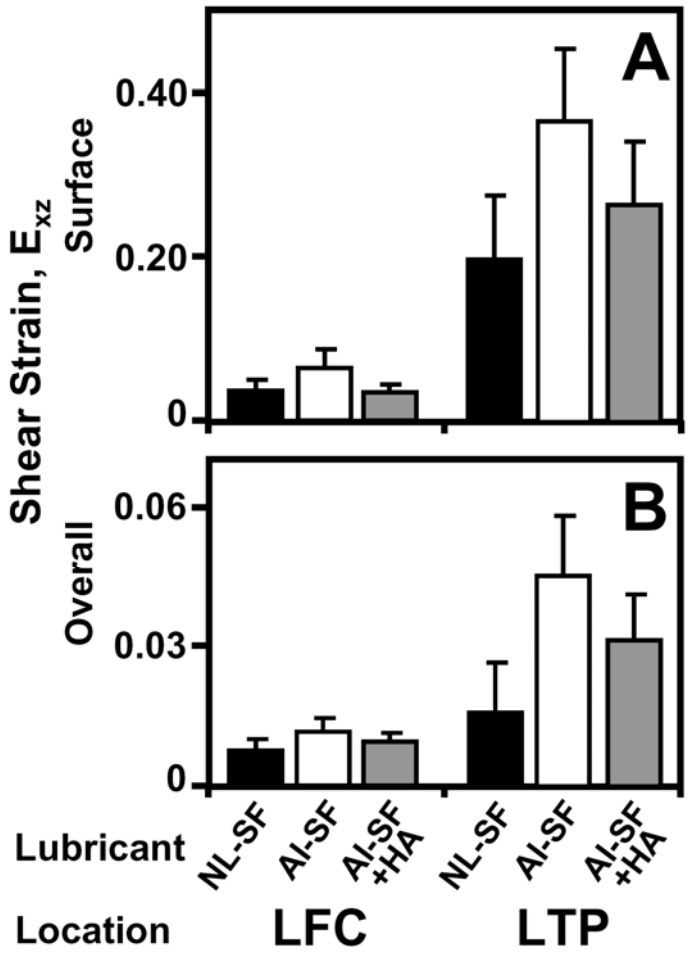

Figure 5.5: Effect of acute injury lubrication (NL-SF, AI-SF, or AI-SF+HA) on (**A**) peak surface and (**B**) overall shear strain for both lateral femoral condyle (LFC) and tibial plateau (LTP) samples.

5.5 Discussion

The present results indicate synovial fluid function, as reflected by cartilage shear deformation during tibio-femoral cartilage articulation, is markedly affected by acute injury, while supplementation with HA partially restores SF function. As indicated by surface and overall $\Delta x_{1/2}$ being ~1.8-fold higher, E_{xz} reached a steady-state peak and surfaces slid at greater Δx when samples were tested with AI-SF than with NL-SF as lubricant (Figure 3). When AI-SF was supplemented with HA (AI-SF+HA), E_{xz} reached a peak and surfaces slid at lower Δx than with AI-SF alone, as indicated by surface and overall $\Delta x_{1/2}$ being only ~0.9 to ~1.6-fold greater than samples tested with NL-SF as lubricant. When surfaces were sliding and peak deformation was achieved, cartilage E_{xz} near the surface and overall increased ~1.6 to 2.9-fold when samples were lubricated with AI-SF compared to NL-SF (Figure 4). When HA was added to AI-SF and used to lubricate samples, E_{xz} near the surface and overall were reduced compared to AI-SF, being only ~0.9 to ~2.0-fold greater than samples tested with NL-SF as lubricant. Effects of lubrication on LFC E_{xz} were similar to that for LTP cartilage ($p<0.05$), but were not statistically significant ($p=0.2$-0.25). Magnitudes of E_{xz} were consistently greater in LTP cartilage than LFC cartilage for all experimental cases, being ~7- and ~3-fold greater near the surface and overall, respectively.

The present study addresses the biomechanical environment (i.e. compression and sliding) of articulating tibio-femoral cartilage during normal joint loading. Osteochondral samples were taken from the lateral femoral condyle and donor-

matched tibial plateau, where such surfaces articulate in apposition and against one another within the joint [14]. Such regions are load-bearing, and tibio-femoral cartilage undergoes a wide range of compression (3-20%) [4, 12, 31] and sliding (~0.1 m/s) during normal activities (estimated from refs [33] and [28]). The loading parameters of present study mimic the high compressive loading (13% compression in this study) and low sliding velocity (0.1mm/s in this study) during contralateral toe-off and heel rise phases of gait [33] (when surface interaction is likely to be high) as well as the relative loading and sliding of physiologically articulating cartilage surfaces (i.e. femoral cartilage against tibial cartilage).

Furthermore, the role of the SF lubricant component of the boundary condition of articulation was analyzed in the present study. Articular cartilage surfaces were lubricated with SF from the contra-lateral normal (NL-SF) and acutely injured (AI-SF) joint to mimic normal and injured lubrication conditions during loading. Since samples were mechanically tested following an hour of stress relaxation, boundary mode lubrication was likely dominant [35], and the pattern of cartilage deformation and strain is consistent with other biomechanical studies, both of cartilage properties measured separately and of cartilage deformation during articulation. In addition, samples were tested with AI-SF supplemented with HA (AI-SF+HA) to analyze a tribosupplementation type of therapy with added HA as lubricant [2]. HA was added to AI-SF to bring the total supplemented HA concentration to be ~1 mg/ml. Such a concentration was selected so final levels of HA in AI-SF+HA would be within the range (0.3-1.3 mg/ml) [19, 20, 30] [17] reported in normal equine SF. Whether other

tribosupplements, such as PRG4 or LUB-1, the engineered variant of PRG4, [5] have similar effects, remains to be established.

While equine SF was used to lubricate human articular cartilage and SF function may be species dependent, SF from equine joints did reduce E_{xz} in human cartilage during loading. Normal SF from bovine joints reduced boundary mode friction between bovine cartilage surfaces [26] and human cartilage E_{xz} (~50%) compared to saline [34]. The current tests were conducted with human articular cartilage being lubricated with equine SF during tibio-femoral articulation. Resultant E_{xz} near the surface and overall were 50% lower when samples were tested with normal equine SF (NL-SF) compared to previous studies using PBS [36]. Since the function of equine SF, of reducing E_{xz} in human cartilage, was preserved compared to the function of saline, the lubricating function of equine SF appears to be species independent. This is consistent with findings that equine SF lubricates bovine cartilage, as indicated by boundary-mode friction, just as well as bovine SF [1].

Acute injury alters SF function to reduce cartilage shear deformation, with surfaces sliding after greater Δx during tibio-femoral articulation. Consistent with the events described for cartilage-on-cartilage articulation [35], tibio-femoral cartilage articulation involved four sequential events: adherence, adherence and shear deformation, surface detachment as shear deformation peaks, and sliding with maintenance of peak shear (Figure 6A). Acute injury significantly reduces the ability of SF to reduce surface interaction (as indicated by boundary-mode friction) during cartilage-on-cartilage articulation [1], which would be predicted to result in surface detachment at greater Δx magnitudes (Figure 6B, III). Increased Δx at which surfaces

detach and slide would result in greater peak cartilage E_{xz}. When samples were lubricated with AI-SF, overall $\Delta x_{1/2}$ markedly elevated, indicating surface detached at

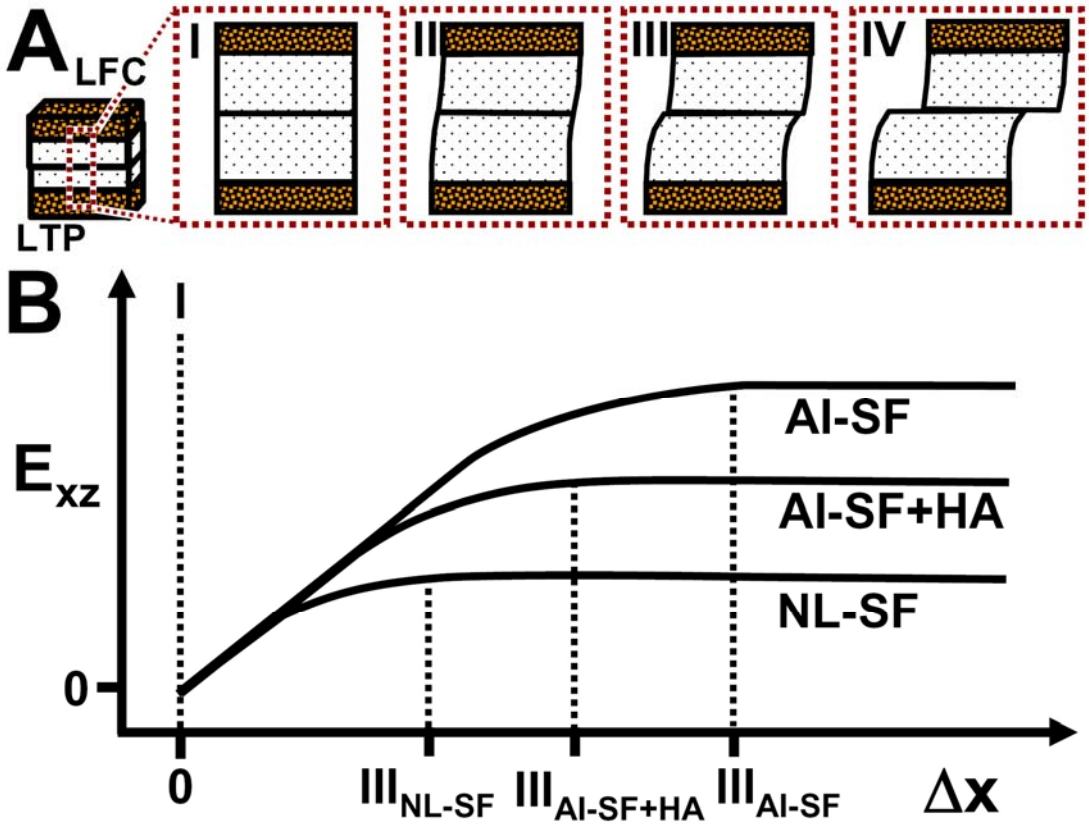

With Acute Injury Lubrication and HA Supplementation**Figure 5.6:** (**A**) Schematic of the four sequential events ((**I**) adherence, (**II**) adherence and deformation, (**III**) detachment, and (**IV**) sliding) that occurs during tibio-femoral cartilage articulation and (**B**) representative shear strain (E_{XZ}) versus applied lateral displacement (Δx) diagrams with markers indicating where detachment (**III**) occurs for each lubricant condition.

greater Δx magnitudes than when NL-SF was used as a lubricant (Figure 6B). Collectively, such results suggest articular surfaces detached and slid later with AI-SF as lubricant, due to increased surface interaction, and caused an elevation in peak E_{xz}.

The ability of tribosupplementation by HA to reduce cartilage shear deformation was significant but did not appear to fully restore tissue mechanics. As indicated by overall $\Delta x_{1/2}$ reducing towards normal, surfaces slid at lower Δx and resulted in lower peak E_{xz} when samples were tested with AI-SF supplemented with HA as lubricant than with AI-SF alone. However, resultant E_{xz} was generally higher (~0-98%) when samples were tested with AI-SF+HA than NL-SF as lubricant despite differences being not statistically significant (p=0.3-0.5). Such results indicate tribosupplementation by HA alone does not fully restore SF function following acute injury. While cells and gross debris were clarified from SF, residual blood and minuscule debris could still be present and may have interfered with lubricant molecules interacting synergistically [25] to reduce surface interaction, and thus resultant tissue shear, during loading. Despite shear being higher when samples were tested with AI-SF+HA than NL-SF as lubricant, HA supplementation (AI-SF+HA) reduced E_{xz} by ~20-50% compared to lubricant conditions without HA supplementation (AI-SF) (Figure 4).

The greater shear deformation in cartilage from the tibia than the femoral condyle is consistent with studies on *in vitro* tibio-femoral cartilage shear deformation. Differences in shear deformation between LFC and LTP cartilage are a reflection of the cartilage from femoral condyles being stiffer in shear than the cartilage from the tibial plateau. Analogous to the current study, osteochondral

samples from the tibial plateau and femoral condyle were previously tested mechanically with articular surfaces in apposition, but with PBS as lubricant [36]. Resultant cartilage E_{xz} near the surface and overall were found to be ~80% higher in tibial cartilage than femoral cartilage, being consistent with the current differences in E_{xz} near the articular surface between LFC and LTP samples (~81-87%) for all lubricant cases. However, differences in overall E_{xz} between LFC and LTP cartilage decreased from ~75% with AI-SF as lubricant to 69% with AI-SF+HA as lubricant and to ~52% with NL-SF as lubricant. Such results suggest normal lubrication reduces the relative differences in overall shear deformation between articulating surfaces.

The present study provides insight into the effects of acute injury on SF function, as indicated by cartilage mechanics, during tibio-femoral joint articulation and tribosupplementation to restore SF function following acute injury. The results collectively suggest acute injury impairs the function of SF to reduce interaction between articulating surfaces, which causes surfaces to detach later than normal, elevating cartilage shear deformation. Tribosupplementation of HA to AI-SF reduces elevated shear deformation by reducing surface interaction as indicated by surfaces detaching and sliding sooner than without added HA (AI-SF). Reduced SF function, as indicated by friction, is positively associated with cartilage wear in mice joints [11], suggesting altered SF function contributes to cartilage degeneration. Impaired SF function may contribute to cartilage wear through elevated tissue E_{xz}. Excessive E_{xz} that results from altered SF function may result in damage to cells and matrix, analogous to excessive compression [3, 13, 18, 29], and contribute to post-injury cartilage degeneration and wear. Tribosupplementation of HA to biomechanically

deficient SF in the knee is a current clinical treatment for osteoarthritis and postulated to have chondroprotective effects [2]. While extensive investigations have been performed to determine clinical outcomes of HA supplementation and shown to be variable [2, 32], studies to elucidate specifically the efficacy of tribosupplementation with HA to restore SF function have been limited. The present findings suggest tribosupplementation with HA restores SF function to modulate cartilage shear deformation to some degree.

5.6 Acknowledgments

We like to thank co-authors Seung Hyun Chris Kim, Jennifer M. Antonacci, and Dr. C. Wayne McIlwraith for their contributions to this work. We thank the many residents and staff at Dr. Lotz's Laboratory at the Scripps Research Institute for harvesting and providing the human tissue used in this study. This work was supported by the NIH and Howard Hughes Medical Institute through the Professors Program Grant to UCSD for Dr. Robert L. Sah.

5.7 References

1. Antonacci JM, Ballard BL, Schumacher BL, Sah RL: Role of hyaluronan in bovine synovial fluid in the boundary lubricating of articular cartilage. *Trans Orthop Res Soc* 33:625, 2008.

2. Brockmeier SF, Shaffer BS: Viscosupplementation therapy for osteoarthritis. *Sports Med Arthrosc* 14:155-62, 2006.

3. Chen C-T, Bhargava M, Lin PM, Torzilli PA: Time, stress, and location dependent chondrocyte death and collagen damage in cyclically loaded articular cartilage. *J Orthop Res* 21:888-98, 2003.

4. Eckstein F, Hudelmaier M, Putz R: The effects of exercise on human articular cartilage. *J Anat* 208:491-512, 2006.

5. Flannery CR, Zollner R, Corcoran C, Jones AR, Root A, Rivera-Bermudez MA, Blanchet T, Gleghorn JP, Bonassar LJ, Bendele AM, Morris EA, Glasson SS: Prevention of cartilage degeneration in a rat model of osteoarthritis by intraarticular treatment with recombinant lubricin. *Arthritis Rheum* 60:840-7, 2009.

6. Frank EH, Grodzinsky AJ, Koob TJ, Eyre DR: Streaming potentials: a sensitive index of enzymatic degradation in articular cartilage. *J Orthop Res* 5:497-508, 1987.

7. Fung YC. A First Course in Continuum Mechanics. 2nd ed. Englewood Cliffs: Prentice-Hall; 1977.

8. Fung YC. Biomechanics: Mechanical Properties of Living Tissues. 2nd ed. New York: Springer-Verlag; 1993.

9. Gratz KR, Sah RL: Experimental measurement and quantification of frictional contact between biological surfaces experiencing large deformation and slip. *J Biomech* 41:1333-40, 2008.

10. Jay GD: Lubricin and surfacing of articular joints. *Curr Opin Orthop* 15:355-9, 2004.

11. Jay GD, Torres JR, Rhee DK, Helminen HJ, Hytinnen MM, Cha CJ, Elsaid K, Kim KS, Cui Y, Warman ML: Association between friction and wear in diarthrodial joints lacking lubricin. *Arthritis Rheum* 56:3662-9, 2007.

12. Kersting UG, Stubendorff JJ, Schmidt MC, Bruggemann GP: Changes in knee cartilage volume and serum COMP concentration after running exercise. *Osteoarthritis Cartilage* 13:925-34, 2005.

13. Loening A, Levenston M, James I, Nuttal M, Hung H, Gowen M, Grodzinsky A, Lark M: Injurious compression of bovine articular cartilage induces apoptosis before detectable mechanical damage. *Trans Orthop Res Soc* 24:42, 1999.

14. Mow VC, Hayes WC, eds. Basic Orthopaedic Biomechanics. 2nd ed. New York: Raven Press; 1997.

15. Mow VC, Huiskes R. Basic Orthopaedic Biomechanics and Mechano-Biology. 3rd ed. Philadelphia: Lippincott Williams & Wilkins; 2005.

16. Noyori K, Takagi T, Jasin HE: Characterization of the macromolecular components of the articular cartilage surface. *Rheumatol Int* 18:71-7, 1998.

17. Palmer JL, Bertone AL, McClain H: Assessment of glycosaminoglycan concentration in equine synovial fluid as a marker of joint disease. *Can J Vet Res* 59:205-12, 1995.

18. Patwari P, Gaschen V, James IE, Berger E, Blake SM, Lark MW, Grodzinsky AJ, Hunziker EB: Ultrastructural quantification of cell death after injurious compression of bovine calf articular cartilage. *Osteoarthritis Cartilage* 12:245-52, 2004.

19. Rowley G, Antonas KN, Hilbert BJ: Quantitation of hyaluronic acid in equine synovia. *Am J Vet Res* 43:1096-9, 1982.

20. Saari H, Konttinen YT, Tulamo RM, Antti-Poika I, Honkanen V: Concentration and degree of polymerization of hyaluronate in equine synovial fluid. *Am J Vet Res* 50:2060-3, 1989.

21. Sah RL, Grodzinsky AJ, Plaas AHK, Sandy JD: Effects of static and dynamic compression on matrix metabolism in cartilage explants. In: *Articular Cartilage and Osteoarthritis,* ed. by KE Kuettner, Schleyerbach R, Peyron JG, Hascall VC, Raven Press, New York, 1992, 373-92.

22. Sarma AV, Powell GL, LaBerge M: Phospholipid composition of articular cartilage boundary lubricant. *J Orthop Res* 19:671-6, 2001.

23. Schinagl RM, Gurskis D, Chen AC, Sah RL: Depth-dependent confined compression modulus of full-thickness bovine articular cartilage. *J Orthop Res* 15:499-506, 1997.

24. Schinagl RM, Ting MK, Price JH, Sah RL: Video microscopy to quantitate the inhomogeneous equilibrium strain within articular cartilage during confined compression. *Ann Biomed Eng* 24:500-12, 1996.

25. Schmidt TA, Gastelum NS, Nguyen QT, Schumacher BL, Sah RL: Boundary lubrication of articular cartilage: role of synovial fluid constituents. *Arthritis Rheum* 56:882-91, 2007.

26. Schmidt TA, Sah RL: Effect of synovial fluid on boundary lubrication of articular cartilage. *Osteoarthritis Cartilage* 15:35-47, 2007.

27. Schumacher BL, Block JA, Schmid TM, Aydelotte MB, Kuettner KE: A novel proteoglycan synthesized and secreted by chondrocytes of the superficial zone of articular cartilage. *Arch Biochem Biophys* 311:144-52, 1994.

28. Shelburne KB, Torry MR, Pandy MG: Muscle, ligament, and joint-contact forces at the knee during walking. *Med Sci Sports Exerc* 37:1948-56, 2005.

29. Thibault M, Poole AR, Buschmann MD: Cyclic compression of cartilage/bone explants in vitro leads to physical weakening, mechanical breakdown of collagen and release of matrix fragments. *J Orthop Res* 20:1265-73, 2002.

30. Tulamo RM: Comparison of high-performance liquid chromatography with a radiometric assay for determination of the effect of intra-articular administration of corticosteroid and saline solution on synovial fluid hyaluronate concentration in horses. *Am J Vet Res* 52:1940-4, 1991.

31. Van de Velde SK, Bingham JT, Gill TJ, Li G: Analysis of tibiofemoral cartilage deformation in the posterior cruciate ligament-deficient knee. *J Bone Joint Surg Am* 91:167-75, 2009.

32. Waddell DD: Viscosupplementation with hyaluronans for osteoarthritis of the knee: clinical efficacy and economic implications. *Drugs Aging* 24:629-42, 2007.

33. Whittle M. Gait Analysis: An Introduction. 3rd ed. Oxford; Boston: Butterworth-Heinemann; 2002.

34. Wong BL, Bae WC, Chun J, Gratz KR, Sah RL: Biomechanics of cartilage articulation: effects of lubrication and degeneration on shear deformation. *Arthritis Rheum* 58:2065-74, 2008.

35. Wong BL, Bae WC, Gratz KR, Sah RL: Shear deformation kinematics during cartilage articulation: effect of lubrication, degeneration, and stress relaxation. *Mol Cell Biomech* 5:197-206, 2008.

36. Wong BL, Sah RL: Cartilage mechanicals during tibio-femoral articulation: local and overall compressive and shear deformation and properties. *J Biomech* Submitted, 2009.

37. Yamada K, Healey R, Amiel D, Lotz M, Coutts R: Subchondral bone of the human knee joint in aging and osteoarthritis. *Osteoarthritis Cartilage* 10:360-9, 2002.

CHAPTER 6

EFFECT OF A FOCAL ARTICULAR DEFECT ON CARTILAGE ARTICULATION DURING PATELLO-FEMORAL ARTICULATION

6.1 Abstract

Objective: To determine the deformation of cartilage near and in apposition of a focal articular defect during patello-femoral articulation.

Methods: Bovine osteochondral blocks from the trochlea (TRO) and patella (PAT) were apposed, compressed 12%, and subjected to sliding under video microscopy. Samples, lubricated with synovial fluid, were tested as intact and then with a full-thickness defect in the center of patellar cartilage. Shear (E_{xz}), axial (E_{zz}), and lateral (E_{xx}) strains were determined as a function of depth at varying lateral regions from the defect edge for TRO and PAT cartilage.

Results: For articulation with a focal defect, TRO cartilage partially filled the defect and then pushed and plowed over the defect edge following lateral motion. Consequently, surface strains of PAT cartilage with a defect were ~2-8x lower in shear and ~1.4x higher in compression than intact cartilage. At 20% depth, E_{xz} and E_{xx} for PAT cartilage with a focal defect were ~2x and ~10-25x higher than intact

samples, respectively. For TRO cartilage articulating against a focal defect, E_{xz} and E_{zz} near the surface and at 20% tissue depth were ~2-4x lower than that for articulation with intact cartilage, while lateral strains near the surface transitioned from compression to tension with increasing lateral distance.

Conclusion: The results extend findings of cartilage compression with focal defects by identifying regions that undergo dramatic changes in tissue strain due to lateral motion. In these regions, such altered cartilage mechanics during knee movement may cause focal defects to expand, and bordering cartilage to degenerate progressively.

6.2 Introduction

Focal articular defects are prevalent in symptomatic knees and are associated with accelerating cartilage degeneration. In patients evaluated arthroscopically, focal defects were found in 20-60% of all symptomatic knees, occurring most frequently in the medial condyle and patella, which are load-bearing regions (Figure 6.1) [1, 6, 19, 36]. With an average area of 2.1 cm^2, focal defects typically range from 0.5 to 4 cm^2 in area, and extend beyond half the cartilage thickness in depth in 50% of all diagnosed articular defects[19]. With continued joint loading and time, untreated defects enlarge[34] and accelerate cartilage volume loss[5, 37], exhibiting signs of cartilage degeneration near the focal defect[21, 23]. While such findings suggest that the presence of a focal defect predispose joints to secondary osteoarthritis, the mechanism by which it causes cartilage within the proximity of a focal defect to progressively degenerate remains to be elucidated.

With the presence of a focal defect, cartilage mechanics during loading markedly changes and may contribute to the progressive degeneration of cartilage. Under axial compression alone, contact stress and stress gradients are elevated in areas of cartilage near the edges of a focal defect[3, 15]. As a result, macroscopic tissue deformation[2] and local strains [13] [14] are markedly increased in cartilage near the defect edge. However, tissue deformation under compression and following lateral motion, which both occur during physiologic joint movement, in the presence of a focal defect remains to be elucidated. Elevated strains can reach levels that induce cell death[22, 25] and matrix damage[28], and thus, changes in the cartilage strains

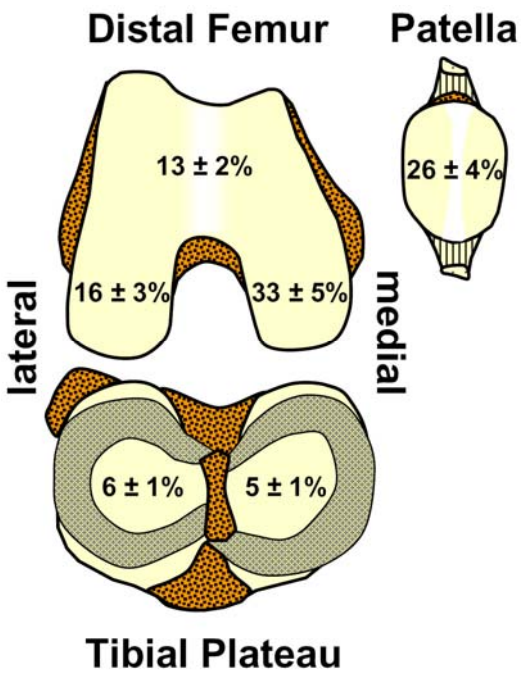

Figure 6.1: Anatomical distribution of focal articular defects averaged from four previous arthroscopy studies on the prevalence of cartilage defects in symptomatic knees[1, 6, 19, 36].

resulting from a focal defect may become injurious to cartilage and induce degeneration. Characterization of the effects of a focal defect on cartilage deformation during articulation would further the understanding of focal defect cartilage mechanics and elucidate the role of mechanical strain in cartilage degeneration associated with focal defects.

During knee movement, articular surfaces contact, compress, and articulate against each other. Within the knee, patellar cartilage contacts and slides against trochlear (also known as the femoral groove) cartilage during normal joint movement and loading (Figure 6.2A) [27]. Under applied compressive loads of ~1.5 times the body weight, patello-femoral cartilage compresses ~10% of its overall thickness *in vitro* following 14 minutes of static loading [18]. While following knee bending, patellar cartilage alone compresses about ~5-10% overall *in vivo* [8]. Collectively, such results provide mechanical parameters for the *in vitro* testing of patello-femoral cartilage articulation that would be within the physiologic range of joint loading.

Recently, several studies have measured intra-tissue strains of cartilage under compression alone and compression with shear during cartilage-on-cartilage articulation. Such studies used video microscopy [30] and image correlation to track the displacement of fidicial markers [12, 33] to determine local and overall deformation of cartilage with a resolution sufficient to resolve small magnitudes (~1%) of strain. More recently, osteochondral blocks from the tibia and femoral condyle were compressed in apposition and subjected to lateral shearing motion with this experimental approach to mimic the biomechanical environment during joint movement[39]. Using this configuration, osteochondral samples from the patella and

trochlea can be apposed (Figure 6.2A,B) as well and tested to examine the effects of a focal articular defect on cartilage deformation during compression and lateral motion (Figure 6.2C), further elucidating the effect of a focal defect on cartilage mechanics during joint movement.

Therefore, the hypothesis of this study was that during patello-femoral cartilage articulation, the cartilage deformation of the patella and trochlea are markedly altered with the presence of a focal articular defect. The specific objective of this study was to determine the effects of a focal articular defect, created in the patellar tissue, on the local and overall strains of the patellar and trochlear cartilage during compression and sliding motion.

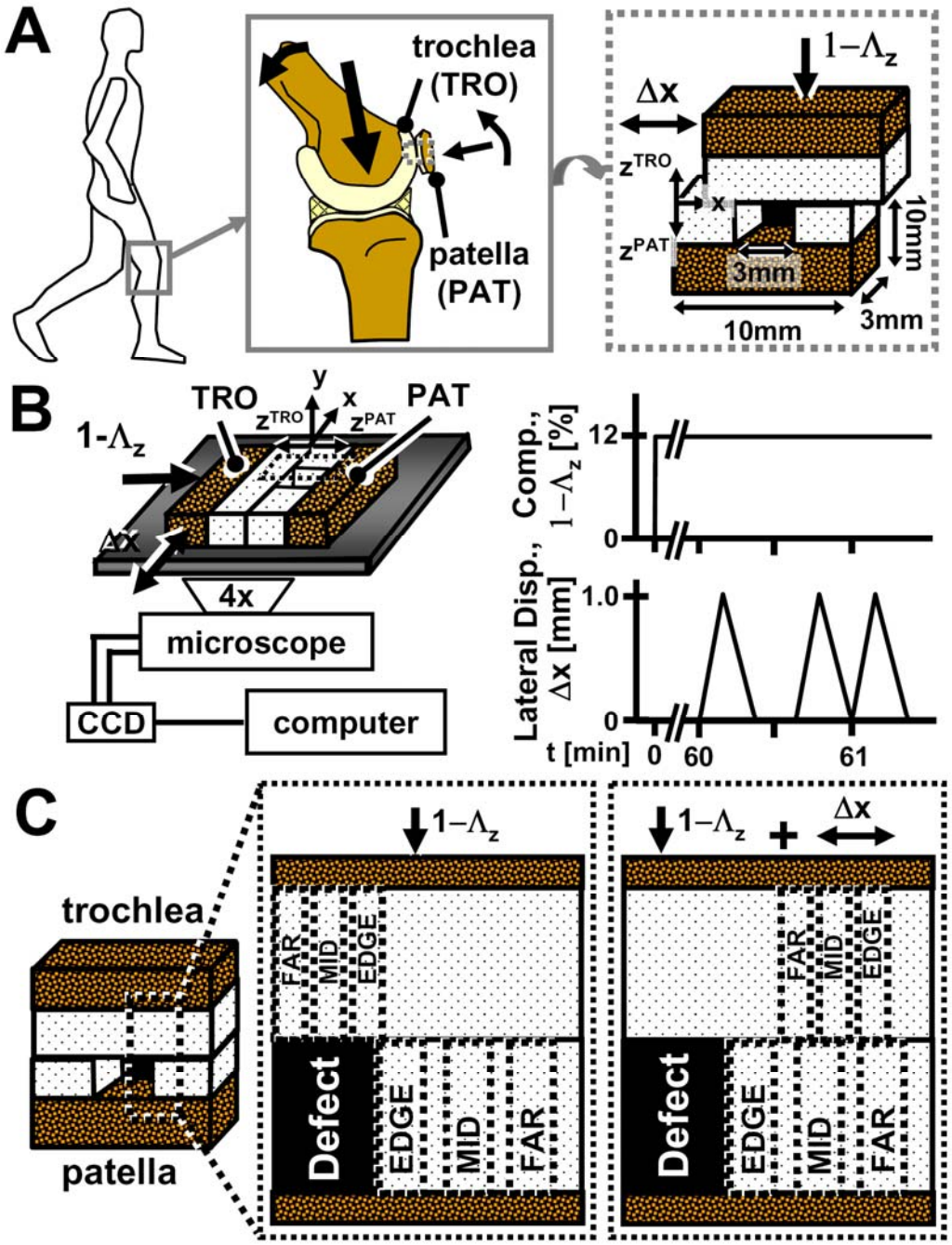

Figure 6.2: Schematic of (**A**) knee joint movements at multiple scales, (**B**) experimental setup and loading protocol for micro-shear testing, (**C**) and locations of sub-regions (EDGE, MID, FAR) used for statistical analysis of strains in patella and trochlear cartilage.

6.3 Materials and Methods

Sample Isolation And Preparation

Osteochondral cores with macroscopically normal cartilage were harvested from the trochlea (TRO) and patella (PAT) of four adult bovine animals (1-2yrs). Using a low speed drill press with custom stainless steel coring bits, a 10 mm diameter osteochondral core was isolated from both the trochlea and donor-matched patella of each joint in a manner similar to that described previously[31]. During isolation, tissue was constantly irrigated with 4^{o}C phosphate buffered saline (PBS) containing proteinase inhibitors (PI) [9]. The TRO and PAT cores were then each trimmed using a low-speed saw with a 0.3 mm thick diamond edge blade (Isomet^{TM}, Buehler, Lake Bluff, IL) to yield one ~rectangular block for biomechanical testing as described previously[38]. Each rectangular block had a cartilage surface area of ~3x10 mm^2 and a total thickness of ~1 cm (Figure 6.2A). Each sample consisted of one TRO and one donor-matched PAT block.

Prior to mechanical testing, samples were stained and lubricated. First, samples were bathed for ~2-4 h at 4^{o}C in PBS+PI and propidium iodide (20 μg/ml) to fluorescently highlight cell nuclei. Subsequently, blocks were bathed in normal bovine synovial fluid (SF) containing PI and propidium iodide (20 mg/ml) at 4^{o}C for 12-16 h to lubricate surfaces. The SF was pooled from adult bovine knees, stored at -80^{o}C, and characterized previously for boundary lubrication properties [31] and for levels of lubricant molecules (~1 mg/ml of hyaluronan and 0.45 mg/ml of proteoglycan 4 [26]).

Experimental Design

To characterize the effect of a focal defect on cartilage deformation during articulation, samples were mechanically tested first as intact and then retested with a focal defect. In between tests, samples were rinsed, allowed to reswell, and incubated for ~2-4 h in PBS+PI and then in SF+PI for an additional 12-16h at 4ºC. Following the mechanical testing of intact samples and reincubation, a full thickness, 3 mm wide focal articular defect was created in the center of the patellar cartilage (Figure 6.2A) as described previously[13]. Briefly, 3 vertical incisions (perpendicular to the articular surface) that extended through the calcified cartilage layer were made; one in the center of the chondral surface and one on each side of the center incision (1.5 mm away). An additional incision was made along the bone starting at the center vertical incision, cutting towards each edge until the cartilage was released. The width of the focal defect was chosen so that the ratio of sample contact area to defect area matched that of the patello-femoral joint contact area to the defect area of a relatively small focal defect (< 1cm^2).

Micro-Scale Shear Testing

Samples were microscale shear tested in a manner similar to that described previously [39]. Briefly, each TRO and PAT pair was secured in a custom bi-axial loading chamber mounted onto an epi-fluorescence microscope for digital video imaging [29] with cartilage surfaces in apposition (Figure 6.2B). The chamber secured the PAT block at the bone and allowed in-plane movement of the apposing mobile TRO block with orthogonally positioned plungers interfaced with either a micrometer

(for axial displacement; Model 262RL; Starrett Co., Athol, MA) or motion-controller (for lateral displacement; Model MFN25PP; Newport, Irvine, CA). Subsequently, an axial displacement was applied (~40 μm/s) to the bone portion of the TRO sample to induce 12% compression ($1-\Lambda_z$, where Λ_z is the stretch ratio [11]) of the overall (i.e. TRO and PAT) cartilage thickness (Figure 6.2B) determined from gross images. Samples were then allowed to stress relax for 1h which was determined to be sufficient to reach an approximate equilibrium stress for the current sample geometries [38].

As described previously[39], cartilage deformation was captured during shear loading separately in the TRO and PAT cartilage following axial compression. Three sets of applied lateral displacements (Δx), each consisting of +1 mm and then −1 mm (returning to initial position) was applied at 100 μm/s to the bone portion of the TRO block (Figure 6.2B) to induce relative lateral motion. The first set, followed by a ~12 s pause, was for preconditioning [31], while the second and third set was recorded for the PAT and TRO blocks for analysis, respectively. The sliding velocity was chosen based on the range of velocities (0-0.1 m/s) occurring during the loading (stance) phase of gait [32, 35]. To capture the shear deformation and sliding during patello-femoral cartilage articulation, sequential fluorescence images were taken separately for PAT and TRO cartilage at 4 frames/s before and during the application of lateral displacements. Resultant images with a field of view of ~3×2 mm^2 encompassed the entire cartilage thickness and a partial view of the apposing surface.

Data Collection and Calculations

Acquired digital micrographs from microscale tests were analyzed as described previously [12, 38] in MATLAB 7.0 (Mathworks, Inc., Natick, MA) to determine the depth-varying and overall deformation in cartilage. Evenly distributed cell nuclei (~250 cells/mm^2) served as fiducial markers and were tracked by maximizing cross-correlation of regions surrounding each marker to the preceding, and then initial frames. Displacements of uniformly-spaced (10 pixel) mesh points in the region of interest were calculated from local affine mappings of nuclei during deformation, and displacement gradients were determined by finite difference approximation. Subsequently, Lagrangian shear (E_{xz}), axial (E_{zz}), and lateral (E_{xx}) strains were determined relative to the unloaded state [10] and when articular surfaces were sliding (~0.8 mm of applied lateral displacement), at which time, strains were relatively constant.

To assess depth-variation and the effect of lateral location on resultant strains, local strains were averaged depth-wise and plotted as a function of tissue depth at various lateral distances from the defect edge. First, sample thickness was normalized and divided into 8 intervals, with 4 intervals being 0.083 times the normalized thickness near the articular surface (i.e. 0 to 0.333) and 0.167 times for the remaining tissue depth (i.e. 0.333 to 1). To reduce noise and consolidate data, strains were then averaged at the same normalized depth interval for lateral regions (~0.2mm x full cartilage thickness) at (EDGE), ~0.4 mm (MID) and ~0.8 mm (FAR) away from the defect edge for PAT cartilage (Fig. 1C) to yield a depth-profile at varying lateral distances from the defect edge. While for TRO cartilage, strains were averaged depth-

wise at lateral regions (~0.15mm x full cartilage thickness) at (EDGE), ~0.3 mm (MID), and ~0.5 mm (FAR) away from the defect edge. For intact tissue, intra-tissue strains in corresponding lateral regions were determined similarly. Overall strain values were determined as the mean of all local values.

Statistical Analysis

Data are reported as mean ± standard error of the mean (SEM), unless noted otherwise. Repeated measures ANOVA was used to determine the effects of a focal defect (intact versus defect), tissue depth, and lateral location from the defect edge (EDGE, MID, FAR) on local and overall strains. Differences between defect and intact samples at various lateral locations were assessed by planned pair-wise comparisons. Systat 10.2.05 (Systat Software, Richmond, CA) and Microsoft Office Excel 2003 (Microsoft Corporation, Redmond, WA) were used to perform all statistical analyses.

6.4 Results

As intact, deformation of PAT and TRO cartilage was similar qualitatively, being depth-varying during axial compression as well as during lateral motion. Cartilage thickness was similar between intact samples, being 1.97 ± 0.13 mm and 1.93 ± 0.14 mm in thickness for PAT and TRO cartilage, respectively. Under compression alone, axial deformation of intact PAT and TRO cartilage were similarly depth-varying, being highest near the surface and lowest near the tidemark. Also during compression, shear and lateral deformation were low (<0.01) for both PAT and TRO surfaces. During lateral motion, shear deformation was depth-varying for both intact PAT and TRO cartilage, being highest at the surface and decreasing monotonically with increasing tissue depth. Changes in axial and lateral deformation during lateral motion were not apparent.

Following the creation of a focal defect in the patellar cartilage, gross deformation of TRO and PAT cartilage was altered qualitatively during axial compression and lateral motion. Under compression alone, TRO cartilage directly in apposition of the focal defect "mushroomed" into and partially filled the empty defect region (Figure 6.3). As a result, PAT cartilage adjacent to the defect edge appeared to collapse or compress further, causing the tissue to laterally "bulge" outward just beneath the articular surface. With lateral motion, the region of TRO cartilage partially filling the focal defect plowed over and further compressed the defect edge, eventually becoming compressed as it slid over the PAT cartilage surface

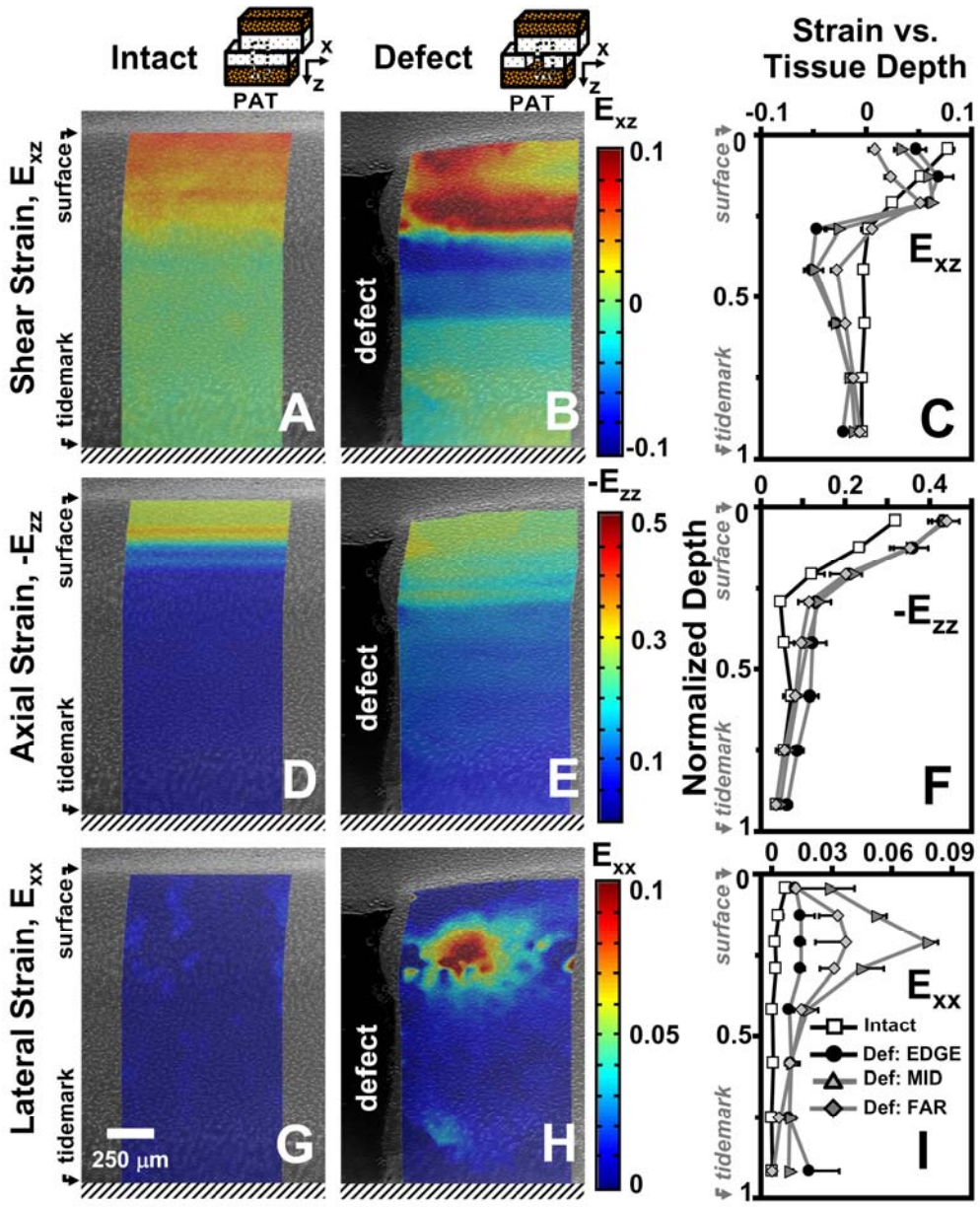

Figure 6.3: Representative micrographs of patellar cartilage as (**A**,**D**,**G**) intact or (**B**,**E**,**H**) with a focal defect with superimposed colormaps of (**A**,**B**) shear (E_{xz}), (**D**,**E**) axial ($-E_{zz}$), and (**G**,**H**) lateral (E_{xx}) strain maps (color maps) when articulating against trochlear samples after articular surfaces have slid. The boundaries of strain maps encompass the corresponding deformed states. Local (**C**) shear (E_{xz}), (**F**) axial ($-E_{zz}$), and (**I**) lateral (E_{xx}) strain averaged depth-wise versus normalized tissue depth for patella cartilage as intact or with a focal defect. For samples with a focal defect, strains were also determined as a function of lateral distance from the defect edge (EDGE, MID, FAR). Values are mean ± SEM.

Patellar Cartilage Deformation

Shear Strain (E_{xz}) – Following compression and lateral articulation, E_{xz} of PAT cartilage was depth-varying without (i.e. intact) and with a focal defect (Figure 6.3A,B), and markedly changed with a focal defect ($p<0.05$). As intact, cartilage E_{xz} did not apparently vary with lateral location ($p=0.6$) and decreased monotonically ($p<0.001$) from ~0.8 near the surface to relatively low magnitudes (≤ 0.01) near the tidemark (Figure 6.3C). With a focal defect, cartilage E_{xz} was also depth-varying ($p<0.001$); however, strains peaked at ~20% tissue depth and became a minimum at ~40% depth for all lateral locations (Figure 6.3C). Near the surface, E_{xz} of cartilage with a defect tended ($p=0.07$) to be ~2-8x lower than that for intact (Figure 6.4A). With increasing lateral distance from the defect edge, surface E_{xz} decreased from ~0.05 to 0.01 for cartilage with a defect ($p<0.01$), while remained constant for intact samples. At 20% tissue depth, E_{xz} was ~2x higher for cartilage with a defect than intact samples at all lateral distances ($p<0.01$), being significantly higher at EDGE ($p<0.05$) and MID ($p<0.01$) regions (Figure 6.4B). Overall, E_{xz} of cartilage with a defect was 4-5x times lower ($p<0.05$) than that for intact cartilage and did not vary markedly with lateral location ($p=0.15$) (Figure 6.4C).

Axial Strain (E_{zz}) – Patella $-E_{zz}$ decreased significantly with depth from the articular surface ($p<0.001$) for both intact and defect samples (Figure 6.3D-F), and was markedly higher for cartilage with a focal defect ($p<0.05$). With increasing tissue depth, $-E_{zz}$ decreased significantly ($p<0.001$) from 0.32 and 0.43 near the surface to ~0.04 near the tidemark for both intact and defect samples, respectively (Figure 6.3F).

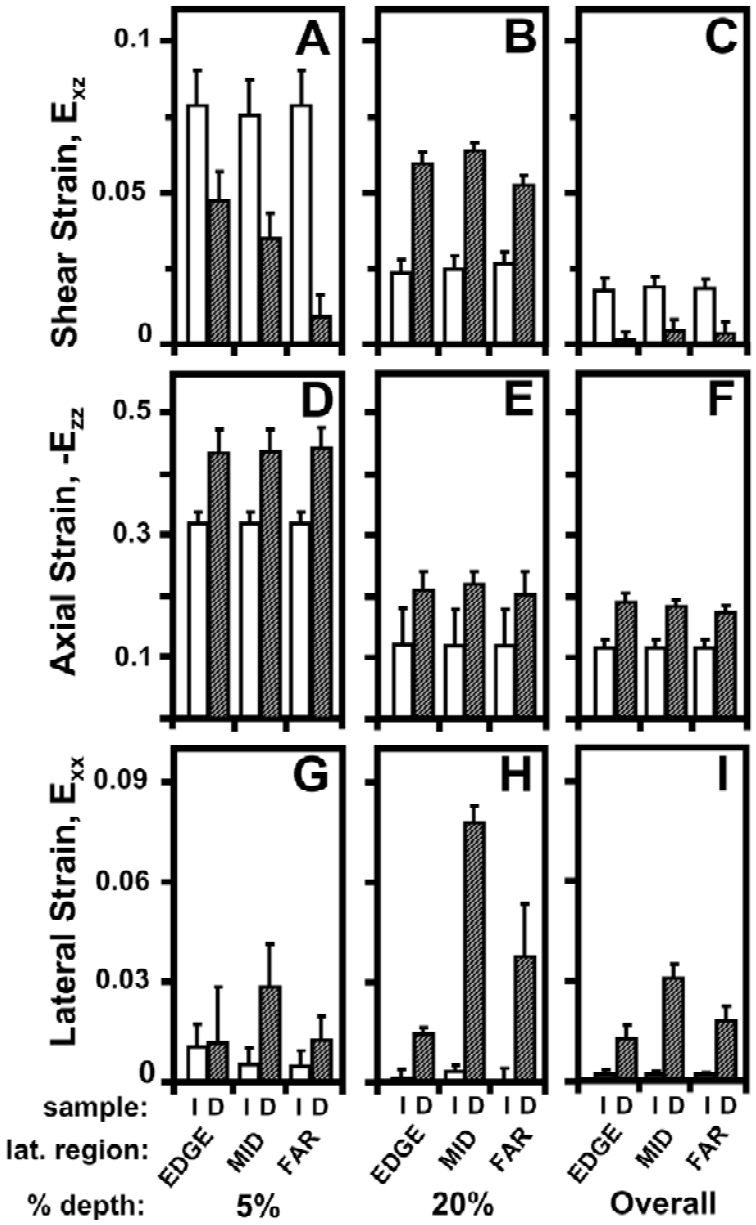

Figure 6.4: Effect of a focal defect (intact (I) versus defect (D)) on (**A**-**C**) shear, (**D**-**F**) axial, and (**G**-**I**) lateral strain (**A**,**D**,**G**) near the articular surface, (**B**,**E**,**H**) at 20% tissue depth, and (**C**,**F**,**I**) overall on patellar cartilage during articulation.

Near the articular surface (Figure 6.4D) and overall (Figure 6.4F), $-E_{zz}$ of cartilage with a defect was ~1.4x higher ($p<0.05$) than that of intact cartilage. At 20% tissue depth, cartilage $-E_{zz}$ with a defect was ~1.8x greater than intact cartilage $-E_{zz}$ (Figure 6.4E); however, differences were not significant ($p=0.2$). Cartilage $-E_{zz}$ with and without a defect did not vary with lateral location near the surface ($p=0.25$) and at 20% depth ($p=0.7$), being similar to overall $-E_{zz}$ of intact cartilage (Figure 6.4D-F). However, overall $-E_{zz}$ of cartilage with a focal defect decreased with increasing lateral distance from the defect edge ($p<0.01$).

Lateral Strain (E_{xx}) – Resultant E_{xx} for intact cartilage did not vary significantly with tissue depth ($p=0.2$) and lateral location ($p=1.0$) (Figure 6.3G), while for cartilage with a defect, E_{xx} varied with tissue depth ($p<0.001$) and lateral region ($p<0.01$) (Figure 6.3H). For all lateral regions, E_{xx} remained negligible (≤ 0.01) for intact cartilage throughout tissue depth and peaked at ~20% depth for defect samples (Figure 6.3I). Near the articular surface, E_{xx} for cartilage with a defect was 1.1-5x higher than that for intact cartilage (Figure 6.4G), however differences were not statistically significant ($p=0.4$). While surface E_{xx} for defect samples reached a peak in the MID lateral region, E_{xx} near the surface did not vary significantly ($p=0.6$) with lateral distance for both intact and defect samples. At 20% tissue depth (Figure 6.4H) and overall (Figure 6.4I), cartilage E_{xx} peaked at a value of ~0.08 in the MID lateral region for cartilage with a focal defect ($p<0.01$) and was significantly higher than E_{xx} for intact cartilage at this lateral region ($p<0.01$).

Trochlear Cartilage Deformation

Shear Strain (E_{xz}) – During patello-femoral cartilage articulation, E_{xz} varied with tissue depth for trochlear cartilage in articulation with both an intact and defect-containing surface, and markedly decreased when TRO samples were slid against a focal defect than when slid against an intact surface (Figure 6.5A,B). With increasing depth from the articular surface, E_{xz} decreased markedly from ~0.1 and ~0.03-0.04 near the surface to low magnitudes (≤0.01) near the tidemark for TRO cartilage in articulation with an intact and defect-containing surface, respectively (Figure 6.5C). Cartilage E_{xz} of TRO samples articulating against a focal defect was ~2-3x lower than that for samples articulated against intact cartilage near the surface (Figure 6.6A), at 20% tissue depth (Figure 6.6B), and overall (Figure 6.6C) for all lateral regions. Differences were statistically significant near the surface ($p<0.05$), while differences at 20% depth ($p=0.17$) and overall ($p=0.11$) displayed strong trends. Local (0.4-0.6) and overall E_{xz} (0.2) did not vary laterally for TRO cartilage in articulation with intact and a defect-containing PAT cartilage.

Axial Strain (E_{zz}) – Similar to trochlear E_{xz}, $-E_{zz}$ decreased significantly with depth from the articular surface ($p<0.001$) for both intact (Figure 6.5D) and defect cases (Figure 6.5E), and was markedly lower for TRO cartilage in articulation with a focal defect than with an intact surface. With increasing depth from the articular surface, $-E_{zz}$ decreased markedly from ~0.36 and ~0.1-0.15 near the surface to ~0.05 and ~0.01 near the tidemark for TRO cartilage in articulation with an intact and defect-containing surface, respectively (Figure 6.5C). Surface and overall $-E_{zz}$ of cartilage

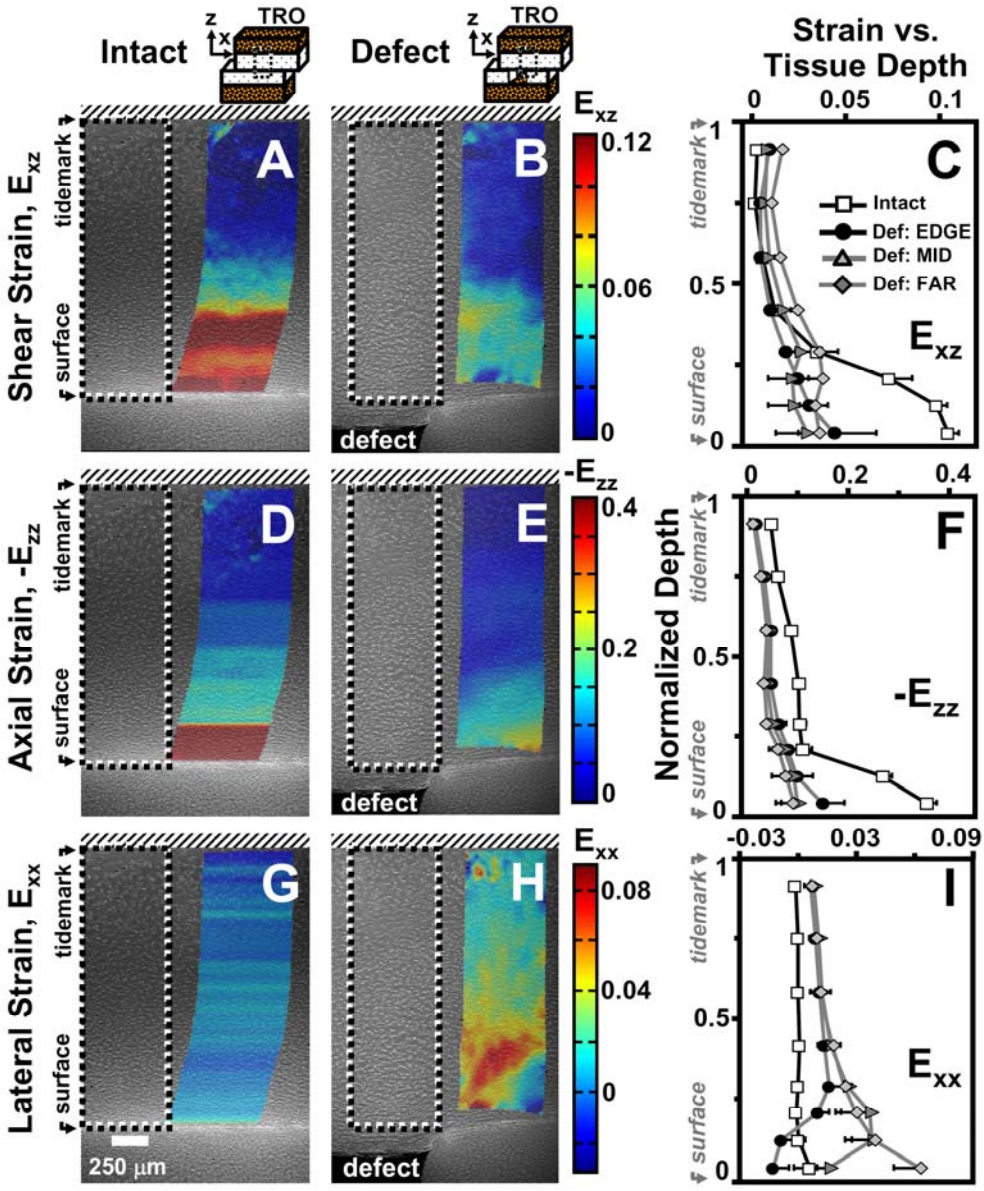

Figure 6.5: Representative micrographs of trochlear cartilage with superimposed colormaps of (**A**,**B**) shear (E_{xz}), (**D**,**E**) axial ($-E_{zz}$), and (**G**,**H**) lateral (E_{xx}) strain maps (color maps) when in apposition with patellar cartilage as (**A**,**D**,**G**) intact or (**B**,**E**,**H**) with a focal defect during lateral motion. Dashed lines (– –) encompass the analyzed regions prior to lateral motion, while the boundaries of strain maps encompass the corresponding deformed states. Local (**C**) shear (E_{xz}), (**F**) axial ($-E_{zz}$), and (**I**) lateral (E_{xx}) strain averaged depth-wise versus normalized tissue depth for trochlear cartilage as intact or with a focal defect. For samples apposing a focal defect, strains were also determined as a function of lateral distance from the defect edge (EDGE, MID, FAR). Values are mean ± SEM.

articulating against a defect was ~2-4x lower ($p<0.01$) than that of cartilage in articulation against an intact surface. At 20% tissue depth, cartilage $-E_{zz}$ for defect cases was ~1.4-1.8x lower than that for intact cases (Figure 6.4E); however, differences were not significant ($p=0.3$). Effects of lateral location were not apparent ($p=0.3$) on $-E_{zz}$ at 20% depth, while surface and overall $-E_{zz}$ tended ($p=0.1$) to decrease with increasing lateral distance.

Lateral Strain (E_{xx}) – Similar to patellar E_{xx}, the depth-variation as well as the magnitudes of E_{xx} were markedly different for TRO cartilage in articulation against an intact surface than that against a focal defect. When in articulation with intact PAT cartilage, TRO cartilage E_{xx} remained negligible (≤ 0.01) with tissue depth ($p=0.6$) for all lateral regions (Figure 6.5G), while for samples in articulation against a defect, E_{xx} varied markedly with tissue depth ($p<0.05$) and lateral region ($p<0.01$) (Figure 6.5H). At the FAR lateral region, E_{xx} decreased monotonically with increasing tissue depth, while at MID and EDGE lateral regions, peaked at ~20-30% tissue depth (Figure 6.5I). Near the surface, differences in E_{xx} between intact and defect cases were not statistically significant ($p=0.3$), but with increasing lateral distance, E_{xx} increased from -0.01 to 0.06 ($p<0.05$) for trochlear cartilage in articulation with a defect (Figure 6.6G). For samples sliding against a defect, TRO E_{xx} tended to be higher than that for samples in articulation against intact cartilage at 20% depth ($p=0.1$) (Figure 6.6H) and overall ($p=0.08$) at all lateral regions (Figure 6.6I). For defect cases, E_{xx} peaked ($p<0.05$) in the MID lateral region at 20% depth and decreased ($p<0.01$) with increasing lateral distance overall. For intact samples, E_{xx} at 20% depth and overall remained negligible (<0.01) for all lateral regions.

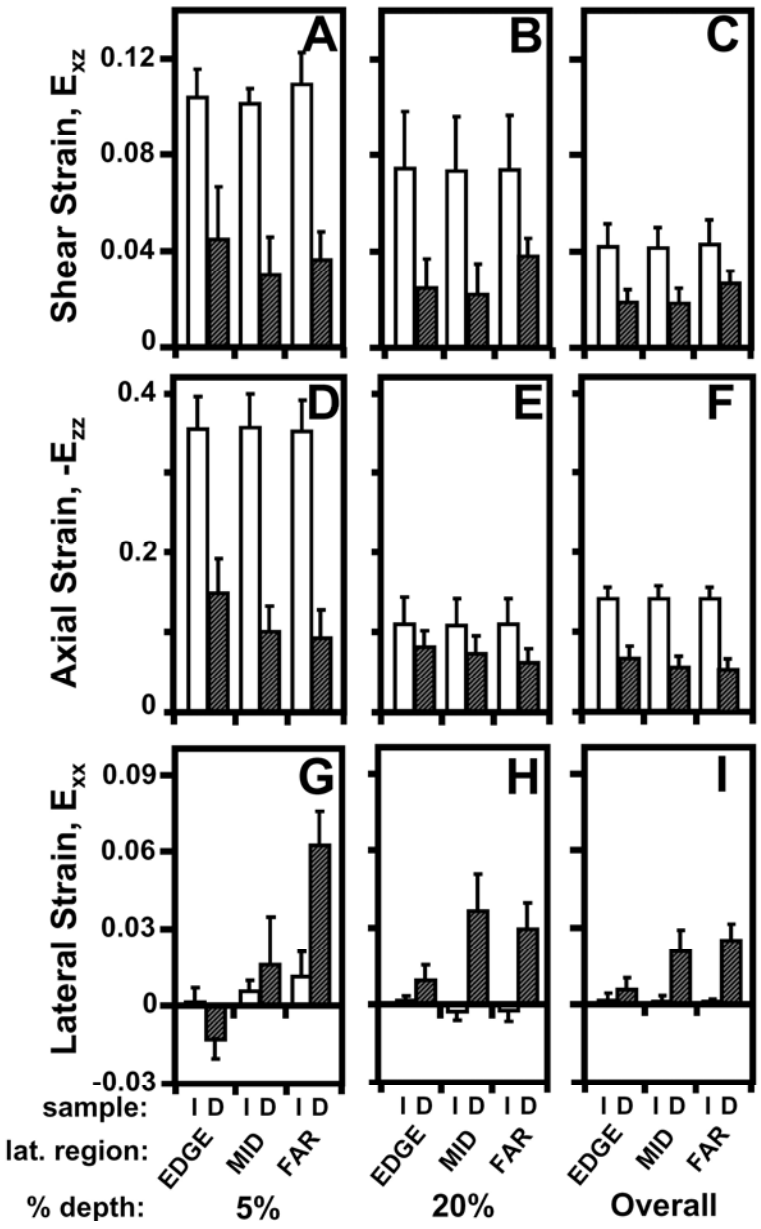

Figure 6.6: Effect of a focal defect (intact (I) versus defect (D)) on (**A**-**C**) shear, (**D**-**F**) axial, and (**G**-**I**) lateral strain (**A**,**D**,**G**) near the articular surface, (**B**,**E**,**H**) at 20% tissue depth, and (**C**,**F**,**I**) overall of trochlear cartilage during articulation.

6.5 Discussion

This study elucidated the deformation of cartilage within the proximity of, and directly in apposition to, a focal articular defect during patello-femoral cartilage articulation. As the TRO surface displaced forward laterally, the tissue partially filling the focal defect pushed and then plowed over the proximal defect edge. As a result, PAT cartilage proximal to the defect sheared markedly less (~70-700%) near the surface and more (~50-60%) at 20% tissue depth than intact cartilage following lateral motion (Figure 6.7). PAT cartilage near the focal defect also compressed more (30-40%) than intact cartilage, causing the tissue to laterally expand ~10-25x more at 20% tissue depth than intact cartilage as TRO cartilage translated laterally over the proximal defect edge. For regions directly in apposition to the focal defect, TRO cartilage sheared and compressed as it slid over the defect edge, but strains were lower in magnitude (~50-70%) than when it slid over intact cartilage. As the TRO surface plowed over the proximal defect edge, TRO cartilage near the surface also compressed laterally at the EDGE region, while expanded laterally at MID and FAR regions. Collectively, the current results indicate that with lateral articulation, the tissue deformation of both the cartilage adjacent to, and in apposition to, a focal defect are altered drastically by the presence of a focal articular defect, extending the findings of strain analysis of cartilage when compressed [13, 14].

Under compression and prior to lateral motion, the tissue deformation of cartilage near, and in apposition to, a focal defect are consistent with previous

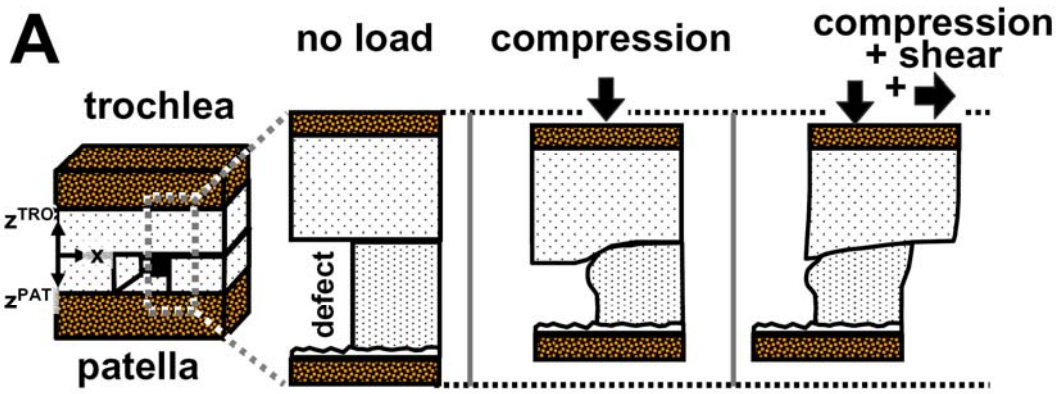

B

location	strain	relative changes in strain compared to intact		
trochlea	E_{xz}	—	↑↑	↓↓
	$-E_{zz}$	—	↓↓↓	↓↓
	E_{xx}	—	↑	↑↑
patella	E_{xz}	—	↑↑	↓↓/↑↑*
	$-E_{zz}$	—	↑	↑↑
	E_{xx}	—	—	↑↑↑

Figure 6.7: (**A**) Schematic depicting the effect of a focal defect on tissue deformation of trochlear and patellar cartilage when unloaded, compressed, and compressed and sheared in apposition. (**B**) Table of relative changes in shear (E_{xz}), axial ($-E_{zz}$), and lateral (E_{xx}) strains compared to normal intact cartilage (i.e. without a focal defect) for both trochlear and patellar cartilage when they are unloaded, compressed, and compressed and sheared in apposition. *With a focal defect, E_{xz} increased locally at ~20% tissue depth, while decreased near the surface and overall compared to intact cartilage.

studies [13, 14]. For the current defect samples, PAT cartilage near the focal defect collapsed inward into the defect, and the apposing TRO cartilage partially filled the empty defect to a tissue depth of ~10% when compressed, being consistent with previous qualitative descriptions [2, 13, 14]. As a result, similar trends in intra-tissue strains were consistent with previous reports [13, 14], with E_{xz} and $-E_{zz}$ of cartilage near the defect being elevated, and strain of TRO cartilage in apposition to the focal defect increasing laterally (E_{xx}) and in shear (E_{xz}), and decreasing axially ($-E_{zz}$) (Figure 6.7) (data not reported).

The biomechanical environment (i.e. compression and sliding) and boundary conditions of knee joint loading were considered in the experimental design of the present study. During joint loading, patello-femoral cartilage likely undergoes high compressive strain (5-10%) [7] and low sliding velocities (estimated from refs [35] and [32]) during contralateral toe-off and heel rise phases of gait [35], which were mimicked in this study by 12% compression and a 0.1 mm/s sliding velocity. To replicate the physiologic articulation and lubrication of cartilage surfaces, osteochondral samples were isolated from the trochlear and patella of the same knee and tested in apposition with normal bovine synovial fluid. Since deformation was measured following an hour of stress relaxation, the patterns of strain were likely to be representative of that occurring after prolonged cyclic loading and sliding. Although, samples were tested under a matching overall compressive strain instead of an identical compressive load which would occur physiologically, significant elevations in stains due to the presence of a focal defect were noted despite the conservative axial loading protocol. Furthermore, the aggregate modulus of human [4] and bovine [29]

cartilage are both depth-varying; and thus, changes in deformation in bovine cartilage due to a focal defect would likely be applicable for human cartilage.

While patellar cartilage was analyzed up to the articular surface, the region near the trochlear surface (~10% of tissue depth), which partially filled the defect, could not be analyzed because cell nuclei were unable to be tracked during lateral motion. The instantaneous compression of this region as it slid over the defect edge resulted in the loss of visible cells. However, regions directly in apposition of the defect edge (EDGE) prior to lateral motion were tracked appropriately near the surface. Thus, strains in other lateral regions (MID, FAR) of the trochlear cartilage may be slightly (~10-15%) underestimated and may be more similar to the values of the EDGE lateral region.

The dramatic elevation in cartilage strains near a focal defect during lateral articulation may be related, and contribute to, the progressive tissue degeneration associated with focal defects. With joint loading and time, increased fibrillation and decreased matrix staining were noted in regions adjacent to a focal defect in animal models [21, 24]. Also, untreated defects in human knee joints have been shown to enlarge [34] and be associated with cartilage volume loss [5, 37]. Such indicators of degeneration in cartilage near a focal defect may be related to the elevated strains characterized in such regions during lateral articulation in this study. Markedly elevated strains likely make cartilage susceptible to damage in these regions, such as cell death [22, 25] and matrix damage [28], which can be induced by high magnitudes of compression. With repeated loading during joint movement, the increased E_{xz} and E_{xx} at 20% tissue depth, as well as the elevated $-E_{zz}$ near the surface, may all

contribute to inducing tissue damage and cell death in cartilage regions near the focal defect edge. Thus, focal defect may enlarge due to the induction of damaging levels of strain to the bordering regions of cartilage.

For cartilage in direct apposition to focal defects, the reduction in localized strains during lateral articulation may be related to the low incidences of two focal defects being in direct apposition (i.e. "kissing lesions"). Focal defects found on both apposing cartilage surfaces were found in only ~2% of the symptomatic knees arthroscopically diagnosed with focal defects [1]. The low number of incidences of kissing lesions may be attributed to the fact that a focal defect present in one cartilage surface does not translate to elevating strains in the apposing surface. Instead, the presence of a focal defect on one surface reduces E_{xz} and $-E_{zz}$ in the apposing tissue. Thus, a second apposing chondral defect is unlikely to develop from a pre-existing focal defect on the opposing cartilage surface since strain magnitudes are lowered. Kissing lesions may instead come about with the lesions being initiated concurrently at the time of injury. Also directly apposing defects may occur when one focal defect enlarges and progresses to be full thickness in depth, causing the apposing intact surface to eventually be in articulation against the subchondral bone and become susceptible to abrasive wear.

The changes in cartilage tissue deformation were elucidated in the present study for a relatively small focal defect, which could also be representative of the cartilage strains near the edges of osteochondral grafts following mosaicplasty procedures. During patello-femoral joint articulation, the unloaded contact area between intact surfaces[36] is reduced by ~30% for surfaces with a relatively small (~1

cm^2) focal defect. This was mimicked in the present study with sample contact area being reduced from 30 mm^2 to ~21 mm^2 following the creation of a 3 mm wide focal defect. Relatively small focal defects were addressed to elucidate how changes in mechanical deformation may contribute to the degeneration of surrounding cartilage. Furthermore, large empty regions exist between the implanted osteochondral grafts immediately following mosaicplasty, and when loaded, tissue strains near the empty regions are likely similar to those near the edge of a focal defect. Although moderate to good outcomes have been reported for mosaicplasty [17], such abnormal strains in cartilage near the graft edges may be involved in causing the early osteoarthritic changes noted in some of the patients (~17%) following this procedure [16].

The deformation of cartilage surrounding a focal defect during lateral motion is likely dependent upon the contact between apposing articular surfaces. Depending on the size or location of a focal defect on the joint surface, a focal defect can be completely or partially within the contact area of an apposing surface. For focal defects in complete contact, the entire defect is axially loaded and articulated over laterally by the apposing surface. For focal defects in partial contact, the apposing surface slides over only a portion of the defect, which would cause deformations to be higher than completely contacted defects since loads are concentrated to a smaller area. In the current study, focal defects were in complete contact with the apposing surface; and thus, both defect edges were articulated against. In addition, deformation was observed in the proximal edge and at a time when surfaces were sliding. Future studies could be conducted to investigate focal defects in partial contact, the peak

deformation of the distal edge, and the deformation of the proximal edge during lateral articulation (i.e. kinematics).

The present study suggests that focal articular defects drastically alter cartilage deformation of both apposing cartilage surfaces not only during axial loading, but also during lateral articulation. Focal defects, which a majority (~61%) has been associated with acute injury or trauma [19], markedly alter the mechanical environment of cartilage, and the resulting abnormal strains may be injurious to cells and matrix. Mechanically induced cell death and tissue loss reduce cell population and likely compromise the overall biosynthetic response of the tissue [20]. While for the remaining viable cells that may continue to experience injurious levels of strain, their metabolic activities are markedly altered [22, 28]. As a result, tissue repair and remodeling responses are likely compromised, eventually leading to changes in cartilage structure by degeneration and wear. Thus, the changes in cartilage deformation associated with focal effects during both axial loading and lateral articulation may contribute to the enlargement of focal defects and predispose joints to secondary osteoarthritis. Future studies investigating the mechanical consequences of focal defects on cell and tissue matrix could further elucidate the relationship between focal defects and osteoarthritis.

6.6 Acknowledgments

This work was supported by NIH and Howard Hughes Medical Institute through the Professors Program Grant to UCSD for Dr. Robert L. Sah. We thank Chris Kim and Alexander Cigan for their help with the sample preparations.

6.7 References

1. Aroen A, Loken S, Heir S, Alvik E, Ekeland A, Granlund OG, Engebretsen L: Articular cartilage lesions in 993 consecutive knee arthroscopies. *Am J Sports Med* 32:211-5, 2004.

2. Braman JP, Bruckner JD, Clark JM, Norman AG, Chansky HA: Articular cartilage adjacent to experimental defects is subject to atypical strains. *Clin Orthop Relat Res* 430:202-7, 2005.

3. Brown TD, Pope DF, Hale JE, Buckwalter JA, Brand RA: Effects of osteochondral defect size on cartilage contact stress. *J Orthop Res* 9:559-67, 1991.

4. Chen SS, Falcovitz YH, Schneiderman R, Maroudas A, Sah RL: Depth-dependent compressive properties of normal aged human femoral head articular cartilage: relationship to fixed charge density. *Osteoarthritis Cartilage* 9:561-9, 2001.

5. Cicuttini F, Ding C, Wluka A, Davis S, Ebeling PR, Jones G: Association of cartilage defects with loss of knee cartilage in healthy, middle-age adults: a prospective study. *Arthritis Rheum* 52:2033-9, 2005.

6. Curl WW, Krome J, Gordon ES, Rushing J, Smith BP, Poehling GG: Cartilage injuries: a review of 31,516 knee arthroscopies. *Arthroscopy* 13:456-60, 1997.

7. Eckstein F, Hudelmaier M, Putz R: The effects of exercise on human articular cartilage. *J Anat* 208:491-512, 2006.

8. Eckstein F, Lemberger B, Stammberger T, Englmeier KH, Reiser M: Patellar cartilage deformation in vivo after static versus dynamic loading. *J Biomech* 33:819-25, 2000.

9. Frank EH, Grodzinsky AJ, Koob TJ, Eyre DR: Streaming potentials: a sensitive index of enzymatic degradation in articular cartilage. *J Orthop Res* 5:497-508, 1987.

10. Fung YC. A First Course in Continuum Mechanics. 2nd ed. Englewood Cliffs: Prentice-Hall; 1977.

11. Fung YC. Biomechanics: Mechanical Properties of Living Tissues. 2nd ed. New York: Springer-Verlag; 1993.

12. Gratz KR, Sah RL: Experimental measurement and quantification of frictional contact between biological surfaces experiencing large deformation and slip. *J Biomech* 41:1333-40, 2008.

13. Gratz KR, Wong BL, Bae WC, Sah RL: The effects of focal articular defects on intra-tissue strains in the surrounding and opposing cartilage. *Biorheology* 45:193-207, 2008.

14. Gratz KR, Wong BL, Bae WC, Sah RL: The effects of focal articular defects on cartilage contact mechanics. *J Orthop Res* 27:584-92, 2009.

15. Guettler JH, Demetropoulos CK, Yang KH, Jurist KA: Osteochondral defects in the human knee: influence of defect size on cartilage rim stress and load redistribution to surrounding cartilage. *Am J Sports Med* 32:1451-8, 2004.

16. Haklar U, Tuzuner T, Kocaoglu B, Guven O: [Mosaicplasty technique in the treatment of osteochondral lesions of the knee]. *Acta Orthop Traumatol Turc* 42:344-9, 2008.

17. Hangody L, Fules P: Autologous osteochondral mosaicplasty for the treatment of full-thickness defects of weight-bearing joints. Ten years of experimental and clinical experience. *J Bone Joint Surg* 85-A, Supplement 2:25-32, 2003.

18. Herberhold C, Faber S, Stammberger T, Steinlechner M, Putz R, Englmeier KH, Reiser M, Eckstein F: In situ measurement of articular cartilage deformation in intact femoropatellar joints under static loading. *J Biomech* 32:1287-95, 1999.

19. Hjelle K, Solheim E, Strand T, Muri R, Brittberg M: Articular cartilage defects in 1,000 knee arthroscopies. *Arthroscopy* 18:730-4, 2002.

20. Hunziker EB, Quinn TM: Surgical removal of articular cartilage leads to loss of chondrocytes from the wound edges. *Trans Orthop Res Soc* 25:185, 2000.

21. Jackson DW, Lalor PA, Aberman HM, Simon TM: Spontaneous repair of full-thickness defects of articular cartilage in a goat model. A preliminary study. *J Bone Joint Surg Am* 83-A:53-64, 2001.

22. Kurz B, Jin M, Patwari P, Cheng DM, Lark MW, Grodzinsky AJ: Biosynthetic response and mechanical properties of articular cartilage after injurious compression. *J Orthop Res* 19:1140-6, 2001.

23. Lefkoe TP, Anastasatos J: Repair of two millimeter defects in a rabbit model of articular step-off. *Trans Orthop Res Soc* 18:723, 1993.

24. Lefkoe TP, Trafton PG, Ehrlich MG, Walsh WR, Dennehy DT, Barrach HJ, Akelman E: An experimental model of femoral condylar defect leading to osteoarthrosis. *J Orthop Trauma* 7:458-67, 1993.

25. Loening A, Levenston M, James I, Nuttal M, Hung H, Gowen M, Grodzinsky A, Lark M: Injurious mechanical compression of bovine articular cartilage induces chondrocyte apoptosis. *Arch Biochem Biophys* 381:205-12, 2000.

26. Mazzucco D, Scott R, Spector M: Composition of joint fluid in patients undergoing total knee replacement and revision arthroplasty: correlation with flow properties. *Biomaterials* 25:4433-45, 2004.

27. Mow VC, Huiskes R. Basic Orthopaedic Biomechanics and Mechano-Biology. 3rd ed. Philadelphia: Lippincott Williams & Wilkins; 2005.

28. Quinn TM, Allen RG, Schalet BJ, Perumbuli P, Hunziker EB: Matrix and cell injury due to sub-impact loading of adult bovine articular cartilage explants: effects of strain rate and peak stress. *J Orthop Res* 19:242-9, 2001.

29. Schinagl RM, Gurskis D, Chen AC, Sah RL: Depth-dependent confined compression modulus of full-thickness bovine articular cartilage. *J Orthop Res* 15:499-506, 1997.

30. Schinagl RM, Ting MK, Price JH, Sah RL: Video microscopy to quantitate the inhomogeneous equilibrium strain within articular cartilage during confined compression. *Ann Biomed Eng* 24:500-12, 1996.

31. Schmidt TA, Sah RL: Effect of synovial fluid on boundary lubrication of articular cartilage. *Osteoarthritis Cartilage* 15:35-47, 2007.

32. Shelburne KB, Torry MR, Pandy MG: Muscle, ligament, and joint-contact forces at the knee during walking. *Med Sci Sports Exerc* 37:1948-56, 2005.

33. Wang CC, Deng JM, Ateshian GA, Hung CT: An automated approach for direct measurement of two-dimensional strain distributions within articular cartilage under unconfined compression. *J Biomech Eng* 124:557-67, 2002.

34. Wang Y, Ding C, Wluka AE, Davis S, Ebeling PR, Jones G, Cicuttini FM: Factors affecting progression of knee cartilage defects in normal subjects over 2 years. *Rheumatology (Oxford)* 45:79-84, 2006.

35. Whittle M. Gait Analysis: An Introduction. 3rd ed. Oxford; Boston: Butterworth-Heinemann; 2002.

36. Widuchowski W, Widuchowski J, Trzaska T: Articular cartilage defects: study of 25,124 knee arthroscopies. *Knee* 14:177-82, 2007.

37. Wluka AE, Ding C, Jones G, Cicuttini FM: The clinical correlates of articular cartilage defects in symptomatic knee osteoarthritis: a prospective study. *Rheumatology (Oxford)* 44:1311-6, 2005.

38. Wong BL, Bae WC, Chun J, Gratz KR, Sah RL: Biomechanics of cartilage articulation: effects of lubrication and degeneration on shear deformation. *Arthritis Rheum* 58:2065-74, 2008.

39. Wong BL, Sah RL: Cartilage mechanicals during tibio-femoral articulation: local and overall compressive and shear deformation and properties. *J Biomech* Submitted, 2009.

CHAPTER 7

CONCLUSIONS

7.1 Summary of Findings

This dissertation has incorporated certain aspects of physiologic joint loading into a novel *in vitro* experimental approach to achieve the overall objective of this work: *To further the understanding of normal cartilage mechanics during articulation as well as provide insight into the effects of degeneration, lubrication, and a focal articular defect on it.* A novel mechanical testing system was developed that compressed and slid apposing cartilage samples to mimic the compression and relative sliding of cartilage surfaces during joint movement. The resulting tissue deformation was captured by video microscopy, from which, cartilage strains and corresponding moduli were determined. The major findings of this dissertation were:

1. Chapter 2 – Following compression and relative sliding, cartilage shear deformation varies with tissue depth, being highest near the articular surface and monotonically decreasing with tissue depth. Such shear deformation reflects the local shear modulus of cartilage. Furthermore, cartilage shear deformation increases markedly with mild degeneration and is lower with synovial fluid (SF) lubrication than with saline as surface lubricant.

a. For intact femoral cartilage, peak shear strain was highest near the surface and decreased to negligible magnitudes (<0.01) near the tidemark. This depth-variation in shear deformation was a reflection of the shear modulus, being ~0.18 MPa near the surface and increasing with depth to a value of ~3-4 MPa near the tidemark.

b. With mild degeneration, cartilage shear strain near the surface and overall increased ~5- and ~2-fold, respectively. Shear modulus near the surface decreased ~3-fold with degeneration. Overall shear modulus decreased ~1.2-fold with degeneration, but differences were not statistically significant.

c. With SF as lubricant, cartilage shear deformation was ~50% lower than with saline as lubricant for both normal and degenerated cartilage.

2. Chapter 3 - Four main events occur during cartilage-on-cartilage articulation, and SF lubrication reduces peak shear deformation by allowing surfaces to slide sooner. In addition, the dominating mode of lubrication transitions from interstitial fluid pressurization near the onset of loading to boundary mode with prolonged loading.

    a. The four main events that occurred during cartilage-on-cartilage articulation were (1) adherence between apposing cartilage surfaces prior to lateral motion, (2) shear deformation of cartilage increasing at the onset of lateral motion while surfaces remained adhered, (3) detachment of cartilage surfaces as shear deformation peaked with continued lateral

motion, and (4) maintenance of peak shear deformation while surfaces were sliding.

b. With SF lubrication, cartilage shear reached 50% of its peak values at a lower applied lateral displacement than with saline, suggesting articular surfaces were able to slide sooner with SF and result in the lower cartilage peak shear.

c. While differences in shear strain were not apparent between lubricant groups after 5 minutes of stress relaxation, shear strain of cartilage with saline as lubricant was ~50% higher than that of cartilage tested with SF after 60 minutes of stress relaxation.

3. Chapter 4 – During tibio-femoral cartilage articulation, cartilage deformation is depth-varying and asymmetric, being greater in tibial cartilage than femoral cartilage. Such deformation was reflective of their respective compressive and shear moduli.

   a. Follow axial compression, compressive strain of both tibial and femoral cartilage was depth-varying, being highest at surface and decreasing monotonically with increasing depth from the articular surface. Near the surface and overall compressive strain of tibial cartilage was ~2x greater that in femoral cartilage.

   b. Similar to compressive strain, shear strain of tibial and femoral cartilage was depth-varying following compression and lateral motion. Shear strain in tibial cartilage was ~8x and 4x greater than that in femoral cartilage near the surface and overall, respectively.

c. Compressive modulus was lowest near the surface and highest near the tidemark for tibial and femoral cartilage, and was 1.7x greater in femoral cartilage than in tibial cartilage near the surface and overall.

d. Shear modulus was similarly depth varying, being lowest near the surface and highest near the tidemark for both tibial and femoral Shear modulus was 8x higher near the surface, and 3x higher overall, in femoral cartilage than that in tibial cartilage.

4. Chapter 5 - Acute injury impairs SF function, elevating cartilage shear strain during tibio-femoral cartilage articulation, while HA supplementation partially restores SF function as indicated by the reduction in cartilage shear towards normal magnitudes.

    a. For both tibial and femoral cartilage lubricated with AI-SF, peak shear strain was ~80% and ~50-200% higher near the surface and overall, respectively, than with NL-SF as lubricant.

    b. Following HA supplementation to AI-SF, peak shear was reduced from values with AI-SF alone by 30-50% near the surface and 20-30% overall.

5. Chapter 6 - Intra-tissue strains of cartilage in both apposing surfaces markedly change following the creation of a focal defect during lateral articulation, with the strains of cartilage near the defect edge typically elevating and the deformation of cartilage in direct apposition to the defect being reduced.

    a. For cartilage adjacent to the leading edge of the defect, shear and lateral strains are ~2x and ~10-25x higher than that for intact cartilage at 20%

depth. Near the surface, axial strains were 1.4x higher for cartilage near a focal defect than that of intact cartilage.

b. For cartilage in direct apposition to a focal defect, shear and axial strains were 2-4x lower than that for cartilage articulation against intact cartilage near the surface and overall. Lateral strains transitioned from lateral compression to tension with decreasing distance to the defect.

7.2 Discussion

The resultant shear deformation during cartilage-on-cartilage articulation characterized in Chapters 2 and 3 may be a necessary mechanical stimulus for tissue homeostasis. Moderate levels of compression and shear strain stimulate proteoglycan and protein biosynthesis [17] and have been shown to result in greater matrix gene expression than under dynamic compression alone [13]. Furthermore, static compression combined with moderate shear strain promotes PRG4 secretion, while dynamic compression alone does not [22]. Such results suggest shear strain further supplements cartilage metabolism as well as induces unique metabolic responses (i.e. PRG4 secretion) that are necessary for cartilage maintenance and function. The moderate magnitudes of shear strain that results during joint articulation may therefore likely stimulate matrix synthesis as well as lubricant molecule secretion. Without it, cartilage metabolism may not be optimal, and lubricant molecule secretion from cartilage may be totally absent, making cartilage shear strain a vital mechanical stimulus for cartilage homeostasis.

Elevations in cartilage shear stain, found to be associated with degeneration and deficient lubrication in Chapters 2 and 3, may make cartilage more susceptible to tissue degeneration and wear. Following injurious levels of compression, reduced matrix synthesis [18, 27], cell death [7, 21], and matrix damage [23] [24]occur. While direct effects of elevated shear strain on chondrocytes and matrix have yet to be investigated, some previous studies do suggest elevated shear magnitudes may also be injurious. After relatively low indentation amplitudes, cell death was observed in areas of high local shear strains [3]. Also, with increasing applied shear stress, the matrix metabolism of seeded chondrocytes decreases [25]. With increased cell death, the ability of remaining chondrocytes to maintain and repair its surrounding matrix is drastically compromised due to a reduction in cell population. Also the remaining viable cells which continue to experience supra-normal magnitudes of strain likely have reduced metabolic activity [18, 24]. Elevated shear strain in cartilage may adversely modulate tissue response by reducing the abilities of cartilage to remodel and repair. Thus, prolonged exposure of elevated shear strains that may be a result of surface degeneration or deficient lubrication may contribute to furthering cartilage wear and cause the progressive degeneration of cartilage.

The findings of Chapter 5 provide insight into the consequences of acute injury on cartilage mechanics due to changes in lubrication function as well as its role in the pathogenesis of OA. The lubricating function of SF to reduce friction between articulating surfaces reduces in acute injury [1, 11] and inflammatory arthritis [11], and is thought to play a role in the pathogenesis of OA. Chapter 5 in this dissertation further elucidates how elevated friction resulting from reduced SF function may

contribute to cartilage degeneration. The results of Chapter 5 indicate the elevated friction between cartilage surfaces lubricated with SF from acutely injured joints causes surfaces to stick longer and slide at higher magnitudes of lateral displacement during lateral motion. As a result, cartilage tissue shears more, and shear strains are markedly higher than if surfaces were lubricated with normal functioning SF. Thus, the compromised friction-reduction function of SF associated with acute injury predisposes cartilage to degeneration by causing higher shear strains in cartilage during the articulation and sliding of cartilage.

The findings of Chapter 5 also provide insight into whether the tribosupplementation of HA to SF of acutely injured joints restores the function of SF and is mechanically beneficial to cartilage. A current clinical treatment for osteoarthritis is the intra-articular injection of HA to failing SF in the knee, which is postulated to have chondroprotective effects. Although investigations on clinical outcomes of HA supplementation have been extensive, few studies have investigated the efficacy of supplemented HA to restore SF function directly and prevent cartilage degeneration. The findings of Chapter 5 indicate HA supplementation partially restores SF function and appears to be mechanically beneficial to cartilage, reducing cartilage shear strains toward normal magnitudes. As a result, cartilage shear strains, which may be injurious with SF following acute injury, may be reduced to levels that are not harmful and within a safe range following HA supplementation. By reducing cartilage shear strain with added HA, the degeneration of cartilage may be possibly prevented following acute injury.

While such results suggest HA supplementation has a positive effect on the mechanical function of cartilage and motivate the use of it as a treatment, the effects of HA supplementation are likely time-dependent. The effects of HA supplementation presented in Chapter 5 are likely temporary, being dependent on the retention of the injected HA within the SF and synovial joint. For knee joints, increased permeability of the synovium associated with arthritic joints [4, 5, 8, 9, 12, 19, 26] would increase the likelihood of the injected HA leaching out. Further investigations to delineate the time-dependent effects of HA supplementation on SF function and the ability of injected HA to be retained in the synovial joint are needed. However, the reduction in cartilage shear strain immediately following the addition of HA to injury SF indicates biomechanical lubricants injected intra-articularly as a therapeutic treatment may be promising.

In Chapter 6, the results describe localized strains in cartilage near a focal defect elevating during lateral articulation, which may play a large role in the progressive cartilage degeneration associated with focal defects. The elevation in localized strains laterally, axially, and in shear of cartilage near a focal defect may bring about significant physiological responses. Such changes in mechanical deformation may be related to the histopathological changes (i.e. increased fibrillation and decreased GAG) found in similar regions of cartilage in animal models with artificially created focal defects [16, 20]. The high shear, axial, and lateral strains experienced during lateral articulation likely makes cartilage susceptible to damage, such as cell death and matrix damage. Especially after repeated cycles of loading during joint movement, the elevated strains may induce tissue damage and cell death

in tissue regions near the focal defect edge and cause the focal defects to enlarge and bordering cartilage to degenerate.

For the cartilage surface in direct apposition to focal defects, the reduction in localized strains reported in Chapter 6 may be a reason for the rare incidences of directly apposing focal defects (i.e. “kissing lesions”). Focal defects found on both apposing cartilage surfaces were found in only ~2% of the symptomatic knees arthroscopically diagnosed with focal defects [2]. The low incidences of kissing lesions may be attributed to the fact that a focal defect present in one cartilage surface does not translate to elevating strains in the apposing surface. Instead, the presence of a focal defect on one surface reduces localized strains in the apposing surface. Thus, it is unlikely kissing lesions develop from a pre-existing focal defect based on these results. Kissing lesions may instead come about with the lesions being initiated concurrently at the time of injury or with one focal defect enlarging and progressing to be full thickness in depth and cause the apposing surface to be in contact with the subchondral bone.

7.3 Future Work

This dissertation work could be expanded upon in a number of directions, which includes the investigation of cartilage articulation against an apposing non-biologic counter surface. Hemiarthroplasty is a common surgical procedure that replaces one half of the joint with an artificial surface and leaves the other half in its native state [10]. As a result, cartilage surfaces are in articulation against a non-

biologic counter surface, typically made of a composite metal or high density polyethylene. Investigating how cartilage deforms in articulation with such materials would elucidate how cartilage mechanics change following such surgical procedures and give insight into reasons why such procedures have been associated with degeneration and wear of the remaining apposed native cartilage [10]. In addition, such studies could also provide insight into which materials as well as surface properties would make an ideal implant that articulates against native cartilage.

Another interesting and clinically relevant direction this work could be taken is the investigation of cartilage deformation during compression and lateral articulation following tribosupplementation of other, or a combination of other, potential lubricant molecules. Chapter 5 investigated the effectiveness of HA supplementation to restore SF function as indicated by cartilage shear deformation. While supplementation of such molecules may reduce friction between articulating surfaces, whether this translates to a reduction mechanical deformation of cartilage during loading remains unknown. Future studies could be performed to investigate the efficacy of therapeutic lubricants molecules, such as PRG4, SAPL, or in combination with HA, to restore the mechanical function of SF to modulate cartilage shear.

The investigations performed in Chapter 6 could be expanded to assess the effects of defect geometry. In the studies presented in Chapter 6, the focal defect was idealized as having perfectly vertical edges. However, focal defects are unlikely to exhibit such geometry in reality. Defect edges that were 100^{o} (open) and 80^{o} (closed) in angle relative to the articular surface did not show distinct differences in deformation under compression alone [14]. However, this would unlikely be the case

during lateral articulation, since a more opened (>90^{o}) angled edge would reduce plowing edge effects and likely reduce resultant deformation. Thus studies to elucidate the effects of defect geometry on cartilage deformation during lateral motion could provide insight into critical parameters, such as defect geometry, that may cause some defects to degenerate more quickly than others.

Future studies could also be performed to elucidate the deformation of the trailing defect edge in Chapter 6. The deformation of the leading defect edge, which experiences oncoming forward lateral motion, was characterized in Chapter 6. At the onset of lateral motion, this edge experiences the forward plowing by the apposing surface and thus deformation was likely highest on this edge as opposed to the trailing edge. However, the deformation of each trailing edge could be markedly different than the leading edge since it does not experience the forward plowing motion. Thus studies that characterize the deformation of the trailing defect edge could give insight into whether some edges of the focal defect are more prone to degeneration and wear than others.

The work of Chapter 6 could also be expanded upon in a very interesting direction by investigating the mechanics of cartilage articulation following the repair of a focal defect. Allograft transplantation is one viable option for the repair focal defects currently implemented in the clinic [6]. However, the mechanical behavior of cartilage following this repair and whether graft transplantation fully restores cartilage mechanics remain to be fully elucidated during loading. The junction between the host cartilage and donor allograft tissue does not integrate with this procedure and remain discontinuous. Such effects are unknown and can be detrimental to the success of this

procedure. One major limitation to this procedure is donor availability, which has motivated the efforts for engineering implantable osteochondral grafts [15]. Thus, cartilage mechanics following the implantation of tissue engineered grafts and whether such treatments are effective in reconstituting the mechanical behavior of cartilage could also be assessed.

While cartilage deformation markedly changed near a focal defect following lateral articulation, whether such magnitudes reach a level that induces cartilage degeneration and wear remain to be investigated. Strains in cartilage near a focal defect are dramatically elevated; however, it remains unknown whether such magnitudes are high enough to induce cell death and matrix damage, early indicators of cartilage degeneration. Studies that investigate such mechanical effects on chondrocyte viability and matrix integrity would further corroborate the hypothesis that focal defects predispose joints to cartilage degeneration and the pathogenesis of OA. In addition, whether cartilage damage and cell death is more prominent during compression or lateral motion could also be elucidated. The notion that strain is the direct mechanism of cartilage degeneration would also be supported if cell death is and matrix damage is shown to be localized in areas of high strains.

Finally, the ultimate goal of for the repair of chondral defects is to prevent further degeneration of the native tissue in addition to restoring the mechanical function of cartilage. Studies that assess the effects of mechanical strain due to a focal defect on chondrocyte viability and matrix damage could be expanded to determine whether filling a defect with either an allograft or engineered osteochondral graft would prevent such adverse biological responses. Such results would be useful in

evaluating the effectiveness of such treatments to repair chondral defects and prevent the progressive degeneration of cartilage associated with focal defects.

7.3 References

1. Antonacci JM, Schmidt TA, Serventi LA, Shu YL, Gastelum NS, Schumacher BL, McIlwraith CW, Sah RL: Effects of joint injury on synovial fluid and boundary lubrication of cartilage. *Trans Orthop Res Soc* 32:156, 2007.

2. Aroen A, Loken S, Heir S, Alvik E, Ekeland A, Granlund OG, Engebretsen L: Articular cartilage lesions in 993 consecutive knee arthroscopies. *Am J Sports Med* 32:211-5, 2004.

3. Bae WC, Schumacher BL, Sah RL: Indentation probing of human articular cartilage: effect on chondrocyte viability. *Osteoarthritis Cartilage* 15:9-18, 2007.

4. Balazs EA: The physical properties of synovial fluid and the special role of hyaluronic acid. In: *Disorders of the Knee,* ed. by AJ Helfet, Lippincott Co., Philadelphia, 1974, 63-75.

5. Balazs EA, Watson D, Duff IF, Roseman S: Hyaluronic acid in synovial fluid. I. Molecular parameters of hyaluronic acid in normal and arthritis human fluids. *Arthritis Rheum* 10:357-76, 1967.

6. Bugbee WD: Osteochondral allograft transplantation. In: *Articular Cartilage Lesions: A Practical Guide to Assessment and Treatment,* ed. by BJ Cole, Malek MM, Springer, New York, 2004, 82-94.

7. Chen CT, Burton-Wurster N, Lust G, Bank RA, Tekoppele JM: Compositional and metabolic changes in damaged cartilage are peak-stress, stress-rate, and loading-duration dependent. *J Orthop Res* 17:870-9, 1999.

8. Coleman PJ, Scott D, Ray J, Mason RM, Levick JR: Hyaluronan secretion into the synovial cavity of rabbit knees and comparison with albumin turnover. *J Physiol* 503 (Pt 3):645-56, 1997.

9. Dahl LB, Dahl IM, Engstrom-Laurent A, Granath K: Concentration and molecular weight of sodium hyaluronate in synovial fluid from patients with rheumatoid arthritis and other arthropathies. *Ann Rheum Dis* 44:817-22, 1985.

10. Dalldorf PG, Banas MP, Hicks DG, Pellegrini VD: Rate of degeneration of human acetabular cartilage after hemiarthroplasty. *J Bone Joint Surg Am* 77-A:877-82, 1995.

11. Elsaid KA, Jay GD, Warman ML, Rhee DK, Chichester CO: Association of articular cartilage degradation and loss of boundary-lubricating ability of

synovial fluid following injury and inflammatory arthritis. *Arthritis Rheum* 52:1746-55, 2005.

12. Fraser JR, Laurent TC, Laurent UB: Hyaluronan: its nature, distribution, functions and turnover. *J Intern Med* 242:27-33, 1997.

13. Grad S, Gogolewski S, Alini M, Wimmer MA: Effects of simple and complex motion patterns on gene expression of chondrocytes seeded in 3D scaffolds. *Tissue Eng* 12:3171-9, 2006.

14. Gratz KR, Wong BL, Bae WC, Sah RL: The effects of focal articular defects on cartilage contact mechanics. *J Orthop Res* 27:584-92, 2009.

15. Hwang J, Görtz S, Sah RL, Bugbee WD: Osteochondral graft transfer - techniques, outcomes, and the future. *US Musculoskeletal Review* 3:75-80, 2009.

16. Jackson DW, Lalor PA, Aberman HM, Simon TM: Spontaneous repair of full-thickness defects of articular cartilage in a goat model. A preliminary study. *J Bone Joint Surg Am* 83-A:53-64, 2001.

17. Jin M, Frank EH, Quinn TM, Hunziker EB, Grodzinsky AJ: Tissue shear deformation stimulates proteoglycan and protein biosynthesis in bovine cartilage explants. *Arch Biochem Biophys* 395:41-8, 2001.

18. Kurz B, Jin M, Patwari P, Cheng DM, Lark MW, Grodzinsky AJ: Biosynthetic response and mechanical properties of articular cartilage after injurious compression. *J Orthop Res* 19:1140-6, 2001.

19. Laurent UB, Fraser JR, Engstrom-Laurent A, Reed RK, Dahl LB, Laurent TC: Catabolism of hyaluronan in the knee joint of the rabbit. *Matrix* 12:130-6, 1992.

20. Lefkoe TP, Trafton PG, Ehrlich MG, Walsh WR, Dennehy DT, Barrach HJ, Akelman E: An experimental model of femoral condylar defect leading to osteoarthrosis. *J Orthop Trauma* 7:458-67, 1993.

21. Loening A, Levenston M, James I, Nuttal M, Hung H, Gowen M, Grodzinsky A, Lark M: Injurious mechanical compression of bovine articular cartilage induces chondrocyte apoptosis. *Arch Biochem Biophys* 381:205-12, 2000.

22. Nugent GE, Aneloski NM, Schmidt TA, Schumacher BL, Voegtline MS, Sah RL: Dynamic shear stimulation of bovine cartilage biosynthesis of proteoglycan 4 (PRG4). *Arthritis Rheum* 54:1888-96, 2006.

23. Patwari P, Cook MN, DiMicco MA, Blake SM, James IE, Kumar S, Cole AA, Lark MW, Grodzinsky AJ: Proteoglycan degradation after injurious

compression of bovine and human articular cartilage in vitro: interaction with exogenous cytokines. *Arthritis Rheum* 48:1292-301, 2003.

24. Quinn TM, Allen RG, Schalet BJ, Perumbuli P, Hunziker EB: Matrix and cell injury due to sub-impact loading of adult bovine articular cartilage explants: effects of strain rate and peak stress. *J Orthop Res* 19:242-9, 2001.

25. Raimondi MT, Moretti M, Cioffi M, Giordano C, Boschetti F, Lagana K, Pietrabissa R: The effect of hydrodynamic shear on 3D engineered chondrocyte systems subject to direct perfusion. *Biorheology* 43:215-22, 2006.

26. Sakamoto T, Mizono, S, Miyazaki, K, Yamaguchi, T, Toyoshima, H, Namiki, O.: Biological fate of sodium hyaluronate (SPH): Studies on the distribution, metabolism, and excretion of ^{14}C-SPH in rabbits after intra-articular administration. *Pharmacometrics* 28:375-87, 1984.

27. Steinmeyer J, Knue S: The proteoglycan metabolism of mature bovine articular cartilage explants superimposed to continuously applied cyclic mechanical loading. *Biochem Biophys Res Commun* 240:216-21, 1997.

APPENDIX A

ACCELERATED STRESS-RELAXATION OF CARTILAGE DUE TO CHONDRAL DEFECTS AND SUBCHONDRAL BONE PLATE PERFORATIONS

A.1 Abstract

Objective: Articular cartilage undergoes hydrostatic pressurization when loaded, predominantly bore by interstitial fluid pressure initially and transiently. Maintenance of this pressure is important for physiologic loading, and prevents pathologic compressive strain in cartilage. Focal articular defects and altered subchondral bone plate (ScBP) permeability are present in cartilage diseases or created in surgical procedures. As a result, pressurization may be affected because cartilage geometry and boundary conditions for fluid flow are altered. Therefore the objectives of this study were to determine the effect of (1) full thickness chondral defects of varying diameter, (2) with or without ScBP perforations, on the time-dependent biomechanical behavior of articular cartilage.

Methods: Sample groups of (a) intact, (b) 1mm defect, and (c) 3mm defect (1mm and 3mm inner diameter annuli, respectively) disks were created from full thickness bovine chondral disks (d=7mm) to model normal cartilage and cartilage with focal

defects, respectively. The test protocol consisted of ramp unconfined compression, stress-relaxation to equilibrium, and then oscillatory compression after each ramp. Each disk was tested twice, using a (i) solid and a (ii) perforated (a 1mm diameter center hole) bottom platen to simulate an impermeable or freely permeable ScBP.

Results: The presence of a defect resulted in diminishing peak stress with increasing defect diameter, while platen perforation had no effect. Equilibrium stress was not altered by either defect or perforation. However, 50% relaxation time constant was lower (i.e., faster relaxation and consolidation) when defects were present and also tended to decrease in a defect-dependent way when a perforated platen was used. Stiffness decreased with the presence of a defect, but did not vary with platen perforation. Phase angle decreased with frequency, and increased with defect size and perforation.

Conclusion: The biomechanical analysis of cartilage explants with boundary conditions mimicking those in health and disease provide translational insights into biomechanical alterations. The results suggest that the integrity of the deep layer of cartilage and subchondral bone is critical for maintaining prolonged cartilage pressurization. Such depressurization may have sequelae that contribute to cartilage deterioration after chondral and/or subchondral bone injuries.

A.2 Introduction

Articular cartilage undergoes hydrostatic pressurization when loaded, resulting in load carriage that is initially and transiently carried predominantly by interstitial fluid pressure [1, 2]. Maintenance of this pressure is important for physiologic loading, and prevents excessive pathologic compressive strain in cartilage [1, 30]. In diseases of cartilage [5], as well as during surgical procedures [26], focal defects are present or created and subchondral bone plate (ScBP) permeability may be altered. Cartilage has a poor capacity to heal itself once damaged [13, 21]; therefore, cartilage will either remain damaged or progressively grow with time that lead to extensive degenerative changes [5].

Untreated cartilage focal defects have been demonstrated to degenerate further, being a risk factor for the onset of progressive cartilage degeneration and osteoarthritis (OA) [14, 15]. *In vivo* animal model studies of untreated chondral [17] and osteochondral defects [16, 20] demonstrated signs of progressive degradation such as cartilage fibrillation and hypocellularity in tissue adjacent to the defect. In recent clinical studies, untreated asymptomatic chondral defects were demonstrated with MRI to degenerate further over a two year period, showing an increase in defect score [10], rate of volume loss [11], and a decrease in total cartilage volume [9]. However, the mechanism(s) causing the progressive degeneration following focal defects remains unclear and requires further investigation.

Impact injuries that cause changes in ScBP permeability (i.e. microcracks) without causing morphological changes in the overlying cartilage tissue have been

shown to initiate degenerative changes in cartilage with continual physiologic loading after initial injury. *In vivo* canine models exhibited indications of altered ScBP (i.e. microcracks and bone bruising) at the time of injury without changes to the overlying articular surface [18, 28]. Cartilage thinning and surface interruptions were present at 6 months post injury [18, 28], and cartilage changes persisted a year while ScBP injuries resolved [29]. Such results imply ScBP injuries can initiate degenerative changes in the overlying cartilage. Many theories, such as bone stiffening [22, 25] and transmission of catabolic agents from the marrow [7], have been proposed as mechanisms initiating the degenerative changes in cartilage following ScBP injury. However, the exact mechanical and biochemical mechanism(s) involved and the pathogenesis of cartilage degeneration following changes in ScBP continues to be debated and remains to be clarified.

In order to elucidate the role of both cartilage defects and ScBP permeability in causing further cartilage degeneration from a mechanical standpoint, mechanical studies of cartilage with focal defects with and without altered boundary conditions are necessary. A limited number of studies have investigated the mechanical effect of chondral defects, alone, on cartilage mechanics. The presence of defects were shown to increase contact stresses at the edges of the defect [4], suggesting that load support is compensated by the adjacent cartilage. In addition, cartilage defects were shown to alter cartilage deformation under compression, increasing tissue strains in both finite element [12]and in vitro models [3].

Subchondral bone plate (ScBP) permeability, which can be altered in disease [5] or by surgical procedures such as microfracture [26], may also be important in

maintaining or altering mechanical behavior of cartilage. Previously, theoretical analysis indicated ScBP perforation results in accelerated consolidation of intact cartilage [23, 27]. Time-dependent mechanical behavior (i.e. strain rates and stress relaxation) in the presence of focal defects and/or altered ScBP permeability has yet to be reported and may give more insight into the mechanical mechanism(s) at which cartilage further degenerates.

The hypothesis of this study is cartilage defects and ScBP permeability, individually or in combination, has a significant affect on the time-dependent mechanical behavior of cartilage because both cartilage geometry and boundary conditions are altered. The presence of chondral defects and a permeable ScBP may separately or additively alter the rate at which fluid exudates from the tissue when loaded. Therefore the objectives of this study were to determine the effect of (1) full thickness chondral defects of varying diameter, (2) with or without a ScBP perforation, on the time-dependent mechanical behavior of articular cartilage.

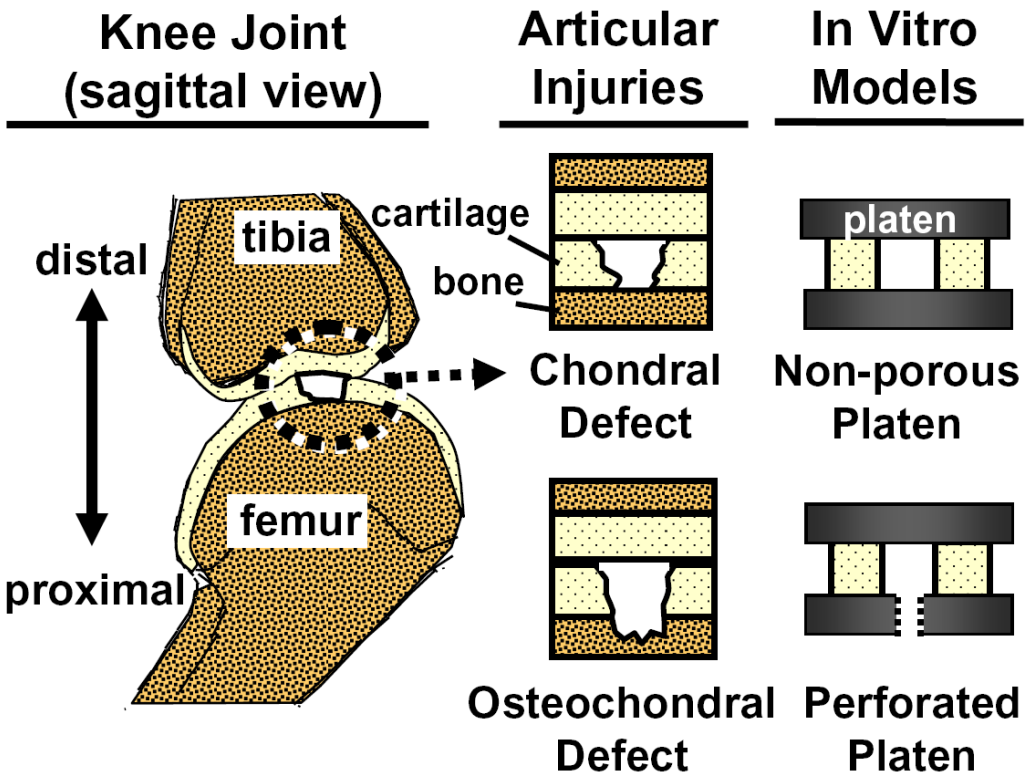

Figure A.1: Schematic of sagittal view of the knee joint, articular injuries that are isolated to the cartilage and extend into the underlying subchondral bone, and the in vitro experimental test models of them.

A.3 Materials and Methods

Sample Isolation And Preparation

Chondral disks were prepared from macroscopically normal patellofemoral grooves of two adult (~2-3 years old.) bovine animals. Osteochondral blocks were first isolated, and then chondral disks with articular surface intact (n =4) were released and punched to a thickness of ~1.5 mm and a diameter of 7 mm from blocks using a sledge microtome and dermal punch. Disks were soaked in phosphate buffered saline (PBS) containing proteinase inhibitors (PI) at 4^0C and stored frozen at -20^0C until testing.

Experimental Design

To examine the effect of focal defects and altered ScBP permeability on the time-dependent mechanical behavior of articular cartilage in *physiological* joints, *in vitro* models were developed that attempted to replicate the mechanical boundary conditions that occur *in vivo* (Figure A.1). Small chondral disks with various size annuli were created and compressed under the displayed conditions to replicate the area of contact between two articulating joints in compression with various articular injuries. A top impermeable platen was used to model an intact apposing cartilage surface, while either an (i) impermeable or (ii) perforated solid bottom platen was used to mimic cartilage boundary conditions that resemble clinically occurring chondral and osteochondral injuries, respectively. Peak and equilibrium stresses, relaxation times, and oscillatory properties were determined to give insight into the

cartilage mechanical behavior *in vivo* as a result of cartilage defects and a perforated ScBP.

Unconfined Compression Testing

Chondral disks were mechanically tested in unconfined configurations to examine the mechanical behavior of cartilage under various geometries and boundary conditions. Disks were thawed in PBS+PI at room temperature (~22^0C), mounted articular surface up between two flat and rigid platens fitted to a uniaxial mechanical test instrument (DynaStat, IMASS, Accord, MA), and subjected to unconfined compression testing. The testing protocol consisted of ramp compression (to 5, 10, and 15% of disk thickness at 1%/sec), stress-relaxation to equilibrium (defined as either a change in stress of less than 0.003MPa in 180 seconds or when a maximum time of 3600 seconds is reached), and then oscillatory compression at equilibrium (at frequencies of 0.01-0.5 Hz and amplitudes of 0.1-0.3%) after each ramp.

Under this mechanical routine, each chondral disk was tested in six permutations (Figure A.2). An (i) impermeable or (ii) perforated (a 1 mm diameter hole) bottom platen was used to model an intact or freely-permeable ScBP, respectively. Each disk was compressed first as (a) intact, then (b) after creation of a 1 mm diameter defect, and finally (c) after enlargement to a 3 mm diameter defect, mimicking full-thickness cartilage defects of different relative sizes, in both aforementioned platen setups to examine the effect of defects and ScBP perforations. Order of compression in the platen setups (i.e. compression of disks in (i) first then (ii) ,or (ii) then (i)) were randomized such that half the samples were compressed in (i)

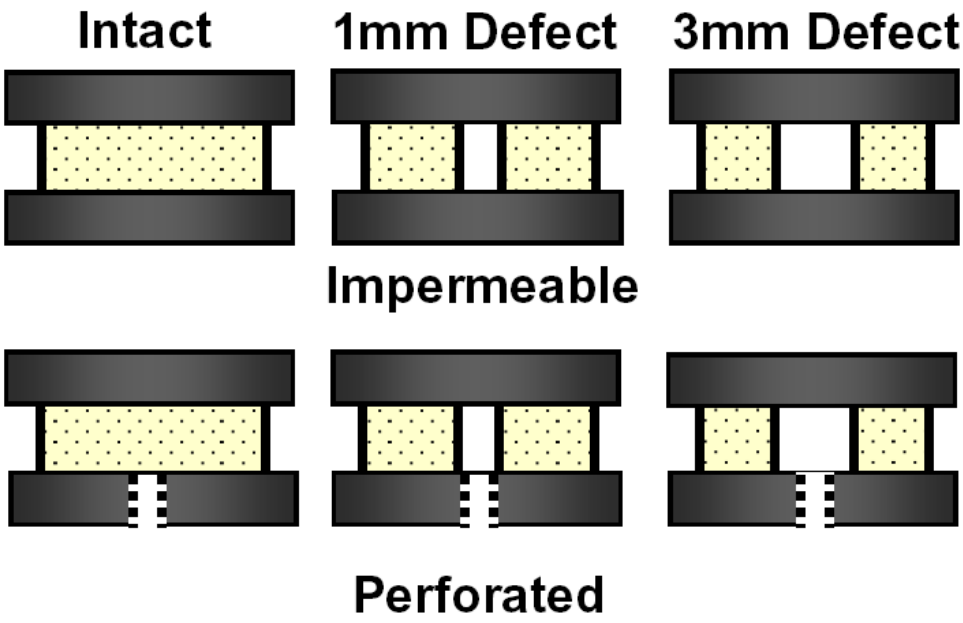

Figure A.2: Schematic of all experimental conditions tested. Samples were tested as first intact, then with a 1 mm defect, and finally with a 3 mm defect with either an impermeable or perforated bottom platen.

first and half were compressed in (ii) first. This was done to eliminate any mechanical effect of performing tests in a particular order. Between tests, disks were allowed to re-swell in PBS+PI for ~1.5 hours to fully re-hydrate the disks.

Data Collection and Calculations

Peak and equilibrium stresses, 50% relaxation time constant ($\tau_{1/2}$), and dynamic stiffness amplitude and phase angles were determined to give quantitative measurements of time-dependent mechanical behavior of cartilage disks loaded under the previously described conditions. Peak and equilibrium stresses were defined as the maximum and minimum stresses recorded, respectively, during the stress-relaxation to equilibrium phase to examine hydrostatic pressurization and solid matrix properties. $\tau_{1/2}$ were determined by calculating the amount of time after peak stress is reached for the measured stress to dissipate to the midpoint between peak and equilibrium stresses, giving a measurement of relaxation (i.e., fluid exudation) rates. Dynamic stiffness amplitude and phase angles were calculated from the collected oscillatory data using previously described methods [8, 19] to examine dynamic cartilage compressive stiffness and relative contribution of fluid flow to energy dissipation in cartilage [19].

Statistical Analysis

The effect of each experimental condition involving platen (i.e., impermeable or perforated), defect (i.e., intact, 1 mm, or 3 mm), and frequency (i.e., stiffness amplitude and phase) were all assessed using repeated measures ANOVA. Where

significant differences were found ($p<0.05$), Bonferroni post-hoc comparisons were made. All statistical analysis was done using SYSTAT 5.2 (Systat, Evanston, IL), and data are expressed, unless otherwise noted, as mean ± standard error of mean (SEM).

A.4 Results

Results for 15% compression are presented, since results at lower amplitude generally showed a similar pattern. During ramp-relaxation, compressive stress increased markedly to a peak and then relaxed (Figure A.3A-C). Peak stress was diminished with increasing defect diameter (Figure A.4A), by 8 and 30%, from intact to 1mm and 3mm defects, respectively ($p=0.01$), respectively. Peak stress did not vary with platen perforation ($p>0.4$). Equilibrium stress did not vary with defect ($p=0.2$) or with platen perforation ($p=0.5$). However, $\tau_{1/2}$ (Figure A.4B) was lower (i.e., faster relaxation) when defects were present ($p<0.005$), decreasing to ~50% of $\tau_{1/2}$ for intact tissue when a 3mm defect was created. $\tau_{1/2}$ also tended to decrease ($p=0.06$) when a perforated platen was used, in a defect-dependent way ($p<0.05$).

During oscillatory testing, variations in dynamic stiffness amplitude (Figure A.3D-F) and phase (Figure A.3G-I) were evident. Stiffness amplitude increased with frequency ($p<0.001$), decreased with the presence of 3 mm defect ($p<0.05$), and did not vary with platen perforation ($p=0.9$). Phase angle decreased with frequency ($p<0.001$), and increased with defect size ($p<0.001$) and perforation ($p<0.001$). There was a significant interaction between frequency and perforation ($p<0.001$), evident by diminishing difference in phase between solid vs. perforated platens (Figure A.3G-I) as frequency increased.

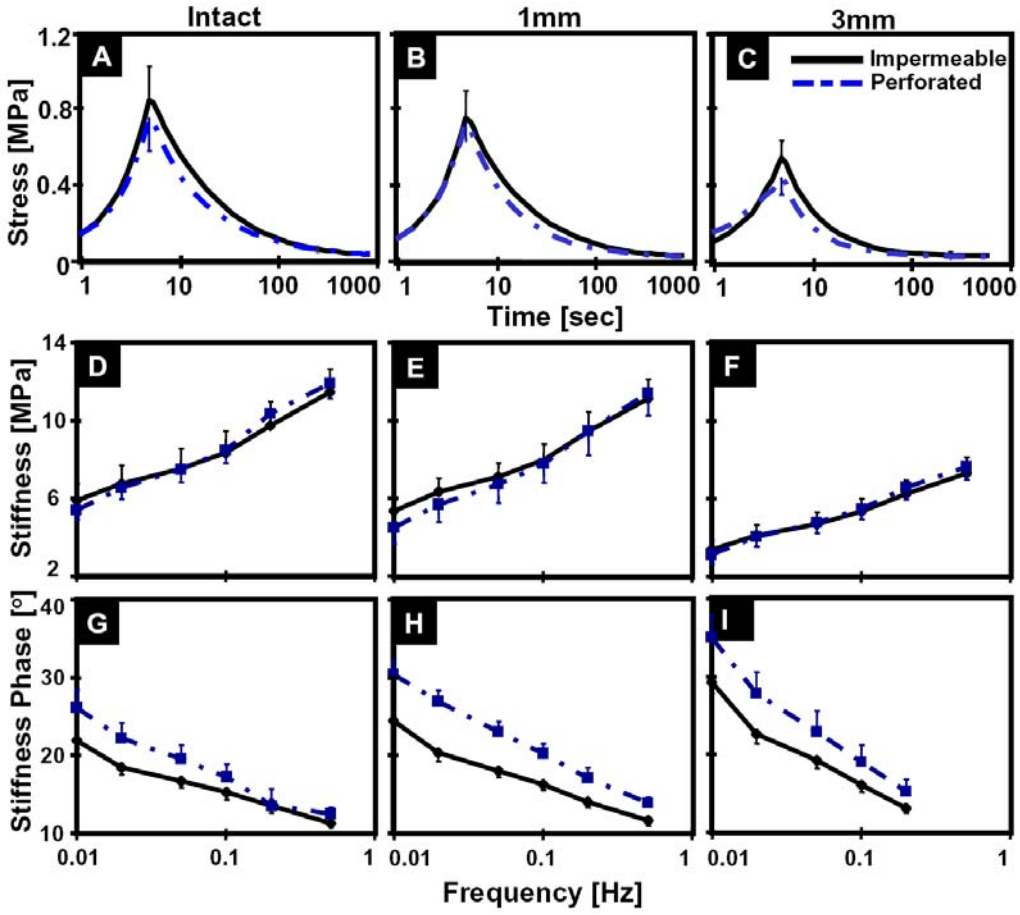

Figure A.3: Stress relaxation plots at 15% strain for cartilage disks, (ADG) intact, (BEH) with 1mm defect, and (CFI) 3 mm defect subjected to (A-C) ramp compression or (D-I) oscillatory testing to determine dynamic stiffness amplitude (DEF) and phase (GHI)

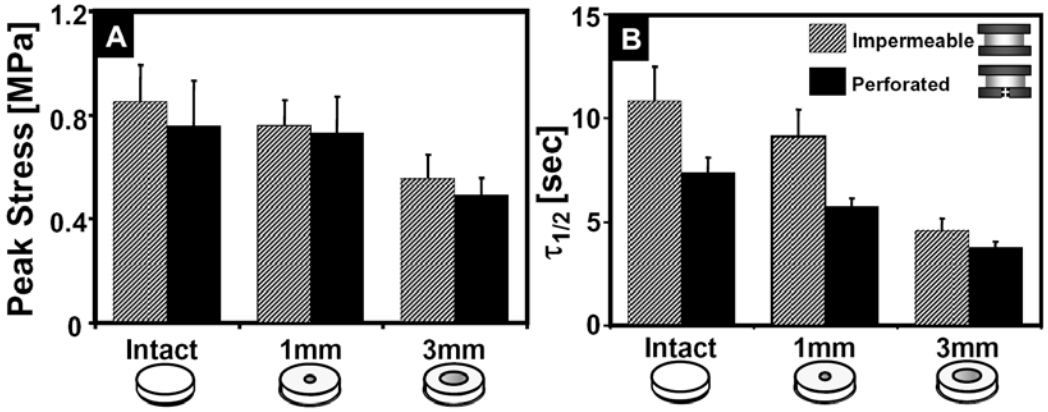

Figure A.4: (A) peak stresses and **(B)** $\tau_{1/2}$ constants ± SEM at 15% strain.

A.5 Discussion

This study utilized *in vitro* models that mimicked chondral defects with and without a compromised subchondral bone plate (ScBP) to elucidate the effects of chondral defects and ScBP perforations on the mechanical response of cartilage under compression. With increasing defect diameter, peak stress diminished with the presence of a defect and was not apparently different between samples tested with an intact platen and a perforated platen. Also, equilibrium stress was not altered by either defect or perforation. When defects were present, 50% relaxation time constant of cartilage was lower (i.e., faster relaxation and consolidation) and tended to decrease in a defect-dependent way when a perforated platen was used. Cartilage stiffness decreased with the presence of a defect, but did not vary with platen perforation. Phase angle decreased with frequency, and increased with defect size and perforation.

Relaxation time constants of cartilage markedly reducing with the presence of a defect suggest chondral defects in cartilage may cause load support to be transferred to solid matrix at a much more rapid rate when compressed. Interstitial fluid bears a majority of the load initially, and with time, this load is transferred to the solid matrix as the fluid exudes out of the cartilage tissue. With a chondral defect, interstitial fluid exits more rapidly, indicated by reduced stress relaxation constants, possibly because the distance to exude out of the matrix is shortened. As a result, cartilage with defects likely consolidates and strains more in the same duration of loading than normal cartilage. Thus, the solid matrix of cartilage is likely more susceptible to further insult and deterioration because of the elevated strains that develop.

The stress relaxation time constants of cartilage being lower with a perforated than an intact bottom platen suggest hydrostatic pressure dissipates more rapidly with a compromised subchondral bone plate than an intact one. Following impact loading, bone bruises and associated microcracks that extend through the ScBP have been observed without any damage in the above cartilage tissue [18, 28]. With time and continued joint loading, the above overly cartilage degenerates and have led some to believe it being caused by the compromised ScBP [6]. The compromised ScBP may contribute to the degeneration of the overlying cartilage by causing the hydrostatic pressure to dissipate more rapidly when loaded, and as a result, cause cartilage to experience greater strains. With greater strains, cartilage is more susceptible to degeneration. Thus, compromised ScBP may lead to cartilage degeneration by accelerating the dissipation of hydrostatic pressure and resulting in elevating cartilage strains.

The decreasing peak stress with increasing defect size suggests cartilage with a chondral defect would experience greater compression than intact cartilage for a given constant load. Articular surfaces during physiologic joint movement experiences a constant load. For current tests, samples were compressed to matching overall compressive strains and found that peaks stresses decrease with increasing defect size. However, if mechanical tests were performed with samples being compressed to matching peak stresses, cartilage with chondral defects would deform more in order to match the peak stress levels of intact cartilage due to loss of contact area. Thus, during physiologic loading, cartilage with chondral defects would experience greater deformation than intact cartilage, being consistent with previous observations [3].

This study has provided insight into effects of chondral defects and ScBP perforations on the initial and transient mechanical response of cartilage. The inability of cartilage to maintain hydrostatic pressure during compressive loading due to chondral defects or ScBP perforations may result in the solid matrix bearing a greater share of the applied load. As a result, the matrix may deform more and experience greater magnitudes of strain overall and locally. Such changes may induce cell death and matrix damage, which have been associated with high compressive strains [24] and impact loading [18]. Thus, the ability of cartilage to maintain hydrostatic pressure during loading may be critical to preventing pathological magnitudes of strain and cartilage degeneration.

A.6 Acknowledgments

I would like to thank co-author Dr. Won C. Bae for his contributions to this work. This work was supported by the San Diego Fellowship for Benjamin L. Wong and by the NIH and Howard Hughes Medical Institute through the Professors Program Grant to UCSD for Dr. Robert L. Sah.

A.7 References

1. Ateshian GA, Lai WM, Zhu WB, Mow VC: An asymptotic solution for the contact of two biphasic cartilage layers. *J Biomech* 27:1347-60, 1994.

2. Ateshian GA, Wang H: A theoretical solution for the frictionless rolling contact of cylindrical biphasic articular cartilage layers. *J Biomech* 28:1341-55, 1995.

3. Braman JP, Bruckner JD, Clark JM, Norman AG, Chansky HA: Articular cartilage adjacent to experimental defects is subject to atypical strains. *Clin Orthop Relat Res* 430:202-7, 2005.

4. Brown TD, Pope DF, Hale JE, Buckwalter JA, Brand RA: Effects of osteochondral defect size on cartilage contact stress. *J Orthop Res* 9:559-67, 1991.

5. Buckwalter JA, Mankin HJ: Articular cartilage: degeneration and osteoarthritis, repair, regeneration, and transplantation. *Instr Course Lect* 47:487-504, 1998.

6. Burr DB: The importance of subchondral bone in the progression of osteoarthritis. *J Rheumatol Suppl* 70:77-80, 2004.

7. Burr DB, Radin EL: Microfractures and microcracks in subchondral bone: are they relevant to osteoarthrosis? *Rheum Dis Clin North Am* 29:675-85, 2003.

8. Chen AC, Bae WC, Schinagl RM, Sah RL: Depth- and strain-dependent mechanical and electromechanical properties of full-thickness bovine articular cartilage in confined compression. *J Biomech* 34:1-12, 2001.

9. Cicuttini F, Ding C, Wluka A, Davis S, Ebeling PR, Jones G: Association of cartilage defects with loss of knee cartilage in healthy, middle-age adults: a prospective study. *Arthritis Rheum* 52:2033-9, 2005.

10. Ding C, Cicuttini F, Scott F, Boon C, Jones G: Association of prevalent and incident knee cartilage defects with loss of tibial and patellar cartilage: a longitudinal study. *Arthritis Rheum* 52:3918-27, 2005.

11. Ding C, Garnero P, Cicuttini F, Scott F, Cooley H, Jones G: Knee cartilage defects: association with early radiographic osteoarthritis, decreased cartilage volume, increased joint surface area and type II collagen breakdown. *Osteoarthritis Cartilage* 13:198-205, 2005.

12. Duda GN, Maldonado ZM, Klein P, Heller MO, Burns J, Bail H: On the influence of mechanical conditions in osteochondral defect healing. *J Biomech* 38:843-51, 2005.

13. Hunter W: On the structure and diseases of articulating cartilage. *Philos Trans R Soc London* 42:514-21, 1743.

14. Hunziker EB: Growth-factor induced healing of partial-thickness defects in adult articular cartilage. *Osteoarthritis Cartilage* 9:22-32, 2001.

15. Hunziker EB, Rosenberg LC: Repair of partial-thickness defects in articular cartilage: Cell recruitment from the synovial membrane. *J Bone Joint Surg Am* 78-A:721-33, 1996.

16. Jackson DW, Lalor PA, Aberman HM, Simon TM: Spontaneous repair of full-thickness defects of articular cartilage in a goat model. A preliminary study. *J Bone Joint Surg Am* 83-A:53-64, 2001.

17. Kim HKW, Moran ME, Salter RB: The potential for regeneration of articular cartilage in defects created by chondral shaving and subchondral abrasion. *J Bone Joint Surg Am* 73-A:1301-15, 1991.

18. Lahm A, Uhl M, Erggelet C, Haberstroh J, Mrosek E: Articular cartilage degeneration after acute subchondral bone damage: an experimental study in dogs with histopathological grading. *Acta Orthop Scand* 75:762-7, 2004.

19. Lee RC, Frank EH, Grodzinsky AJ, Roylance DK: Oscillatory compressional behavior of articular cartilage and its associated electromechanical properties. *J Biomech Eng* 103:280-92, 1981.

20. Lefkoe TP, Trafton PG, Ehrlich MG, Walsh WR, Dennehy DT, Barrach HJ, Akelman E: An experimental model of femoral condylar defect leading to osteoarthrosis. *J Orthop Trauma* 7:458-67, 1993.

21. Mankin HJ: The response of articular cartilage to mechanical injury. *J Bone Joint Surg Am* 64-A:460-6, 1982.

22. Meachim G, Bentley G: Horizontal splitting in patellar articular cartilage. *Arthritis Rheum* 21:669-74, 1978.

23. Mow VC, Bachrach NM, Ateshian GA: The effects of a subchondral bone perforation on the load support mechanism within articular cartilage. *Wear* 175:167-75, 1994.

24. Patwari P, Gaschen V, James IE, Berger E, Blake SM, Lark MW, Grodzinsky AJ, Hunziker EB: Ultrastructural quantification of cell death after injurious compression of bovine calf articular cartilage. *Osteoarthritis Cartilage* 12:245-52, 2004.

25. Radin EL, Parker HG, Pugh JW, Steinberg RS, Paul IL, Rose RM: Response of joints to impact loading. 3. Relationship between trabecular microfractures and cartilage degeneration. *J Biomech* 6:51-7, 1973.

26. Steadman JR, Rodkey WG, Singleton SB: Microfracture technique for full-thickness chondral defects: technique and clinical results. *Oper Tech Orthop* 7:300-4, 1997.

27. Suh JK, Li Z, Woo SL-Y: Dynamic behavior of a biphasic cartilage model under cyclic compressive loading. *J Biomech* 28:357-64, 1995.

28. Thompson RC, Oegema TR, Lewis JL, Wallace L: Osteoarthrotic changes after acute transarticular load: an animal model. *J Bone Joint Surg Am* 73:990-1001, 1991.

29. Thompson RC, Vener MJ, Griffiths HJ, Lewis JL, Oegema TR, Wallace L: Scanning electron-microscopic and magnetic resonance-imaging studies of injuries to the patellofemoral joint after acute transarticular loading. *J Bone Joint Surg Am* 75-A:704-13, 1993.

30. Wu JZ, Herzog W, Ronsky J: Modeling axi-symmetrical joint contact with biphasic cartilage layers--an asymptotic solution. *J Biomech* 29:1263-81, 1996.